2019

Electrochemical Separation of Multivalent Species on a Liquid Bismuth Cathode in LiCl-KCl Eutectic for Used Nuclear Fuel Reprocessing

Michael Woods
Virginia Commonwealth University

Electrochemical Separation of Multivalent Species on a Liquid Bismuth Cathode in LiCl-KCl Eutectic for Used Nuclear Fuel Reprocessing

A dissertation submitted in partial fulfillment of the requirements for the degree of Doctor of Philosophy at Virginia Commonwealth University

by

Michael Woods

Mechanical and Nuclear Engineering, Virginia Commonwealth University

Richmond, Virginia

December 3rd, 2019

Major Professor: Supathorn Phongikaroon, Ph.D, Mechanical and Nuclear Engineering, Virginia Commonwealth University

This is to certify that the dissertation prepared by Michael Woods entitled "Electrochemical Separation of Multivalent Species on a Liquid Bismuth Cathode in LiCl-KCl Eutectic for Used Nuclear Fuel Reprocessing" has been approved by his committee as satisfactory completion of the dissertation requirement for the degree of Doctor of Philosophy.

Graduate Advisory Committee (type name and sign)

	Failed	Passed
Supathorn Phongikaroon		✓
Leonard V Rogers M		✓
Julio C. Alvarez		✓
BRADEN GODDARD		✓
Christina Tang		✓

ACKNOWLEDGMENTS

I would like to first acknowledge and thank my advisor, Dr. Supathorn Phongikaroon. I was drawn to come to VCU by the great Mechanical and Nuclear Engineering program and the beautiful city of Richmond, but I was most excited to have Dr. Supy as a mentor and advisor in this beginning of my career. Thank you for your guidance, time, energy and efforts to improve my professional and personal life. You are never the cockroach. Many thanks to all of the other professors and departmental people at the VCU College of Engineering. Thank you Drs. Sama, Rojas, Goddard, Supy, Mr. Miller, and all of the others for teaching such enlightening classes. Thank you Drs. Alvarez, Tang, and those already mentioned for serving on my dissertation committee. Special thank you to Julie Arendt and the research librarians at VCU who are scarily good at their jobs and who successfully found every obscure article I ever requested.

I also want to acknowledge all of the teammates, coaches, and supporters of the Crew Club at VCU. Rowing each morning on the James and competing around Virginia has given me lifelong memories and some of my closest friendships. It certainly enhanced my VCU experience.

To all of my friends from the research group, Ammon, Dalsung, Riyadh, Samaneh, Hunter, Dimitris, Reggie, George, Ivan, Adam, and Miroslava, thank you for all of your help in the lab and valuable discussions. I was lucky to be a member of such a cohesive research team.

Finally, I want to acknowledge my family for their support. To my Dad, thank you for encouraging me to go in the way I choose. To my Mom, thank you for always being there to talk. To Matthew, Maggie, and Jamie, thank you for all of the fun trips and good times while I have been studying. Lastly, to my fiancée Caroline, thank you for making the last two years immeasurably more fun and for constant patience with me while I completed my PhD.

TABLE OF CONTENTS

LIST OF TABLES

LIST OF FIGURES

LIST OF ABBREVIATIONS AND SYMBOLS

Abbreviation	Meaning
ANL	Argonne National Laboratory
CP	Chronopotentiometry
CPE	Constant Phase Element
CV	Cyclic voltammetry
DSC	Differential Scanning Calorimetry
EBR-II	Experimental Breeder Reactor-II
EIS	Electrochemical impedance spectroscopy
EMF	Electromotive force
ER	Electrorefiner
ICP-MS	Inductively coupled plasma mass spectrometry
INL	Idaho National Laboratory
LBC	Liquid bismuth cathode
LCC	Liquid cadmium cathode
MOX	Mixed oxide
OCP	Open circuit potential
PUREX	Plutonium and uranium recovery extraction
RE	Rare-earth elements
RSS	VCU Radiation Safety Section
SEM-EDS	Scanning electron microscopy with energy dispersive spectrometry
TRU	Transuranic elements
UNF	Used Nuclear Fuel

Symbol	Physical meaning	Unit
a_i	Activity	
C_0	Concentration	mol cm^{-3}
C_{dl}	Double-layer capacitance	F
D	Diffusion coefficient	cm^2 s^{-1}
E	Potential	V
E^0	Standard Reduction Potential	V
E^{0*}	Apparent standard potential	V
E^{eq}	Equilibrium potential	V
E_p	Peak potential for CV	V
η	Activation overpotential	V
F	Faraday's constant	C mol^{-1}
γ	Activity coefficient	
i_p	Peak current	A
n	Number of electrons transferred	
ω	Angular frequency	rad s^{-1}
φ	Phase angle for EIS	rad
R	Universal gas constant	J mol^{-1} K^{-1}
R_{ct}	Charge transfer resistance	Ω
R_s	Solution resistance	Ω
S	Surface area	cm^2
T	Absolute temperature	K
t	time	s

v	Scan rate for CV	$V\ s^{-1}$
W	Warburg diffusion resistance	Ω
X	Mole fraction	
Z	Impedance	Ω

ABSTRACT

Recovery of alkali/alkaline-earth species from the bulk salt medium used in pyroprocessing of used nuclear fuel would allow increases in operational efficiencies and minimization of ultimate waste. A proposed method for separation of some of these species using electrochemical reduction at a liquid Bi cathode has been investigated via cyclic voltammetry (CV), electrochemical impedance spectroscopy (EIS), and scanning electron microscopy with energy dispersive x-ray spectrometry (SEM-EDS) conducted on the LiCl-KCl/liquid Bi system containing Cs, Sr, Ba, or Ce. These studies have provided information about the redox reactions and mass transport occurring in the system, as well as the kinetic properties of the electroactive species at the Bi cathode surface. Furthermore, SEM-EDS characterization of the Bi cathodes after experimentation have suggested the presence or absence of the interested species in the form of Bi intermetallic compounds.

CV studies were performed at temperatures of 723–823 K and concentrations of the target species up to 4.0 wt%. The redox reactions occurring during potential sweeps were observed and diffusion coefficients (D) of the electroactive species calculated. Redox reactions were present in LiCl-KCl systems containing Cs, Ba, and Ce. Values of D for CsCl were calculated to be 0.0176 to 0.945×10^5 cm^2 s^{-1} from the first redox peaks and 0.027 to 1.551×10^5 cm^2 s^{-1} from the second redox peaks. Calculated values of D from the observed redox peaks of $BaCl_2$ ranged from 0.0129 to 0.0993×10^5 cm^2 s^{-1}. Concentration of $BaCl_2$ in the salt did not seem to influence the diffusivity in the studied concentration range up to 4.0 wt%. Although the presence of Sr in the system affected the redox reaction of Li, there were no distinguishable redox peaks which could be measured. Finally, $CeCl_3$ was studied and diffusion coefficients for $CeCl_3$ in the LiCl-KCl salts was calculated to be 1.05 to 8.40×10^5 cm^2 s^{-1}.

EIS methods were also employed to obtain impedance spectra leading to calculations of the exchange current densities (i_0) of the electroactive active redox couple at the Bi cathode. Values of i_0 calculated for the Cs^+/Cs redox couple ranged from 0.0752 to 0.0911 A cm^{-2} for a 0.5 wt% CsCl-LiCl-KCl system at temperatures of 723–773 K. Likewise, values of i_0 measured by EIS for the Ba^{2+}/Ba redox couple at the Bi cathode ranged from 0.0550 to 0.121 A cm^{-2} for concentrations of 0.78–3.0 wt% $BaCl_2$ in LiCl-KCl and temperatures of 723 to 823 K.

Based on the experimental results, a general assessment of the liquid Bi cathode for alkali/alkaline-earth elements recovery in LiCl-KCl salts is presented. Further research of the Bi cathode, including electrochemical reduction of multiple species in LiCl-KCl, is suggested for advancement and progression of the Bi cathode in pyroprocessing technology applications.

Chapter 1 Introduction

Nuclear power contributes significantly to the worldwide demand for energy and its contribution is likely to increase in the future. At the end of 2018, there were 449 operable reactors and 55 more under construction worldwide [1]. These 449 reactors plus two others which were closed down in 2018 created 2563 TWh of clean energy in 2018 [1]. As the generation of nuclear power continues and increases, there is an increasing need to address the long-term storage or recycling of the increasing amount of used nuclear fuel (UNF). The United states alone has 81,901 tonnes heavy metal (tHM) in storage with 2,493 tHM created in 2018 [2]. Alternative to a simple long-term storage and disposal of the UNF is reprocessing because ~95% of the available nuclear energy of fresh fuel is still available after the fuel has been used in a reactor [3]. Reprocessing allows for the fuel elements (i.e. U, Pu, and other actinides) to be recoverable in order to create new mixed-oxide (MOX) fuel for reactors and reduce the amount of nuclear material in the final waste form.

Two methods of reprocessing UNF–aqueous separation and pyroprocessing technology–have been well established and studied. Aqueous separation, utilizing acid and typically a process of plutonium and uranium recovery extraction (PUREX), has been studied extensively by many countries, including the U.S., Russia, and France, where the La Hague facility has the capacity to reprocess 1700 t/yr [4]–[6]. Aqueous reprocessing, and more specifically the PUREX process, separates pure U and Pu via several steps of solvent extractions with nitric acid media. However, this is not ideal for proliferation resistance as it involves separated plutonium product. This fact contributed to the U.S. halting advancement of commercial reprocessing activity in the late 1970s [4]. In contrast, proliferation resistance is a key feature of pyroprocessing technology, where U and Pu are co-deposited with other transuranics electrochemically in molten salt media and are

originally not separated during the process. Details of this technology are discussed in the following section.

1.1 Pyroprocessing Technology

Pyroprocessing technology, also called electrometallurgical process and electrochemical separation, was first developed by Argonne National Laboratory (ANL) to treat metallic fuel from the Experimental Breeder Reactor-II (EBR-II). This process is still operated at Idaho National Laboratory (INL) for this purpose [7]. A flow diagram of the advanced process is shown in Figure 1.1. In this process, the feed product is either fuel from a fast breeder reactor utilizing metal fuel or oxide fuel, which is converted to metallic form via oxide reduction. This feed product is then chopped up and dissolved into LiCl-KCl salts in a large apparatus called an electrorefiner (ER). Here, the fuel claddings are isolated and removed and the useful constituents of the fuel are separated and recovered.

Its advantages in comparison to aqueous reprocessing are the solubility of fuel products in molten salts, decreased cooling time of fuel before reprocessing, combined irradiation-reprocessing facility capability, increased proliferation resistance, decreased long-lived radioactive waste and lower criticality hazard due to the poor neutron moderation properties of the salt [8], [9].

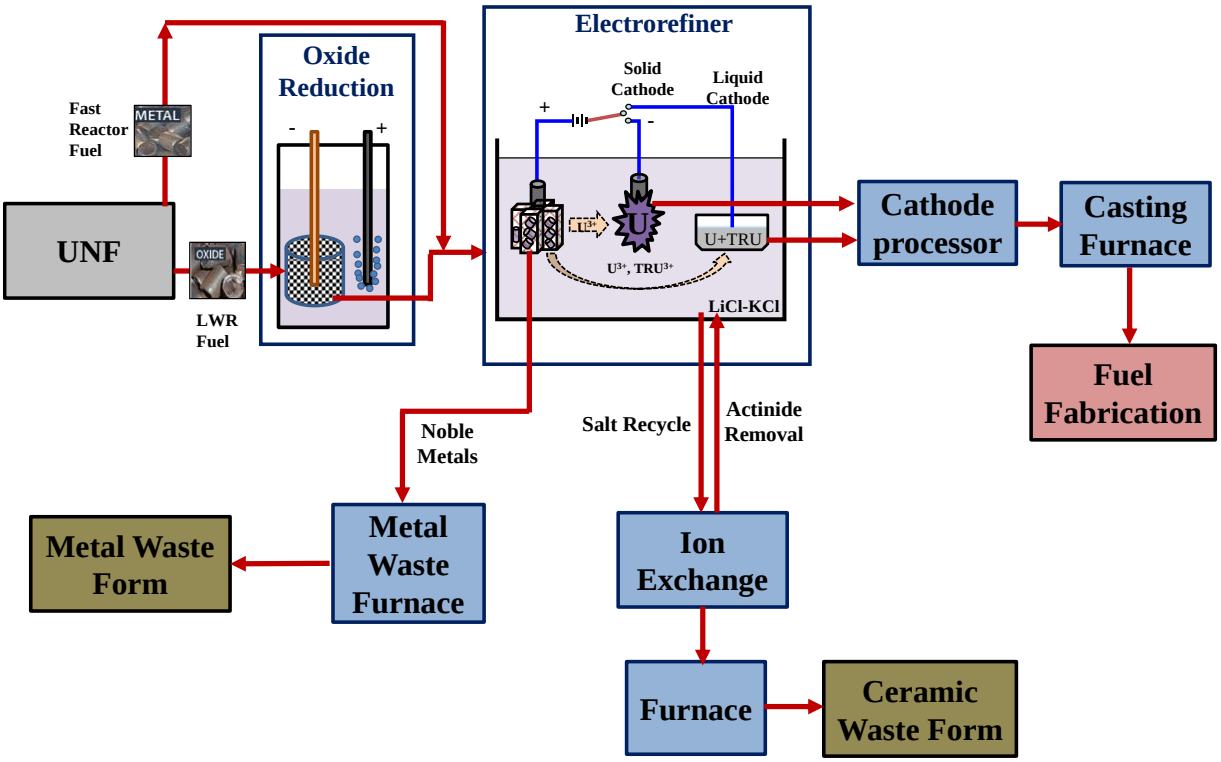

Figure 1.1 Schematic diagram of an advanced pyroprocessing for UNF including electrolytic oxide reduction [10].

1.2 Electrorefiner (ER)

The primary step in pyroprocessing happens with the ER, a diagram of which is presented in Figure 1.2. The general procedure is (1) the used fuel is chopped up and contained in an anode basket, (2) soluble elements are anodically dissolved into LiCl-KCl salts, and (3) U is recovered electrochemically at a solid cathode. A liquid cadmium cathode (LCC) is also able to be applied to recover actinides, including transuranic elements (TRU) and some rare earth fission products due to their low activity coefficients in liquid metals [11], [12]. The metal waste from cladding hulls remains in the anode basket and is removed for treatment as waste. The solid U and Cd cathodes are processed separately via distillation in a vacuum chamber to remove the salt and cadmium and to recover the U/TRU and Pu/U/TRU products [4], [13], [14]

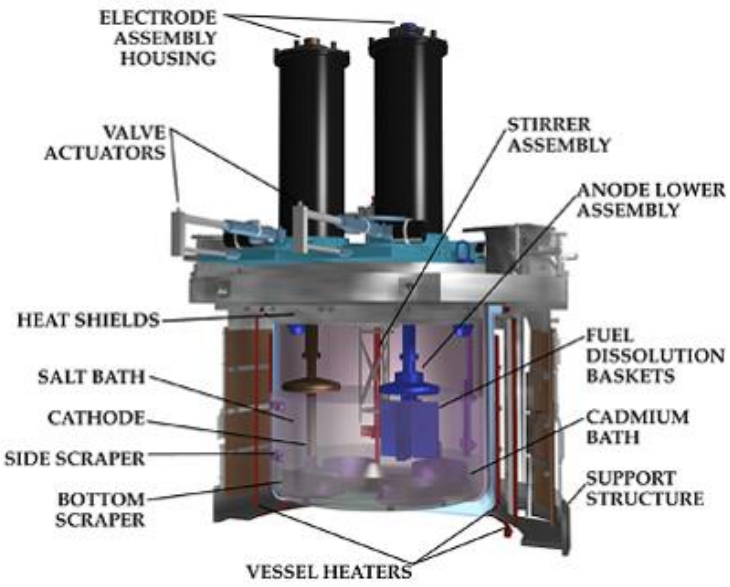

Figure 1.2. Diagram of the Mk-IV Electrorefiner.

Fission products in the ER salts will accumulate as UNF is processed in each batch cycle. The accumulation of these salts degrades the efficiency of the ER by decreasing the electrode reaction which captures U. Therefore, the salt will need to be cleaned of these fission products or otherwise replaced. Furthermore, removal of the radioactive fission products, especially the short-lived isotopes like Cs-137 (half-life of 30.17 y) and Sr-90 (half-life of 28.8 y) can lessen the radioactivity of the bulk salt and make shielding and handling easier. Table 1.1 shows the expected composition of the salt after it has undergone several batches in the ER. The separation of specific fission products from these salts has been the focus of much research and many different techniques, primarily ion exchange [7], [15], [16], and zone freezing [17]–[20].

Table 1.1 The expected composition of waste ER salt after treatment [21].

Composition (mol%)			
LiCl (36.12)	$SrCl_2$ (0.57)	$NdCl_3$ (1.48)	$PuCl_3$ (1.05)
KCl (26.13)	UCl_3 (0.59)	$PmCl_3$ (0.02)	$AmCl_3$ (0.003)
NaCl (29.35)	$BaCl_2$ (0.58)	$SmCl_3$ (0.28)	$PrCl_3$ (0.44)
RbCl (0.26)	$LaCl_3$ (0.47)	$EuCl_3$ (0.02)	YCl_3 (0.34)
CsCl (1.37)	$CeCl_3$ (0.89)	$GdCl_3$ (0.01)	$NpCl_3$ (0.03)

1.3 Motivation

The reprocessing of UNF by electrochemical separation methods has successfully demonstrated the recovery of solid U and a U/Pu mixture via a Cd cathode. However, there is not yet a well-demonstrated technique for the electrochemical separation of other fission products, such as Cs, Ba, and Sr, which remain in the salt after each batch and degrade the performance of the ER. Similar to the way that U and other actinides can be recovered by the LCC because of a shift in reduction potentials of the elements for a cadmium cathode, a liquid Bi cathode might be able to be used to capture other fission products [22], [23]. Although the thermodynamic and electrochemical properties of many rare-earth elements (RE) and actinides have been investigated for the LiCl-KCl/Bi system, there is lack of knowledge for these properties of alkali/alkaline-earths [24]–[26]. A more robust base of electrochemical knowledge is needed in order to confidently assess the potential for application of the liquid Bi cathode in pyroprocessing schemes.

1.4 Goal

The primary goal of this dissertation is to provide fundamental electrochemical and kinetics data for select representative alkali/alkaline-earth and RE fission products in the LiCl-KCl/Bi cathode system. This data can then be used to make a preliminary judgement on the feasibility and

performance of a liquid Bi cathode if added to a pyroprocessing scheme. This electrochemical data was collected via bench-top experiments replicating the ER environment. Electrochemical experiments made use of cyclic voltammetry (CV), electrochemical impedance spectroscopy (EIS), and open circuit potential (OCP) techniques to determine values for important parameters of the process, including redox potentials, diffusivity, and exchange current density of the ions. These parameters have not been well-examined for the LiCl-KCl/Bi system with fission products and this work will provide a basis for future studies of a liquid Bi cathode in the ER environment.

1.5 Approach

A four-phase approach was developed to organize and complete this research. The specific goals of each phase are explained here and a schedule of the performed work for each phase is given in Section 1.5.5.

1.5.1 Phase I: Literature Survey and Experimental Design

In Phase I, an extensive literature review of liquid bismuth in LiCl-KCl systems was performed. This literature review indicated the existing knowledge gaps for the electrochemistry of LiCl-KCl/liquid Bi eutectic systems and informed the experimental design of our system.

1.5.2 Phase II: Measurement of Electrochemical Properties of Fission Products

This phase established the experimental setup, which has been utilized for electrochemical property measurements. The electrochemical behaviors of Cs, Sr, and Ba ions were studied. All experiments have taken place in a glove box of argon atmosphere with O_2 and H_2O levels maintained under 5 ppm, within the Radiochemistry laboratory (Room E4262, East Engineering Building). The argon atmosphere is necessary since the salts are very hygroscopic.

1.5.3 Phase III: Measurement of Electrochemical Properties of Lathanides

In this phase, the experimental and analysis techniques—which have been applied for alkali/alkali-earth in Phase II—were applied to cerium to represent trivalent lanthanides. This work allowed for validation of our experimental system compared to previous studies and expanded on their findings.

1.5.4 Phase IV: Assessment of Bismuth Cathode for use in Pyroprocessing Applications

In this phase, the electrochemical data sets from Phases I–III were compared and analyzed to give an assessment of the bismuth cathode as it could be added into existing pyroprocessing applications. The result is an overview of the scientific benefits and challenges which are present with the addition of the bismuth cathode in the ER.

1.5.5 Project Schedule

The project was completed within three years according to the schedule in Table 1.2, expressly quarterly.

Table 1.2 Timeline of the dissertation experimental work.

Phase	Year 1 (2017)				Year 2 (2018)				Year 3 (2019)			
	1	2	3	4	1	2	3	4	1	2	3	4
I												
II												
III												
IV												

1.6 Organization of the Dissertation

This dissertation is composed of five chapters. Chapter 1 contains the background information, motivation, goal, and approach related to the project. In Chapter 2, a review of relevant experiments and electrochemical methods from literature is presented. Chapter 3 discusses the experimental design and procedures, including preparation of salts for electrochemical experiments and sample analysis by inductively coupled plasma mass spectrometry (ICP-MS) and scanning electron microscopy with energy dispersive spectrometry (SEM-EDS). Chapter 4 presents the results of this research, including values for electrochemical and kinetics parameters, as well as a discussion of the feasibility of a Bi cathode for inclusion in the ER. Chapter 5 summarizes the content of this dissertation and suggests future work. Additional assessments conducted on thermophysical properties of the LiCl-KCl-$BaCl_2$ system as well as data, figures, and tables supporting the body of the chapters are presented in the appendices.

Chapter 2 Literature Survey

There have been many published papers regarding the electrochemical separation of elements within LiCl-KCl eutectic salt. Since the target elements are typically actinides, due to their potential for reuse, or RE elements, due to their electrochemical similarity to the actinides and consequent complication of actinide recovery, there is a still limit on the body of literature for the behavior and separations of alkali/alkaline-earth elements. The purpose of this chapter is to confer the important parameters and behavioral aspects sought after in pyroprocessing experimental research and to review the existing research, which has investigated Cd and Bi cathodes for electrochemical separations. The electrochemical techniques applied for the experimental research will also be covered.

2.1 Review of Electrochemical and Microscopy Techniques

This section presents an overview of the electrochemical and other techniques used in this project to collect experimental data. The electrochemical techniques can be applied to give insight into the mass transfer and kinetics behaviors of selected ions within the LiCl-KCl salt and at the Bi cathode surface.

2.1.1 The Electrochemical Cell and Redox Potentials

The aim of electrochemical experiments are to understand reactions wherein an electron transfer occurs. This means that a species is either being oxidized, losing an electron and gaining a more positive charge, or being reduced, gaining an electron and a more negative charge. These two reactions are referred to as half-reactions. The electrochemical cell of interest to electrochemical experiments is called an electrolytic cell. It consists of two electrodes, a cathode where species are reduced and an anode where species are oxidized, and an electrolyte, a solution or sometimes solid which the electrodes are in contact with and which mediates the movement of

ions to the electrode surface. The two electrodes are connected electrically outside of the cell so that a voltage may be applied which drives the reduction and oxidation reactions. To study the reactions taking place, this connection is made with a potentiostat. The potentiostat applies a voltage to the cell and records the current response at the working electrode. The working electrode is chosen based on which half-reaction is of interest in measuring. The response of the working electrode is measured versus a stable reference electrode that is also in ionic contact with the electrolyte. A reference electrode is an independent half-cell with constant makeup and measures a well-known potential. It completes the half-reaction opposite the working electrode and allows for an accurate measurement. Common choices for a reference electrode include a standard hydrogen electrode, saturated calomel electrode, and silver chloride electrode. The electrode that is not chosen as a working electrode is referred to as the counter electrode. Its purpose is to allow the current to be passed through the cell without producing reactions that interfere with the reaction of interest at the working electrode. This configuration of a cathode, anode, and reference electrode is referred to as a three electrode system.

Applying a current to the electrolytic cell and measuring the potential at the working electrode gives valuable information about the reaction that is taking place at the electrode surface. The half-cell reactions for a species being reduced at the cathode and oxidized at the anode are, respectively,

$$M^+ + e^- \rightarrow M \tag{2.1}$$

$$M \rightarrow M^+ + e^- \tag{2.2}$$

When no external current is applied to the cell, the concentrations of the species are in equilibrium and the cell will possess a potential referred to as the equilibrium potential $E^{eq}_{M^+/M}$.

This reduction-oxidation reaction, called redox, and its equilibrium potential is described by the Nernst equation,

$$E^{eq}_{M^{n+}/M} = E^{0}_{M^{n+}/M} + \frac{RT}{nF}\ln\left(\frac{a_{M^{n+}}}{a_{M}}\right) \quad (2.3)$$

where $E^{0}_{M^{n+}/M}$ is the standard reduction potential, which is the theoretical potential when the cell is reversible at an equilibrium state and the solution concentration is 1 mol L^{-1} at 1 atm and 298 K, R is the universal gas constant (8.314 J mol^{-1} K^{-1}), T is the absolute temperature (K), n is the number of electrons transferred, F is Faraday's constant (96485 C mol^{-1}), and a_i is the activity of the species. For the Bi cathode system, the binary system of Bi with the reduced cation is of interest. Eq. (2.3) can be expressed with respect to this reaction and the activity of the binary system as,

$$E^{eq}_{M^{n+}/M} = E^{0}_{M^{n+}/M} - \frac{RT}{nF}\ln\left(\frac{a_{M(\text{in Bi})}}{a_{M^{n+}}}\right) \quad (2.4)$$

With this relation in mind, the shift of reduction potentials with a Bi cathode due to the low activities of alkali/alkaline-earth species in Bi can be explained. The electromotive force (emf) technique can be applied to measure and give a value for the second term in the right hand side of Eq. (2.4). Using the emf values of Li, K, Sr, and Ba in Bi that have been measured and reported in literature, it is possible to calculate the shifted equilibrium potential of each species in Bi. The standard reduction potentials, emf values for a 5 mol% species in Bi concentration, and shifted equilibrium potentials from literature for the relevant species are given in Table 2.1 and displayed graphically in Figure 2.1. Due to the large emf values of Sr and Ba compared to Li and K, the reduction potentials of Sr and Ba are shifted to more positive values than Li and K. This thermodynamic calculation suggests the ability to reduce Sr and Ba into liquid Bi selectively over Li and K.

Table 2.1 Overview of thermodynamic properties of Bi system species and calculated reduction potential shifts.

M^{n+}/M	E^0 (V) vs Cl-/Cl_2 (g)	emf (V)	E_{eq} (V) vs Cl-/Cl_2 (g)
Li^+/Li	-3.550	0.924	-2.626
K/K	-3.690	0.967	-2.723
Sr^{2+}/Sr	-3.623	1.004	-2.619
Ba^{2+}/Ba	-3.755	1.164	-2.591

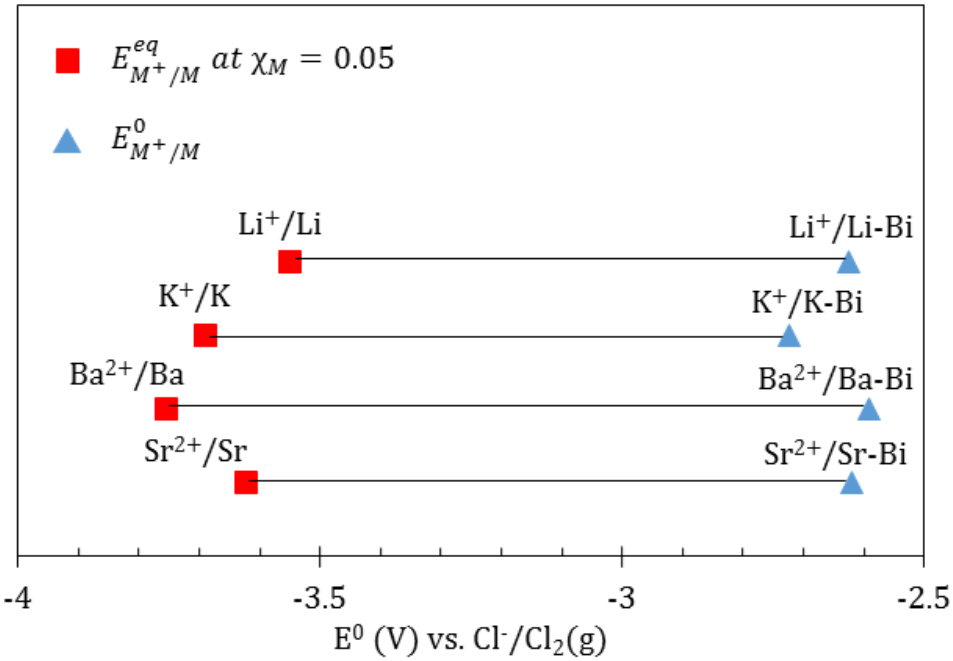

Figure 2.1 Graphical depiction of standard reduction potentials (E^0) and shifted equilibrium potentials in liquid Bi (E^{eq}) based on literature emf values.

To simplify Eq. (2.4), since activities are usually unknown, the standard apparent potential can be used which relies on the concentration of species in the cell since the activity $a_i = \gamma_i * \chi_i$. This apparent standard potential is denoted $E^{0*}_{M^+/M}$ and yields the following expression,

$$E^{eq}_{M^{n+}/M} = E^{0*}_{M^{n+}/M} - \frac{RT}{nF} \ln\left(\frac{\chi_{M(\text{in Bi})}}{\chi_{M^{n+}}}\right) \quad (2.5)$$

This is an important concept for an electrochemical process, especially to the ER, because this apparent standard potential is the one that can be applied to a cell to drive the reaction. That is, a species, such as U^{3+} or Ba^{2+}, can be reduced at the cathode with an applied potential equal to the apparent standard reduction potential.

2.1.2 Open Circuit Potentiometry (OCP)

A necessary component of understanding a redox reaction is knowing the equilibrium or "zero-current" potential. This is done by using the OCP method, where potential in the cell is measured with no applied current flowing through the cell. The system is allowed to rest until the redox couple is present in equilibrium at the cathode surface. The equilibrium potential, which is the steady potential between the oxidant and reductant, is then measured via OCP. Figure 2.2 shows an example of this measurement, where the equilibrium potential can be seen to be about -0.283 V for a certain $BaCl_2$-LiCl-KCl/Bi system.

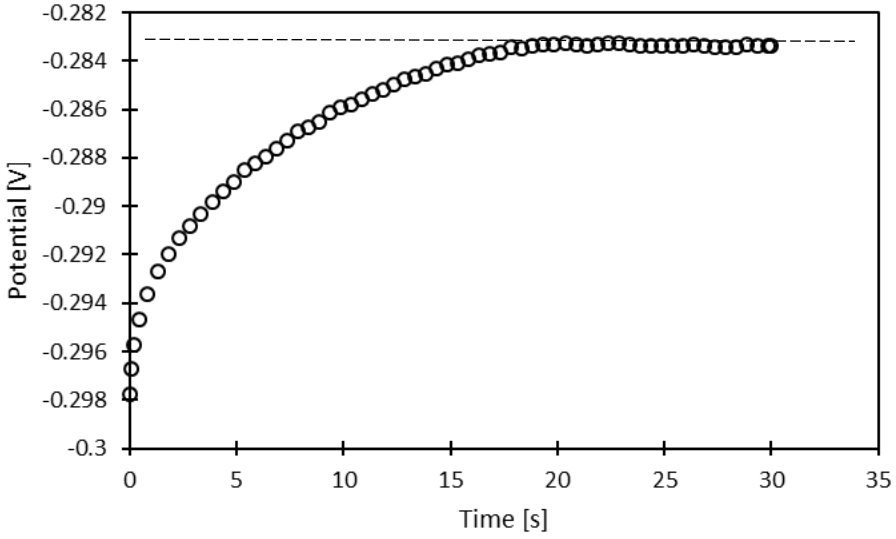

Figure 2.2 Example of OCP measurement for a 2.0 wt% $BaCl_2$-LiCl-KCl/Bi system at 798 K.

The equilibrium potential is useful for calculating the apparent standard potential. When the equilibrium potential is measured at different concentrations, the apparent standard potential can be calculated from the plot of the two, according to Eq. (2.4) for a cathodic peak potential for a reversible soluble/insoluble system in a mole fraction form. The OCP method is also useful in ensuring the electrochemical cell is in equilibrium before conducting experiments. Thus, performing the OCP run before each electrochemical measurement is critical in verifying that the equilibrium condition is present.

2.1.3 Cyclic Voltammetry (CV)

Cyclic voltammetry is a powerful technique because of its ability to quickly give characterization of an electroactive species along with kinetic and mechanistic information when chemical reactions are present [27]. An example of a cyclic voltammogram is shown in Figure 2.3. The potential is swept from positive to negative and then reversed while measuring the current response. The negative current peak corresponds to reduction at the cathode, while the positive current peak corresponds to oxidation of the reduced species.

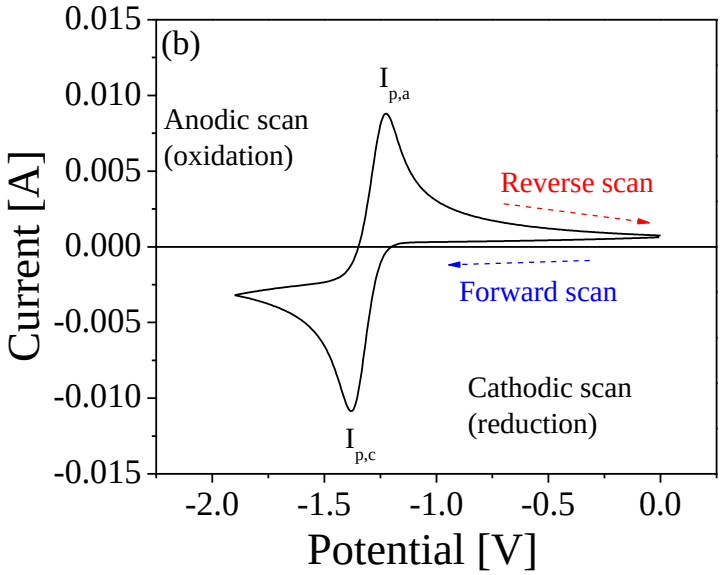

Figure 2.3 Example of a cyclic voltammogram [10].

Mass transfer in an electrochemical cell is governed by diffusion, migration, and convection of the electroactive species [28]. Often the reduction of an electroactive species is diffusion controlled [29], [30]. Then, the diffusion coefficient of a species is important for understanding the reduction behavior. CV can be performed at different scan rates v to give a measurement of the diffusion coefficient D according to the Berzin-Delahay equation for a soluble-insoluble reversible process,

$$i_p = 0.611\ nFSC_0 \left(\frac{nFvD}{RT}\right)^{1/2} \tag{2.6}$$

where i_p is the peak current, n is the number of electrons transferred, S is the surface area of the cathode, and C_0 is the concentration of the electroactive species in the salt. Plotting i_p vs. $v^{1/2}$ will give an experimental value for D based on Eq. (2.6). For all species of this project, the ionic species in the bulk salt is soluble, while the reduced form within the Bi cathode is insoluble.

From the values of diffusion, the activation energy can be calculated since the diffusivity generally follows an Arrhenius relationship, expressed as,

$$D = D_0 \exp(-\frac{E_a}{RT}) \tag{2.7}$$

where D_0 is the pre-exponential factor and E_a is the activation energy (kJ mol^{-1}) for the diffusion. Therefore, by plotting ln(D) versus 1/T, the activation energy can be calculated from the slope.

The CV plot is also useful for calculating the apparent standard potential from the cathodic peak potentials. This is achieved by the following equation [28],

$$E_p = E^{0*} + \frac{RT}{nF}\ln(X) - 0.854\frac{RT}{nF} \tag{2.8}$$

where E_p is the peak potential, X is the mole fraction, and E^{0*} is the apparent standard potential.

Lastly, the CV technique can be used to calculate an approximation of the exchange current density i_0, which describes the ion exchange happening at the liquid cathode surface. The exchange current density is important for understanding the rate of reaction as controlled by ion transfer and is important for kinetic modeling of the system. It is calculated by using the area of linear polarization during a CV scan and plotting the current i vs. activation overpotential η according to the simplified Butler-Volmer equation for very small overpotential regions [31],

$$\mathrm{i} = \mathrm{i}_0 \left(\frac{\mathrm{nF}}{\mathrm{RT}}\right) \eta \tag{2.9}$$

2.1.4 Electrochemical Impedance Spectroscopy (EIS)

EIS is a technique which applies a small current at a potential near the open circuit potential, driving a small reduction at the cathode, and measures the impedance spectra as a function of frequency. For a perturbation of potential with angular frequency ω, the impedance Z(t) can be expressed as a function of the potential E(t) and current response i(t),

$$Z(\mathrm{t}) = \frac{\mathrm{E(t)}}{\mathrm{i(t)}} = \frac{\mathrm{E(0)sin(\omega t)}}{\mathrm{i(0)sin(\omega t + \phi)}} = \mathrm{Z(0)} \frac{\mathrm{sin(\omega t)}}{\mathrm{sin(\omega t + \phi)}} \tag{2.10}$$

where ϕ is the phase angle illustrated in Figure 2.4.

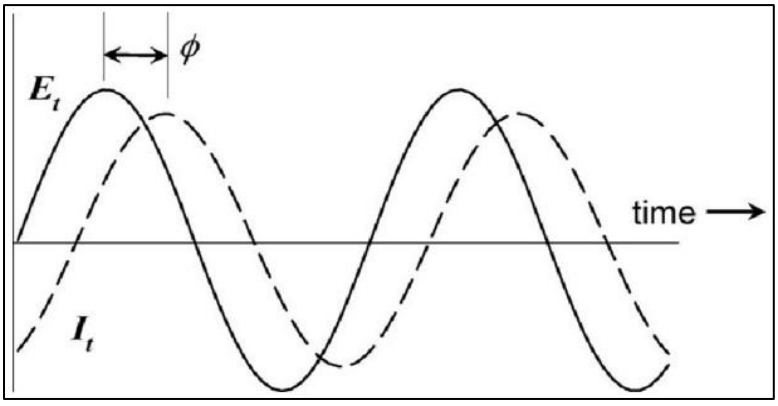

Figure 2.4 Example plots of the potential and current response for the EIS method [32].

When E(t) and i(t) are considered in the complex plane, the equations become,

$$E(t) = E(0)\exp(j\omega t) \tag{2.11}$$

$$i(t) = i(0)\exp(j(\omega t - \phi)) \tag{2.12}$$

where j is the imaginary number, $\sqrt{-1}$. The equation for Z can be then be simplified with these equations and Euler's formula to,

$$Z(t) = Z(0)(\cos\phi + j\sin\phi) = Z(Re) + Z(Im) \tag{2.13}$$

where Z(Re) and Z(im) are the real and imaginary part of the impedance, respectively. This forms the basis for the Nyquist plot, where Z(Re) and Z(Im) are plotted on the x and y axes, respectively.

The Nyquist plots generated by EIS techniques can be fitted to an equation of an equivalent circuit for modeling the system. A proposed circuit for this system is displayed in Figure 2.5 – composed of the bulk solution resistance, a double layer capacitance at the cathode surface, the charge transfer resistance, and the Warburg diffusion related resistance.

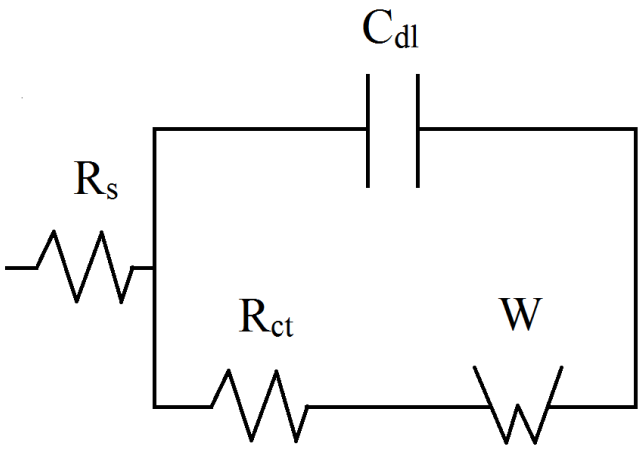

Figure 2.5 Equivalent circuit for the liquid bismuth cathode electrochemical cell, including bulk solution resistance R_s, capacitance of the double layer at the cathode surface C_{dl}, charge transfer resistance R_{ct}, and the Warburg diffusion related resistance W.

This circuit can be represented by the Voigt model for an electrode process, for which the impedance is expressed by the following equation [28],

$$Z(t) = R_s + \frac{1}{\frac{1}{R_{ct}} + \frac{1}{W} + j\omega C_{dl}} = R_s + \frac{R_{ct}}{1 + \frac{R_{ct}}{W} + j\omega R_{ct} C_{dl}} \tag{2.14}$$

To simplify the circuit, a constant phase element can be introduced which represents the Warburg impedance and the double layer capacitance. A constant phase element (CPE) is useful in fitting equivalent circuits because it can represent a resistor, inductor, capacitor, Warburg response, or a combination of these impedances. The impedance of a CPE can be expressed as [33],

$$Z_{CPE}(\omega) = \frac{1}{(j\omega)^{\alpha} Q} \tag{2.15}$$

where Q is the capacitance and α is an exponent that is less than or equal to one. Upon inspection of Eq. (2.14), the second term of the impedance relation is negligible at very high frequency whereas the second term approaches R_{ct} when the frequency is low. Figure 2.6 shows an ideal Nyquist plot for the Voigt model, where R_s and $R_s + R_{ct}$ are easy to find on the x-axis.

The charge transfer resistance is relevant to the redox reaction occurring at the cathode surface, and allows for calculation of the exchange current density according to the following equation [28],

$$R_{ct} = \frac{RT}{nFi_0} \tag{2.16}$$

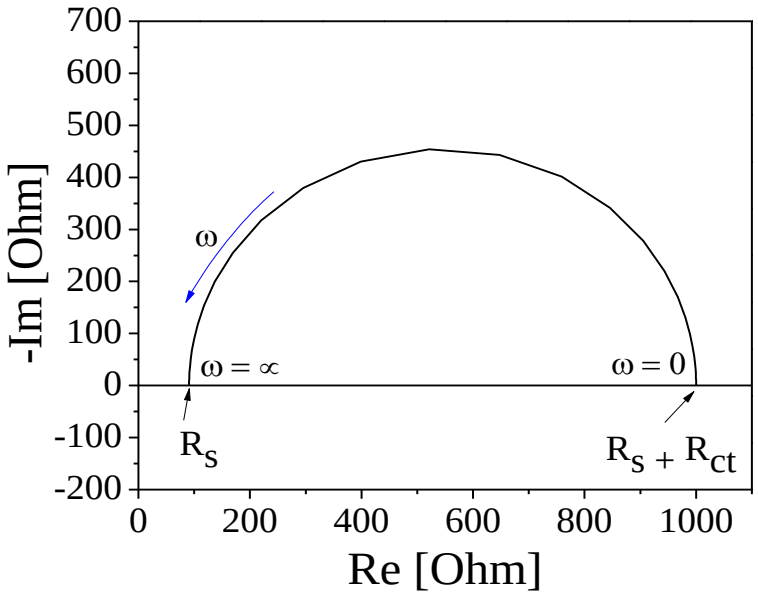

Figure 2.6 The ideal Nyquist plot for the Voigt model, showing how the solution resistance R_s and charge transfer resistance R_{ct} can be read and calculated from the x-axis intercepts [10].

2.2 Liquid Metal Electrodes

Few research studies have been conducted regarding the pyroprocessing application of liquid metal electrodes such as Cd, Bi, Zn, Al, Ga, Pb, and Sn for actinide, rare-earth, and alkali/alkaline-earth separations [34]–[36]. These separations can occur thermodynamically when the liquid metal is used as a solvent for reductive extraction or electrochemically when the liquid metal is used as a cathode [11], [25], [37]. Cd in particular has been widely studied since it has been successfully applied in the ER for recovery of Pu along with U and TRUs. This section will review the relevant studies of electrochemistry at Cd and Bi cathodes, including the similar techniques used in this project.

2.2.1 Liquid Cd Electrode Studies

The inclusion of a cadmium cathode introduces many complexities to the ER system. The primary goal is to reduce Pu ions into intermetallic compounds with Cd. Alongside these processes, U is also reduced making the product proliferation-resistant. However, the Cd also forms

intermetallic compounds and chemically reduces various other actinide, RE, and alkali/alkaline-earth fission products. Many thermodynamic studies have been done to understand the solubility, intermetallic compounds, activity coefficients, distribution coefficients, separation factors, and Gibbs free energies of formation for these systems [11], [25], [45], [29], [38]–[44]. Some of these studies are done by electromotive force measurements and sampling during electrodeposition while the concentrations of species in the salts are changed. Binary phase diagrams are also useful for understanding the intermetallics present in the Cd cathode and can be created from these measured emf values [37].

Another approach of liquid Cd cathode research is using electrochemical techniques to study reactions occurring at the Cd electrode surface to get information about the mass transfer and reaction kinetics, and thermodynamic data such as intermetallic compounds formed and enthalpies of formation for the systems [29], [30], [46]–[49], [34], [39]–[45]. These studies utilize many techniques, such as CV, chronopotentiometry (CP), OCP, and EIS. By comparing the diffusion coefficients and exchange current characteristics obtained from these previous studies, it is possible to obtain the rate-determining steps of the overall redox processes. Although the specific electrochemical property values and characteristics of the actinides, lanthanides, and fission products on the liquid Cd cathode will not be discussed here, it is important to note the body of work that has been performed for a Cd cathode since the techniques and approaches are similar and often useful to apply for studies of the Bi cathode.

2.2.2 Liquid Bi Electrode Studies

The liquid Bi cathode has similarly been studied with an aim of elucidating the electrochemical reactions taking place at the surface and understanding the thermodynamics, intermetallic compounds, and solubility of species from UNF. Few studies focused on the

separation of actinides, RE elements, and alkali/alkaline-earths by thermodynamic or electrochemical reduction techniques into the Bi. This idea is predicated on the idea that Bi could then be distilled from the cathode leaving behind the recovered material, similar to the cathode distillation already designed in this electrochemical process [13], [50].

Being that the most valuable materials within UNF are the actinides, many studies have investigated these elements for separation ability with a liquid Bi cathode. By a reductive extraction process, U, Np, Pu, and Am can be reduced into Bi comparably to Cd by addition of Li, as a reductant [25]. However, there is a significant amount of Li added to the system and also reduced into the liquid Bi during this process. Toda et al. have shown by calculation with thermodynamic parameters that U, Pu, and Am can be favorably separated into Bi compared to Ce [51]. Another way of reducing actinides into the liquid Bi instead of adding a reductant is by electrolysis. Studies of the electrochemical behavior of Th, U, Np, and Pu have shown the reduction of actinide ions into a liquid Bi phase or onto a Bi film electrode as various intermetallic species [23], [26], [30], [47], [48], [52], [53]. The small activities of actinides in a liquid Bi phase due to alloy formation lead to a positive shift of the reduction potential, so these studies have measured the redox potentials along with the diffusion coefficients of the actinide ions in the salt. These studies have shown reversible behavior using the CV technique.

RE elements have similarly been studied for electrochemical separations using liquid Bi in LiCl-KCl. Kurata et al. have shown that the distribution of trivalent REs compared to U is slightly better for Bi than for Cd in LiCl-KCl, reporting separation factors of 10^2–10^6 [25]. Cyclic voltammetry studies of La, Ce, Pr, and Tb have shown quasi-reversible behavior and similar positive potential shifts of RE redox reactions due to a lowered activity of RE in liquid Bi, owing to formation of intermetallic compounds [40], [49], [54]–[56]. For Ce, Castrillejo et al. showed

the formation of two intermetallic compounds, $CeBi_2$ and CeBi, by emf measurements and reported Gibbs energies of formation at 773 K for these compounds of -218.5 kJ/mol and -211.8 kJ/mol, respectively [55].

The separation of alkali/alkaline-earth species from LiCl-KCl via liquid Bi has not been studied as extensively as for actinides and REs. For reductive extraction, the favorable reduction of Sr and Ba versus U by addition of a reductant is lesser for Bi compared to Cd, but still very strong with a separation factor of 10^6–10^7 [25]. For reduction by electrolysis, Sr and Ba have been separated into a liquid Bi cathode in LiCl-KCl salts by constant current electrolysis with coulombic efficiencies of 63–67% [57]. There was significant deposition of Li into the liquid Bi pool, nevertheless the overall idea of alkali/alkaline-earth separation in LiCl-KCl salts was demonstrated. The electrochemical behaviors and separations of Sr^{2+}, Cs^{+} and Ba^{2+} on a graphite, liquid Bi, liquid Pb, or liquid Zn cathode have been studied in KCl, equimolar NaCl-KCl, or LiCl-$CaCl_2$-NaCl salts, reporting quasi-reversible redox reactions and diffusion coefficients [22], [34], [58]–[61]. The values reported for the diffusion coefficient are presented in Table 2.2. Since these studies have dealt with closely related but varied systems – focusing on the electrolyte and cathode composition – they can serve as a reference for this project as it fills in the gaps of fundamental knowledge of LiCl-KCl/Bi systems for alkali/alkaline-earth electrochemical separations.

Table 2.2 Reported diffusion coefficients from literature for alkaline-earth liquid metal studies.

Element	Electrolyte	Cathode	T (K)	D (x10^5 cm^2 s^{-1})	Method	Reference
Sr	KCl	Pb	1073	1.3 ± 0.3	CV conventional	[58]
				1.7 ± 0.2	CV semi-integral	
				1.6 ± 0.2	CV semi-differential	
				1.9 ± 0.7	CP	
				1.46 ± 0.18	CP	
	NaCl-KCl	Pb	1073	1.42	EIS	[61]
		Zn	1023	1.46 ± 0.18	CP	[62]
Ba	NaCl-KCl	Pb	1000	1.3 ± 0.2	CV conventional	[34]
				1.1 ± 0.3	CV semi-integral	
				1.2 ± 0.3	CV semi-differential	
				1.0 ± 0.2	CP	
				1.08 ± 0.16	CP	
		Zn	1023	1.08 ± 0.21	CP	[62]

2.3 Summary

Literature surveys have been performed to review the base of reported information regarding a liquid Bi cathode for a pyroprocessing technology. Most studies regarding the liquid Bi cathode have focused on their separation potential with actinides or RE elements. There is still a large gap of electrochemical and thermodynamic information not yet investigated regarding the alkali/alkaline-earth fission product species. The electrochemical techniques (OCP, CV, EIS) used in this project were reviewed and are derived from previous studies performed in LiCl-KCl salt with a liquid metal electrode. These techniques were then used to perform experiments and derive values for some of the electrochemical properties and missing information systematic parameters, such as redox reactions, diffusion coefficients, exchange current densities, and distribution behavior of the multivalent species in a LiCl-KCl/liquid Bi system.

Chapter 3 Experimental Design

The study of electrochemistry and molten salts requires special equipment and careful experimental designs to isolate the hygroscopic salts from the atmosphere. This chapter will review the equipment and experimental setup—including the glovebox system, ICP-MS, potentiostat, SEM-EDS, electrode materials and preparation, salt preparation, and sample preparations for ICP-MS and SEM-EDS analysis.

3.1 Electrochemistry Equipment

An inert argon glovebox from Innovative Technology has been installed in the Radiochemistry laboratory at the VCU College of Engineering East Hall room E4262 (see Figure 3.1). The O_2 and H_2O levels inside the glovebox were measured by the built in sensors installed in the glovebox circulation system and also occasionally checked and verified by a portable O_2 sensor from Advanced Instruments Inc. placed inside the glovebox (both shown in Figure 3.2). All sample preparations and electrochemical experiments were performed with O_2 and H_2O levels of less than 5 ppm. Periodically, the catalysts within the glovebox purifier system were regenerated with a 5% H in Ar mixture. Although all experimental runs in this study did not use radioactive materials, the glovebox contains radioactive materials. Therefore, all researchers working in this glovebox must complete the radiation safety training through the VCU Radiation Safety Section (RSS) and perform necessary monitoring while conducting research activities. This monitoring includes checking hands, arms, and material exiting the glovebox using the portable Geiger-Muller detectors as shown in Figure 3.3 and conducting weekly swipe tests of the gloves and ante chambers with a liquid scintillation counter (see Figure 3.4). This is in addition to the quarterly surveys of the entire lab space done by the RSS. To achieve and maintain the experimental temperatures of the molten salts, a Kerrlab melting furnace was used initially. Due to several

complications of the temperature controller in long continuous mode, a new Thermo Scientific benchtop muffle furnace was purchased and customized for these experiments shown alongside the Kerrlab furnace in Figure 3.5. Customization included inverting the installed heating element and drilling a hole through the top surface and insulation for electrode insertion into the middle cavity.

An Ohaus balance (see Figure 3.6) was used to measure all salts and other material contents inside the glovebox. Figure 3.7 displays a Biologic Science Instruments VSP-300 potentiostat/galvanostat used for all electrochemical measuremnets. Electrical connections were made from the potentionstat into the glovebox via an electrode connection port installed in the back wall of the glovebox. The provided software from Biologic Science Instruments EC-Lab V11.20 was used for electrochemical data collection and analysis.

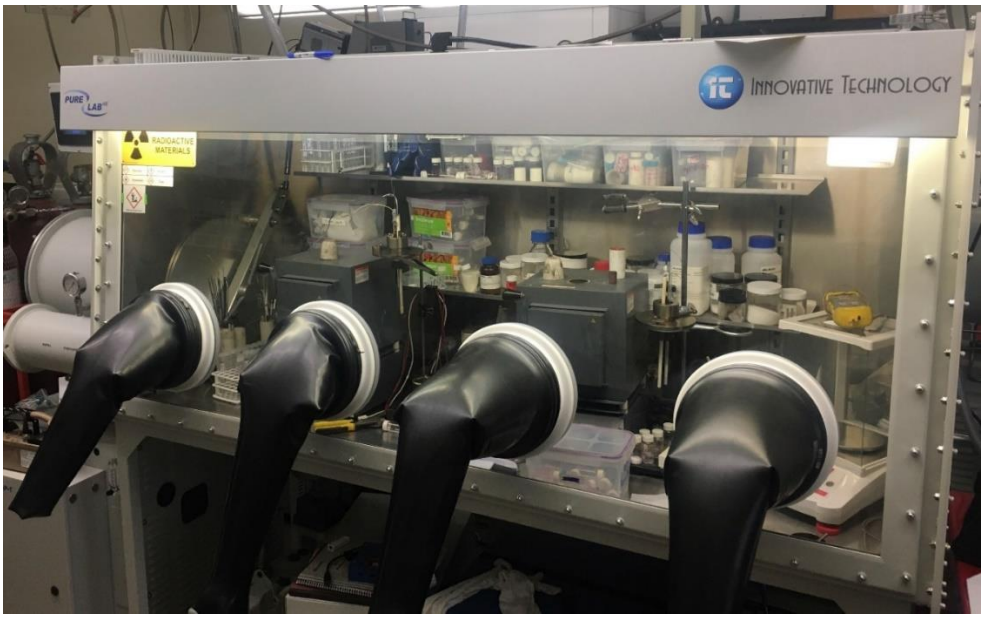

Figure 3.1 Inert argon atmosphere glovebox for molten salt experiments.

Figure 3.2 Glovebox control screen with O_2 and H_2O readings (left), and portable O_2 monitor inside glovebox (right).

Figure 3.3 Geiger-Muller counter for personnel and antechamber monitoring.

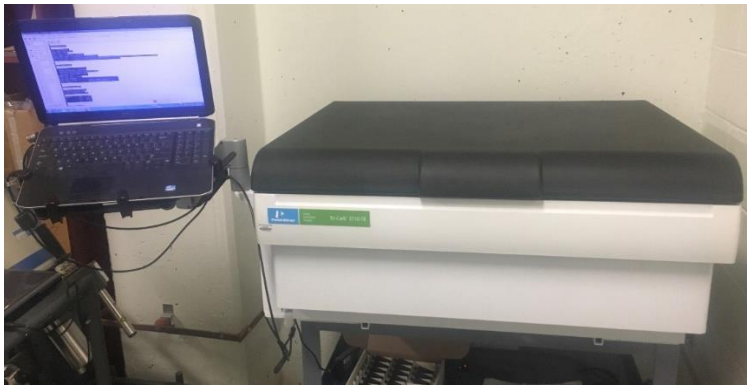

Figure 3.4 PerkinElmer Tri-Carb 3110 TR Liquid Scintillation Counter for radiation contamination monitoring.

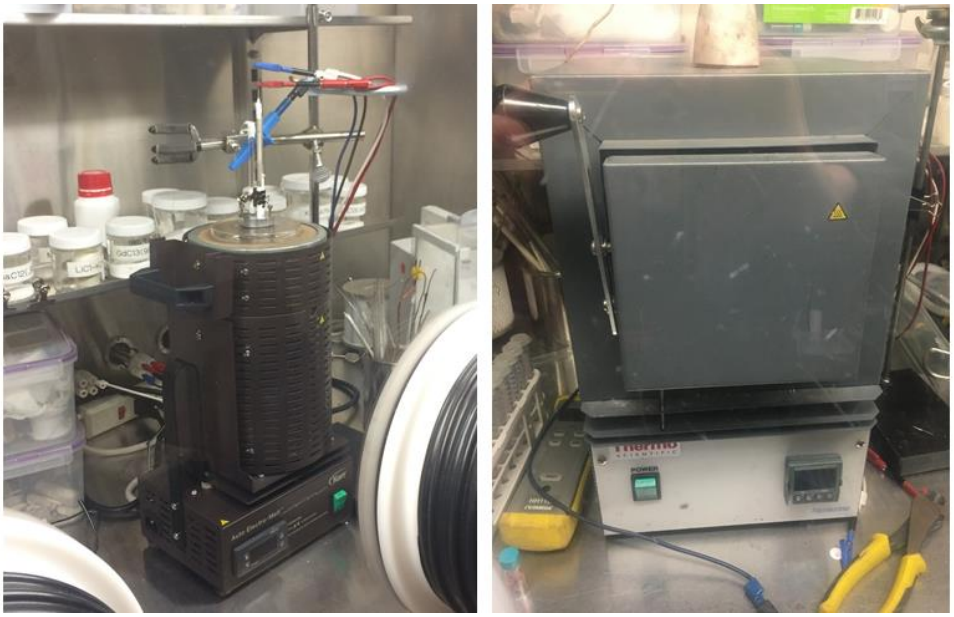

Figure 3.5 Furnaces used for electrochemistry experiments, Kerrlab Automelt (left) and Thermo Scientific Benchtop Muffle Furnace (right).

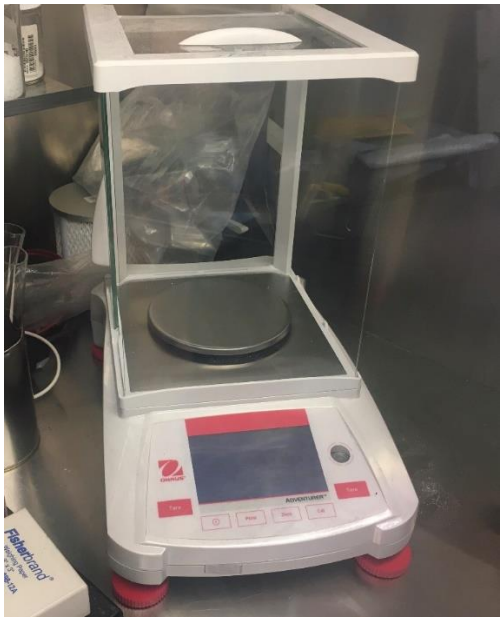

Figure 3.6 Ohaus balance inside glovebox for weight measurements of salts and bismuth.

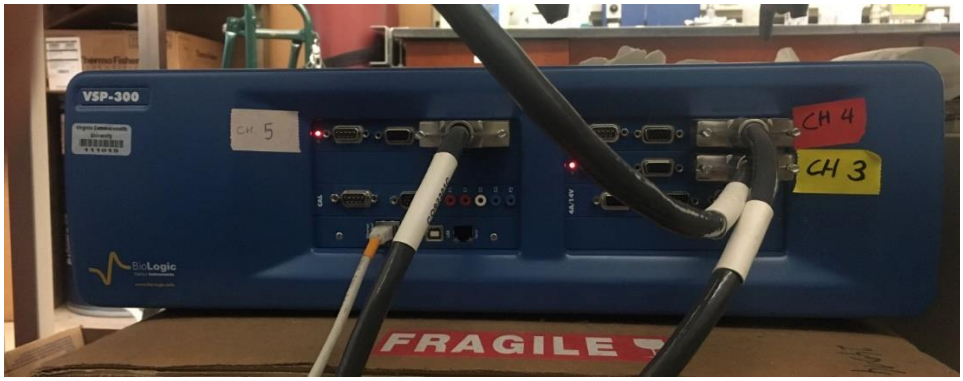

Figure 3.7 Biologic Science Instruments VSP-300 Potentiostat/Galvanostat.

3.2 Experimental Preparation

3.2.1 Crucibles and Reagents

Anhydrous bead type lithium chloride (LiCl, 99.995%), potassium chloride (KCl, 99.95%), silver chloride (AgCl, 99.997%), strontium chloride ($SrCl_2$, 99.995%), cesium chloride ($CsCl_2$, 99.99%), barium chloride ($BaCl_2$, 99.998%), and cerium chloride ($CeCl_3$, 99.9%) were purchased from Alfa Aesar. Salts were prepared and packaged under argon so they were used in the experiments as purchased. Alumina crucibles (Al_2O_3, 99.8%) of size 40 mL and 180 mL were purchased from Coorstek. Prior to experimentation and outside the glovebox, the crucibles were sonicated in 2% HNO_3 acid with ultrapure water and dried in a benchtop oven at 473K for 2 hours. They were then taken into the glovebox. The LiCl-KCl eutectic was prepared by weighing and mixing the beads in a quartz tube with a 58.2:41.8 mol% composition. These salts were then loaded into a 40mL Al_2O_3 crucible and this crucible was then placed into a larger 180 mL Al_2O_3 crucible, which served as a safety crucible in case of spillage or breakage from the 40 mL cruicble. The crucibles were then loaded into the furnace and heated at 573 K for 5 hours minimum in order to further dry out and outgas the salts and crucibles. After this drying process, the salts were raised to the beginning experimental temperature, typically 723K, and allowed to melt and equilibrate

for a minimum 2 hours before electrodes or other salts were added. When electrodes or an addition of salt contents was lowered in the eutectic melt, a minimum of 2 hours was allowed for dissolution or otherwise equilibration of the system before electrochemical experiments were performed. In some cases, at least a 24 hour period was allowed for dissolution and for the system to reach equilibrium. A summary of the experimental reagents and crucibles and their data is provided in Table 3.1.

Table 3.1 Summary of experimental materials.

Material	Form	Purity	Manufacturer
LiCl	Anhydrous beads	99.995%	Alfa Aesar
KCl	Anhydrous beads	99.95%	Alfa Aesar
AgCl	Anhydrous beads	99.997%	Alfa Aesar
$SrCl_2$	Anhydrous beads	99.995%	Alfa Aesar
CsCl	Anhydrous beads	99.99%	Alfa Aesar
$BaCl_2$	Anhydrous beads	99.998%	Alfa Aesar
$CeCl_3$	Anhydrous beads	99.9%	Alfa Aesar
Al_2O_3 crucibles	40 mL	99.8%	Coorstek
“	180 mL	“	“

3.2.2 Bismuth Cathode

Two different types of a liquid Bi cathode were studied, a pool-type and a cup-type. Bismuth needles (99.99%) were purchased from Alfa Aesar. They were packaged in open atmosphere and had visible oxidation on the outside surface. Therefore, to remove oxidation and obtain a pure Bi metal, the Bi needles were melted in the furnace inside the glovebox in a 40 mL alumina crucible at 673 K. A pyrex tube with inner diameter 2 mm was dipped into the Bi metal below the oxidation and a connected syringe used to draw Bi metal up into the tube. This recovered

a pure Bi metal with no visible oxidation. The pyrex tube was then broken open and the new Bi needles recovered for use in experiments.

For the cup-type cathode, a custom made pyrex electrode from a local glass shop, Research Glass, was used and is shown in Figure 3.8. The shaft was 7 mm and open to the attached bottom. A 0.5 mm Mo wire was threaded through the tube and into the bottom cup before addition of approximately 5 g of Bi needles to the cup. The addition of this cathode to the overall electrode assembly and the salts will be discussed in section 3.2.4.

For the pool-type cathode, Bi needles were added to a 40 mL crucible before addition of the salts and melted at 773 K for 1 hour in the glovebox furnace. After visual confirmation of the liquid Bi phase, the system was cooled to room temperature and the LiCl-KCl were added. In one study performed, a 10 mol% Ba in Bi cathode was made. This was done by adding Ba metal (99.9%) acquired from Alfa Aesar to purified Bi needles and melting at 798 K in the 40 mL crucible. The liquidus point for 10 mol% Ba in Bi is approximately 645 K [63]. Needles of this Ba-Bi alloy were then extracted via a 2 mm inner diameter pyrex tube and syringe in a process similar to the pure Bi needle preparation. Then ,the Ba-Bi needles were loaded into a 40 mL crucible and prepared as a pool-type cathode in the same method as for pure Bi. For both the Ba-Bi and the Bi pool-type cathodes, a tungsten rod of diameter 1.5 mm (99.95%) purchased from Alfa Aesar was sheathed with an alumina tube and used to make contact with the liquid metal pool.

Figure 3.8 Cup-type cathode with Bi and Mo wire connection.

The surface area of the Bi cathode was measured after each experimental run. The pyrex cup was broken open and the Bi cathode extracted. Minimal adhesion of the salt to the Bi allowed for a clean extraction. The Bi cathode post-experiments is shown in Figure 3.9.

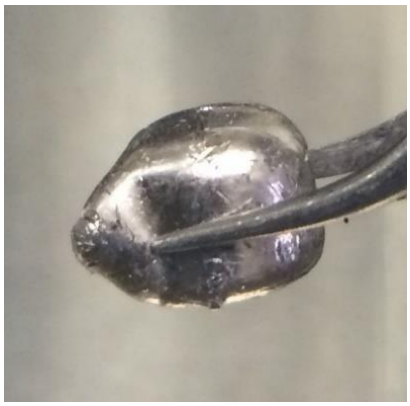

Figure 3.9 Bi cathode post-experiments.

The surface area of the top Bi surface was calculated by using the formula for surface area of an oblate spheroid and multiplying by half to get the surface area of the half spheroid [64],

$$S = \pi a^2 \left(1 + \frac{(\frac{c}{a})^2}{2\sqrt{1-\frac{c^2}{a^2}}} \ln\left(\frac{1+\sqrt{1-\frac{c^2}{a^2}}}{1-\sqrt{1-\frac{c^2}{a^2}}} \right) \right) \quad (3.1)$$

where the parameters a and c are the diameter and height of the half-spheroid, respectively, as shown in Figure 3.10.

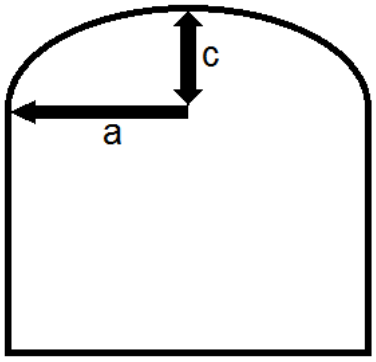

Figure 3.10 Diagram of measurements for calculation of surface area of Bi cathode.

3.2.3 Reference Electrode

All experiments were performed using a Ag/AgCl reference electrode shown in Figure 3.11. The housing of the electrode was custom made by Research Glass and consisted of a 7 mm outer diameter pyrex tube open on one end and on the other closed with a thin wall less than 0.5 mm in thickness. The thin surface allows ionic conduction between the bulk electrolyte and reference electrolyte. The reference electrolyte consisted of 5 mol% AgCl in LiCl-KCl and was prepared by the following steps:

1. Prepare LiCl-KCl eutectic bead mixture in a clean 40 mL crucible.
2. Add the correct amount of AgCl for a 5 mol% composition.
3. Place crucible into glovebox furnace and melt at 773 K for no less than 3 hours.

4. Dip a 2 mm inner diameter pyrex tube into the salts and use a syringe to draw the salt into the tube.
5. Remove the pyrex tube and allow salt to freeze at room temperature.
6. Use a clean 1 mm tungsten rod to push out the salt rod from the tube, or otherwise carefully break open the pyrex tube and recover the salt rods.

For each experiment, approximately 0.5 g of prepared 5 mol% AgCl-LiCl-KCl eutectic was added to a new reference electrode pyrex tube. A 1 mm Ag wire (99.99%) purchased from Alfa Aesar was inserted into the tube with the bottom end submerged in the salts approximately 5 mm from the thin bottom surface and the top end protruding out of the top allowing connection to the potentiostat.

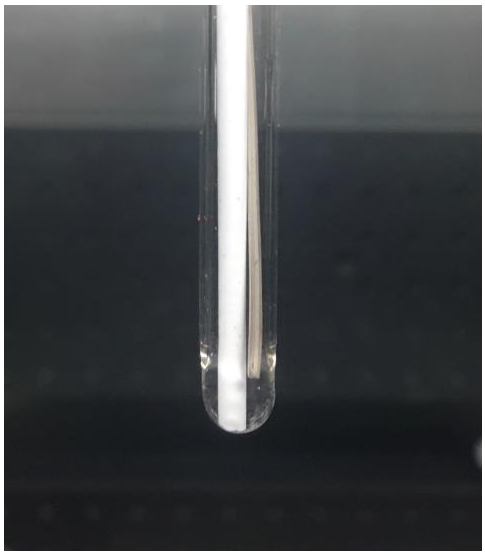

Figure 3.11 Ag/AgCl reference electrode.

3.2.4 Electrode Assembly

All experiments were conducted with a three–electrode setup and a thermocouple submerged in the LiCl-KCl salt. This setup is similar to a study by Yoon et al. and is depicted in Figure 3.12 [44]. The Bi cup-type or pool-type cathode was used as a working electrode. The

counter electrode in all experiments consisted of a 3 mm diameter glassy carbon rod purchased from HTW. This counter electrode was housed in an alumina sheath to insulate it from the steel electrode assembly. A K-type thermocouple probe was purchased from Omega Instruments and housed in an 8 mm outer diameter alumina sheath (99.8%) from Coorstek that was in contact with the salt. These electrodes and thermocouple sheath were held in place by a steel electrode assembly at the top of the furnace. This assembly was custom designed and is shown in Figure 3.13.

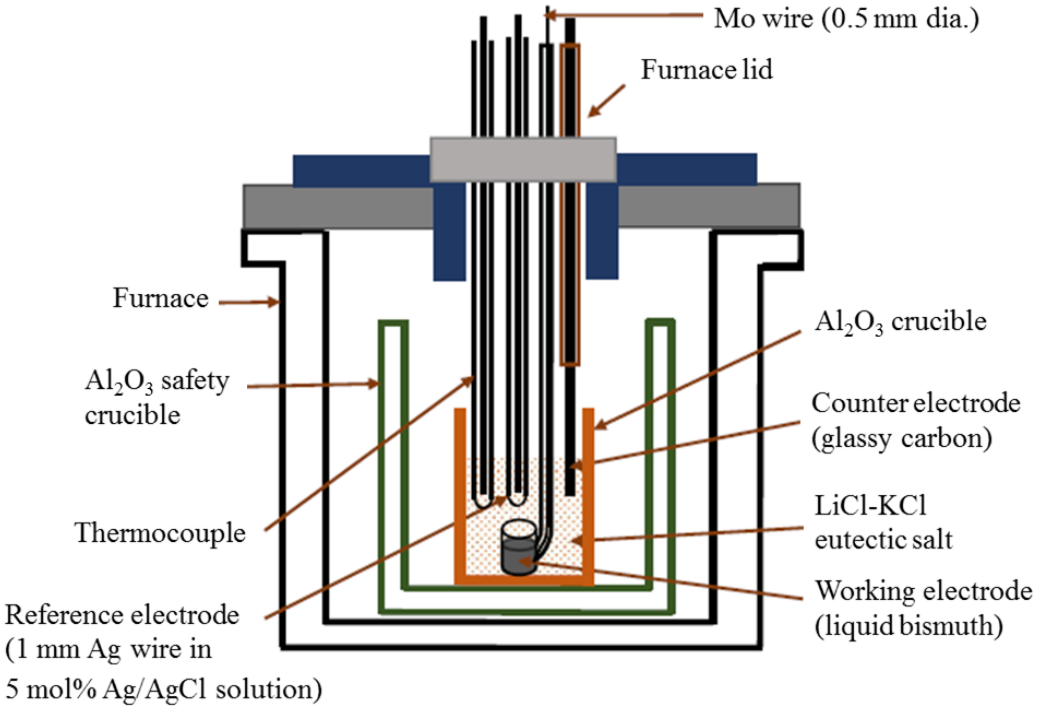

Figure 3.12 Diagram of electrode assembly and furnace.

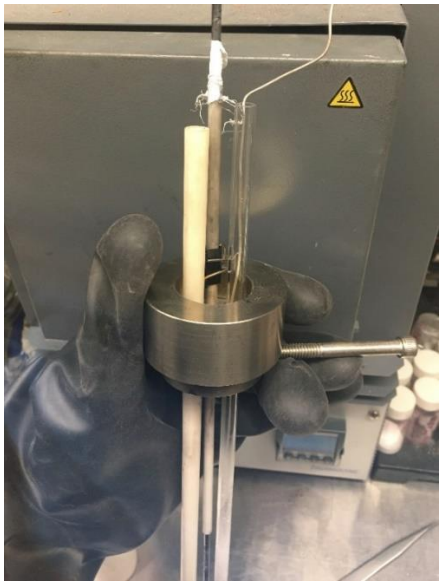

Figure 3.13 Electrode assembly to hold three electrodes and thermocouple sheath.

3.3 Inductively Coupled Plasma Mass Spectrometry (ICP-MS)

Many of the electrochemical experiments performed aimed to measure the properties of salt species at varying concentrations. In order to verify salt species concentrations, salt samples withdrawn during experiments were analyzed by an Agilent Scientific Instruments 7900 ICP-MS (see Figure 3.14). This section will explain the salt sample withdrawal and preparation for ICP-MS analysis.

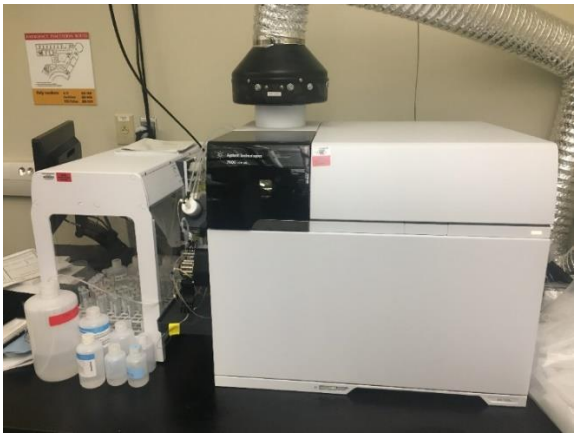

Figure 3.14 Agilent Scientific Instruments 7900 ICP-MS for salt composition analysis.

3.3.1 Sample Preparation

To prepare salt samples for ICP-MS analysis and avoid unnecessary exposure of the samples to the atmosphere, the following procedure was adhered to:

1. Take new 15 mL centrifuge tubes into the glovebox.
2. Measure the weight of the salt sample using the Ohaus balance using the average of three measurements.
3. Load each salt sample into a centrifuge tube and close the lid.
4. Take the loaded centrifuge tubes out of the glovebox.
5. Open the lid and quickly fill the tubes with 10 mL of 2% HNO_3 (prepared with ultrapure water) using an Eppendorf pipette.
6. Close the lid, agitate tube slightly, and wait one day for full dissolution.
7. In new centrifuge tubes, created diluted samples from the stock sample with a dilution factor of 1000 to obtain a sample within the optimal detection range for ICP-MS.
8. Prepare standard samples using multi-element blends CCS1 and CCS4 from Inorganic Ventures with dilution factors of 0.5, 1, 5, 10, 50, 100, 300, 500, and 1000.
9. Run the ICP-MS with the diluted salt samples and calculate concentrations using the known dilution factor.

3.4 Scanning Electron Microscopy with Energy Dispersive Spectrometry (SEM-EDS)

To characterize the bismuth cathodes after electrochemical experiments, a Phenom ProX Desktop SEM-EDS was utilized, shown in Figure 3.15. This desktop system is capable of giving visual information via SEM and elemental identification via EDS regarding deposition and location of intermetallic species within the bismuth cathode samples. This section will review the sample preparation and analysis used for bismuth cathode cross sections in the SEM-EDS.

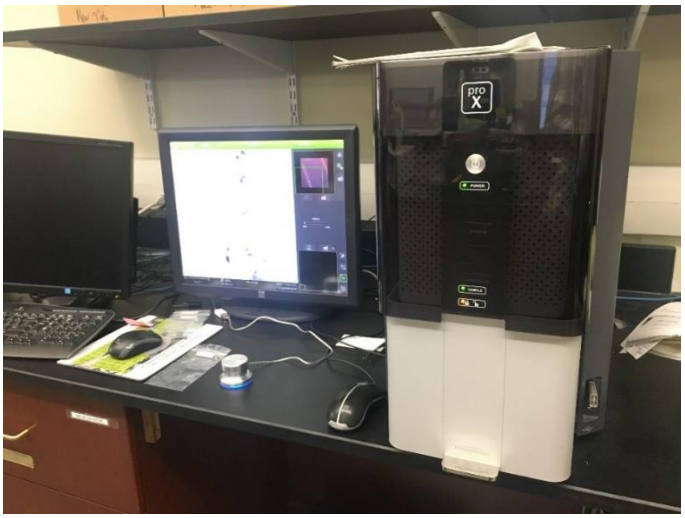

Figure 3.15 Phenom ProX SEM-EDS for bismuth cathode characterization.

3.4.1 Sample Preparation

After electrochemical experiments and recovery of the bismuth cathode, the cathode was prepared for SEM-EDS analysis by the following procedure:

1. Create a vertical central cross section of the cathode by sawing the cathode down the middle from the top with a coping saw with cleaned metal blade
2. Polish the cross section face using 2000 grit sandpaper and ultrapure water
3. Clean surface with ultrapure water and dry
4. Place carbon tape on SEM puck
5. Place bismuth cathode with sample surface up and parallel to the puck surface as shown in Figure 3.16.
6. Place puck into SEM-EDS mount and place into Phenom system.

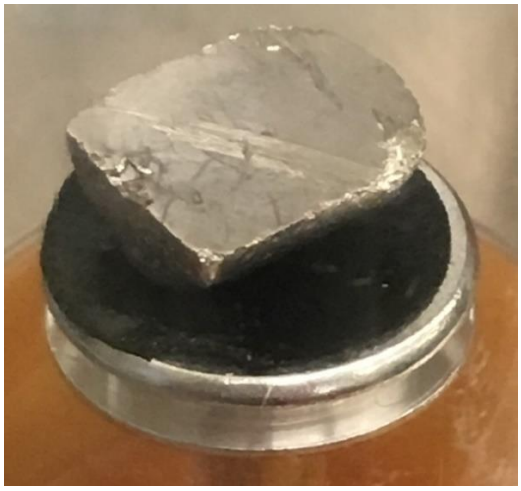

Figure 3.16 Bismuth cathode prepared for SEM-EDS analysis.

Here, it is important to note that the pool-type cathode used in EIS experiments was prepared slightly differently from the cup-type cathode. Due to the size and shape of the pool-type cathode, the cross section was created by breaking the disk-shaped cathode in half, and then cutting a sliver from the middle of the resulting half-disk. This allowed for the radial sliver of the disk to be set upon the SEM sample platform and faced upward for analysis.

3.4.2 Analysis

For SEM-EDS characterization of the cathode cross section, the cathode is first visually scanned by the SEM user for visible heterogeneity in the sample, indicating the presence of multiple phases of material. These are usually apparent as darker and lighter patches within the cross section. When these patches are discovered, the SEM user selects these as target spots for EDS analysis. The Phenom ProX uses 15 kV x-rays to probe the target spot for a period of 90 seconds while it collects spectroscopic information. The software then returns results to the user as a plot of spectral counts and calculated elemental compositions as atomic and weight

percentages. Here, it is important to note that the software allows the user to deselect elements for inclusion in the elemental composition analysis of the spectra. This allows for a better fit of spectral peaks with knowledge of the system being studied. With this in mind, all elements that were included in the spectral elemental composition analysis but known with certainty to not be present in the system (e.g. Mg, Ca, Mn, etc.) were deselected. The deselection allows the elemental composition analysis software to refit the spectral lines and report a more accurate elemental composition analysis.

3.5 Experimental Program

The different elemental species and techniques were chosen for each experimental run. Table 3.2 shows a summary of the experimental program. Only one element was studied in each experimental run. Likewise, CV and EIS experiments were always performed in separate experimental runs.

Table 3.2 Summary of experiments performed and their design.

Experiment	Element	Cathode	Electrochemical Methods	
			CV	EIS
Chapter 4.1	Cs	Bi Cup	X	
	Cs	Bi Pool		X
Chapter 4.2	Sr	Bi Cup	X	
Chapter 4.3	Ba	Bi Cup	X	
		Ba-Bi Pool		X
Chapter 4.4	Ce	Bi cup	X	

3.6 Summary

The experimental materials, apparatus, and preparation procedures were described and explained in this chapter. The inert argon gloveboxes, furnaces, and potentiostat used in the electrochemical experiments were explained. The reagents and their preparations were then covered. This included all salts and crucibles used in the studies and their drying and experimental preparation. The purification of the Bi and assembly of the cup-type and pool-type Bi cathode was covered. The 5 mol% reference electrode and its construction were also explained. The three-electrode setup with thermocouple that was used in experiments was then reviewed. Finally, the sample preparations and analysis for both the ICP-MS salt composition verifications and the cathode characterization by SEM-EDS were discussed, along with the experimental program which was followed for electrochemical experiments.

Chapter 4 Results and Discussion

Electrochemical behaviors of the alkali/alkaline-earth species (Cs, Sr, and Ba) and a lanthanide (Ce) were investigated by CV and EIS techniques. These experiments gave data for evaluation leading to an understanding of the redox reactions for these species, including values for the diffusion coefficient, charge transfer resistance and exchange current density for monovalent, divalent, and trivalent species. These values allow insight into dominating reaction mechanisms and the rates of reactions.

4.1 Studies with Cesium (Cs)

The presence of Cs-137 contributes significantly to the radioactivity of the ER salt. It is possible that the activity of Cs in Bi is small enough comparatively to Li and K to allow the preferred deposition of Cs. Few studies have been performed to evaluate the electrochemical properties of the Cs^+/Cs redox couple on a liquid Bi electrode in LiCl-KCl eutectic salt. Therefore, this project has evaluated some of the electrochemical properties by CV and EIS techniques. Peak currents from the CV studies were used to calculate values for the diffusion coefficient of CeCl in the salt. The exchange current density of Cs^+/Cs at the liquid Bi cathode was also determined at varying temperatures using an EIS technique. The calculated values for exchange current density were quite large compared to the diffusion coefficient and other systems, indicating that the controlling mechanism of the reaction is likely diffusion of Cs^+ ions from the bulk salt to the cathode surface layer.

4.1.1 CV Measurements

CV was performed for Cs systems on a cup-type Bi cathode with the experimental parameters of concentration, temperature and CV scan rates shown in Table 4.1. After performing CV of the pure LiCl-KCl system, an experimental potential window of 0.3 to -1.5 V versus

Ag/AgCl reference electrode was chosen for repeatable voltammograms. It is important to produce repeatable CV data in order to study only the reactions of interest and negate other unwanted influences such as surface area growth of the cathode.

Table 4.1 Experimental parameters for CV experiments of CsCl.

Temperature (K)	723, 748, 773, 798, 823
CsCl Concentration (wt% in LiCl-KCl)	0.5, 1.0, 1.5, 2.0, 3.0, 4.0
Electrical Potential Range (V)	0.3 to -1.55
Scan rate (mV s^{-1})	50, 100, 150, 200
Bi Cathode Surface Area (cm^2)	0.743

Pure LiCl-KCl cyclic voltammograms were obtained at each temperature and scan rate before additions of CsCl. This allowed for a subtraction method to be applied to obtain voltammograms relating only to the reactions of the Cs^+ ions. An example of these voltammograms and subtraction method in shown in Figure 4.1

Subtraction voltammograms representative of the CsCl-LiCl-KCl system on a liquid Bi cathode are shown in Figure 4.2. At the positive end, the reduction occurring at -0.13 V is attributable to free Bi in the system. This behavior was seen during all CV experiments with the liquid Bi cathode. The final rise occurring at the positive end of the anodic scan corresponds to the anodic dissolution of Bi from the cathode. Likewise, the strong reduction occurring at the negative end of the cathodic scan is attributable to the reduction of a Li-Bi alloy in the system, as many other researchers have likewise discovered [53]–[55]. The two redox reactions of interest attributable to the presence of Cs occur with (I) reduction at -1.1 V and oxidation at -0.15 V, and (II) reduction at -1.24 V and oxidation at -0.32 V. The peak potentials moved slightly in the negative direction with increasing scan rate. Thus, the reaction might be quasi-reversible. After all

experiments, the Bi cathode was extracted and the surface area of the working Bi surface was calculated to be 0.743 cm^2 according to Eq. (3.1).

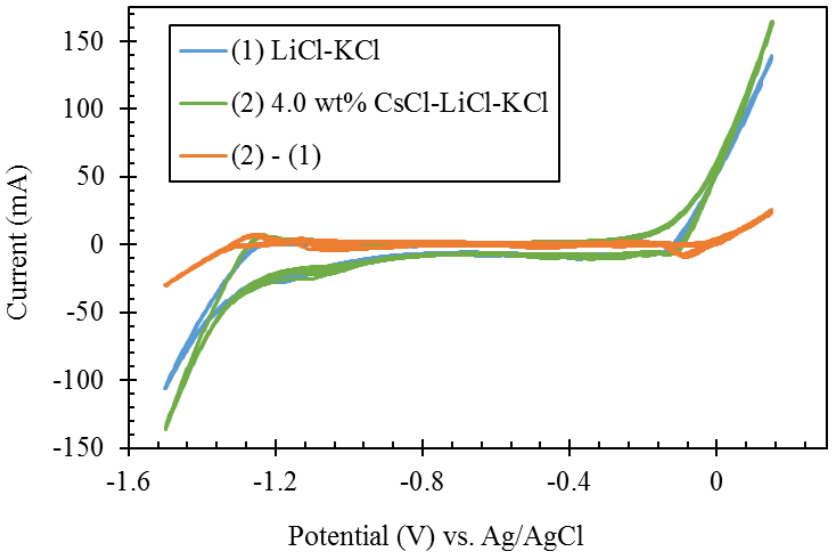

Figure 4.1 Cyclic voltammogram of pure LiCl-KCl, 4 wt% CsCl-LiCl-KCl, and subtraction at 773 K and scan rate 100 mV s^{-1}.

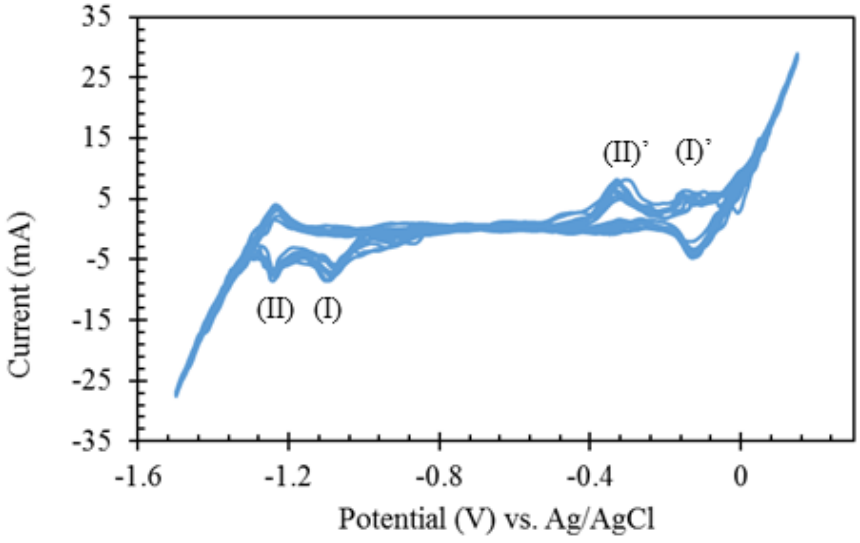

Figure 4.2 Subtraction cyclic voltammograms for the 0.5 wt% CsCl-LiCl-KCl system at 823K and scan rate 100 mV s^{-1}.

The first peak was investigated to determine the diffusion of this species according to Eq. (2.6). These calculated values are displayed in Table 1.1 and shown with respect to inverse temperature in Figure 4.3. An Arrhenius temperature relationship is apparent and activation energy and pre-exponential factor D_0 were calculated according to Eq. (2.7) for peak (I), for which sufficient data was available. These calculated values of the activation energy of diffusion are shown in Table 4.3 and exhibit a large increase with increasing concentration of CsCl in the salt.

Table 4.2 Diffusion coefficients of Cs reduction peak (I) from CV with scan rate 100 mV s^{-1}.

	D ($\times 10^5$ cm^2 s^{-1})				
CsCl concentration	**0.5 wt%**	**1.0 wt%**	**1.5 wt%**	**2.0 wt%**	**3.0 wt%**
723 K	0.498	0.203	0.0359	-	-
748 K	0.857	0.385	0.0615	-	-
773 K	0.945	0.255	0.0679	0.0506	-
798 K	0.759	0.195	0.0832	0.0543	0.0181
823 K	0.867	0.410	0.103	0.0898	0.0176

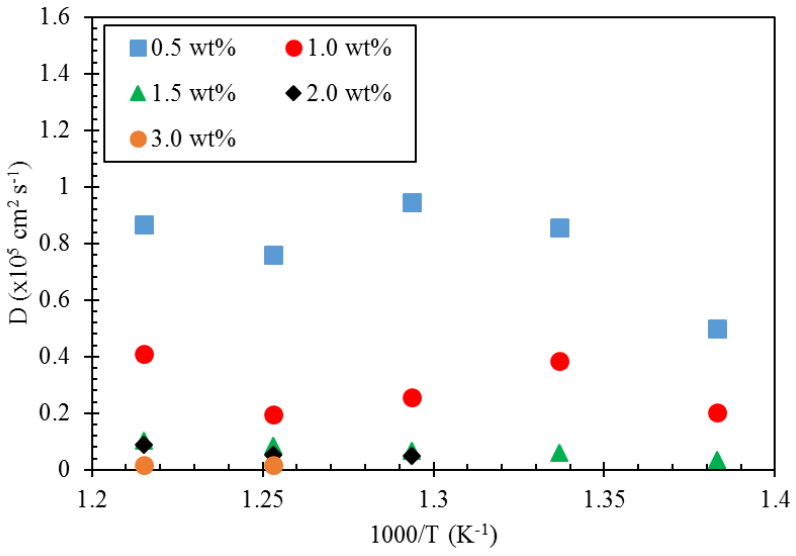

Figure 4.3 Diffusion coefficients of Cs reduction peak (I) from CV with scan rate 100 mV s^{-1}.

Table 4.3 Calculated activation energy of diffusion for CsCl from peak (I) of CV studies.

CsCl Concentration (wt%)	E_a (kJ mol^{-1})	D_0 ($\times 10^5$ cm^2 s^{-1})
0.5	20.3	18
1.0	14.2	2.5
1.5	48.1	120
2.0	60.1	544

The second redox peak (II) was analyzed in a similar fashion to redox peak (I). Calculated diffusion coefficients for the redox species at this peak from the reduction peaks are displayed in Table 4.4 and shown graphically with respect to inverse temperature in Figure 4.4. For both redox peaks (I) and (II), the diffusion coefficient of the active ionic species decreased considerably with increasing concentration.

Table 4.4 Diffusion coefficients of Cs reduction peak (II) from CV with scan rate 100 mV s^{-1}.

	D ($\times 10^5$ cm^2 s^{-1})				
CsCl concentration	**0.5 wt%**	**1.0 wt%**	**1.5 wt%**	**2.0 wt%**	**3.0 wt%**
723 K	1.551	0.546	0.203	0.101	0.027
748 K	0.702	0.326	0.326	0.049	-
773 K	-	0.389	-	0.052	-
798 K	-	0.301	-	-	-
823 K	1.189	0.371	-	-	-

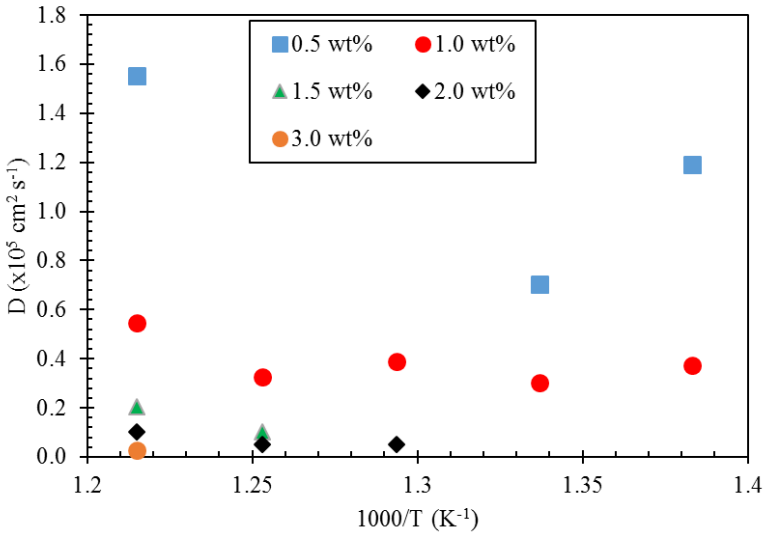

Figure 4.4 Diffusion coefficients of Cs reduction peak (II) from CV with scan rate 100 mV s^{-1}.

4.1.2 EIS Experimental Runs

EIS experiments were selected and conducted for a CsCl-LiCl-KCl system on a Bi pool-type electrode to allow calculation of the exchange current density i_0 of the Cs^+/Cs redox couple on the Bi interface. Table 4.5 provides a list of specific parameters of the experimental runs. After all experiments, the Bi cathode was cooled, extracted, and the surface area calculated to be 5.26 cm^2.

Table 4.5 Experimental parameters for EIS experiments of CsCl.

Temperature (K)	723, 748, 773
CsCl Concentration (wt% in LiCl-KCl)	0.5
Potential amplitude (mV)	10
Frequency Range	50 kHz – 10 mHz
Bi Cathode Surface Area (cm^2)	5.26 cm^2

Figure 4.5 shows impedance spectra for the 0.5 wt% CsCl-LiCl-KCl system at 773 K where the applied potential was increased beyond the equilibrium potential by steps of 1 mV. EIS is ideally performed at the equilibrium potential for calculation of the exchange current density (i_0).

However, as shown in Figure 4.5, the impedance increases dramatically at high frequencies; at low frequencies, there is no ion transfer occurring between the Bi and Cs ions. Therefore, small overpotentials were applied to the system to initiate Cs^+ reduction at the Bi cathode. It can be seen in Figure 4.5 that when the applied overpotential is increased to 2 mV, a diffusion related resistance starts to occur at the low frequencies. This indicates that there is electron transfer at the cathode surface and that the diffusion of Cs^+ ions from the bulk salt to the electrode surface is occurring. Overpotentials were found by this procedure at each experimental temperature and these Nyquist plots were used to fit to an equivalent circuit for calculation of the charge transfer resistance R_{ct}.

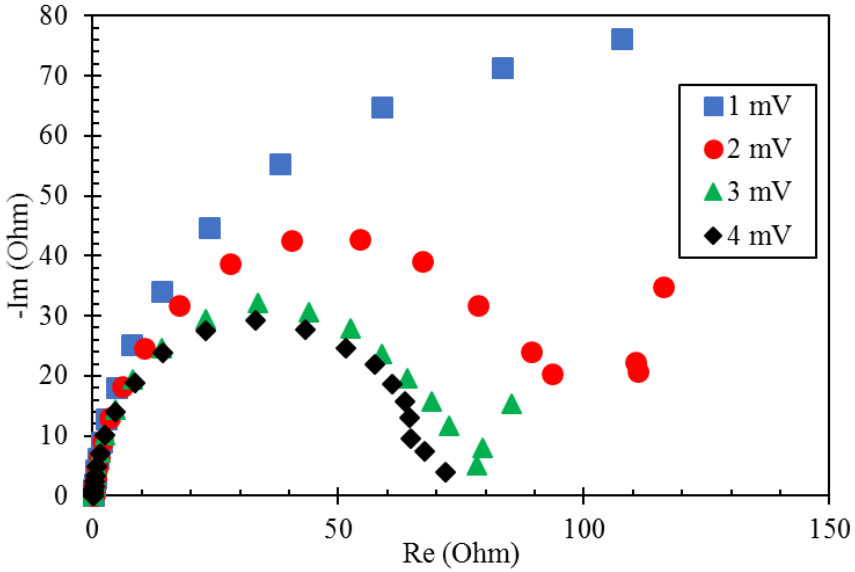

Figure 4.5 Nyquist plot for 0.5 wt% CsCl-LiCl-KCl system at 773 K on a pool-type Bi cathode.

The equivalent circuit chosen is based on the diagram of Figure 2.5 (see detailed explanation in Section 2.1.4). The impedance spectra were first automatically fitted by the Z-fit software from Biologic Scientific Instruments. Then, the fit was manually adjusted by changing the values of some of the equivalent circuit components. This was performed to minimize the relative error to a value below 0.10. The curve was then used to provide a value for the product of

R_{ct} and the surface area of the cathode in the system. From these values, i_0 on the Bi cathode was tabulated. Table 4.6 gives the values of R_{ct}*S and i_o collected from the fits of the impedance spectra for the CsCl containing system. Figure 4.6 displays i_0 values for the Cs^+/Cs reaction versus inverse temperature showing a linear relationship.

When these values for exchange current density and diffusion coefficient are compared with each other and to other similar systems, it can be seen that the exchange current mechanism is much less likely to be the rate-controlling step in deposition than the mass transport of Cs^+ ions from the bulk salt to the cathode surface layer.

Table 4.6 Applied overpotential (η), measured charge transfer resistance (R_{ct}) times electrode surface area (S), and exchange current density (i_0) values at different temperatures for 0.5 wt% CsCl system.

T (K)	η (mV)	R_{ct}*S (Ω cm^2)	i_0 (A cm^{-2})
723	2	0.828	0.0752
748	2	0.739	0.0843
773	2	0.684	0.0911

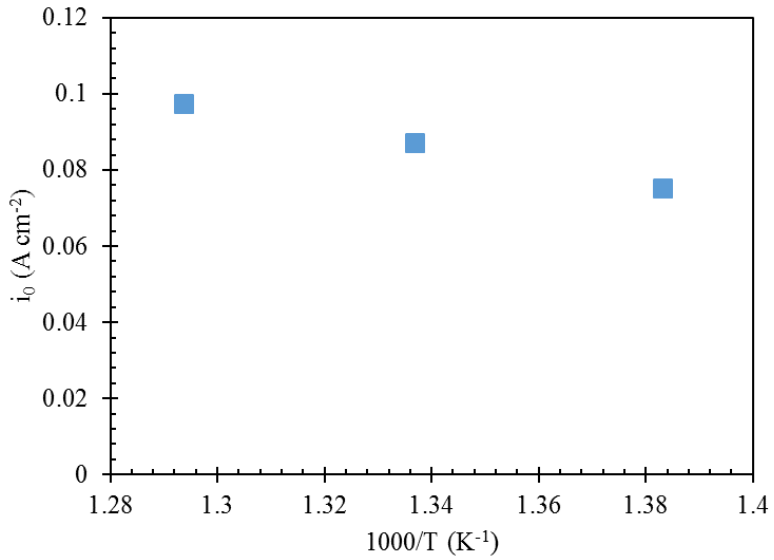

Figure 4.6 Plot of exchange current density versus inverse temperature for the 0.5 wt% CsCl-LiCl-KCl system on a pool-type Bi cathode.

4.1.3 SEM-EDS Experimental Runs

After CV and EIS studies of CsCl-LiCl-KCl systems, the Bi cathodes used were prepared and analyzed by SEM-EDS according to the procedure described in Section 3.3. Analysis of both cathodes yielded no evidence of Cs-Bi intermetallics present. Figure 4.7 shows an SEM picture of the cathode cross section analyzed from the Bi cathode for CV experiments. The target spots are labelled and Figure 4.8 shows the EDS elemental composition analysis of target spot 1, which suggests 100% Bi present. Likewise, Figure 4.9 shows an SEM picture of the cathode cross section analyzed from the Bi cathode for EIS experiments with target spots labelled. Figure 4.10 shows the EDS analysis of the target spot indicating 90.02% Bi composition. Here, the measurement of carbon could be considered as an error; thus, the EDS analysis can be considered to show 100% Bi present in the cathode from EIS studies. These SEM-EDS results merely suggest that Cs does not become an alloy thermodynamically in the CsCl-LiCl-KCl/liquid Bi system.

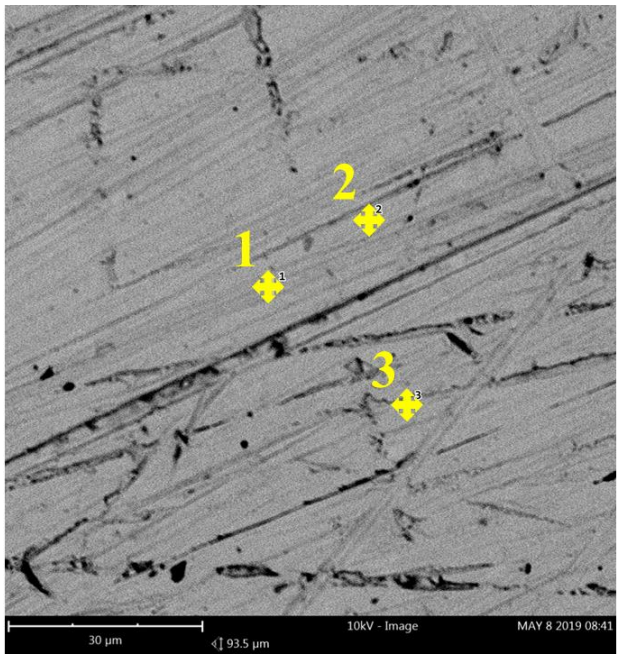

Figure 4.7 SEM picture of Bi cathode used in CV studies of CsCl.

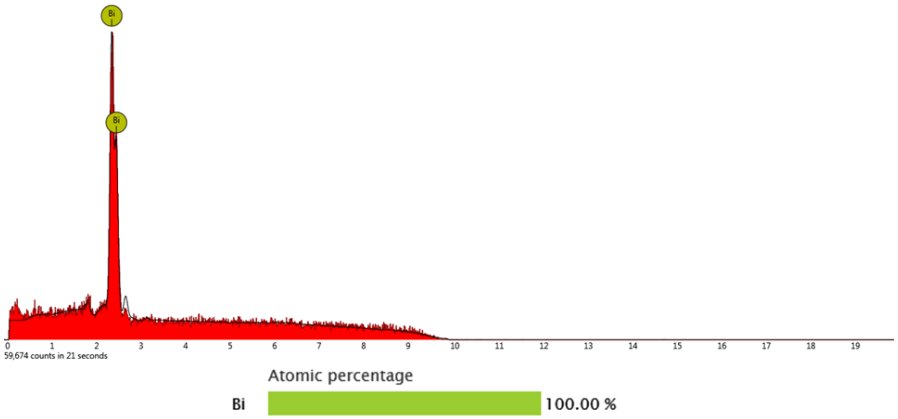

Figure 4.8 SEM-EDS analysis of Bi cathode used in CV studies of CsCl.

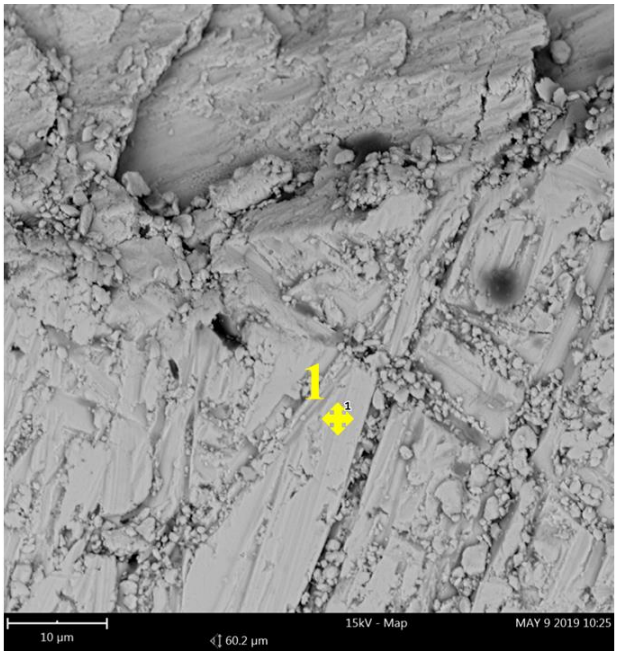

Figure 4.9 SEM picture of Bi cathode used in EIS studies of CsCl.

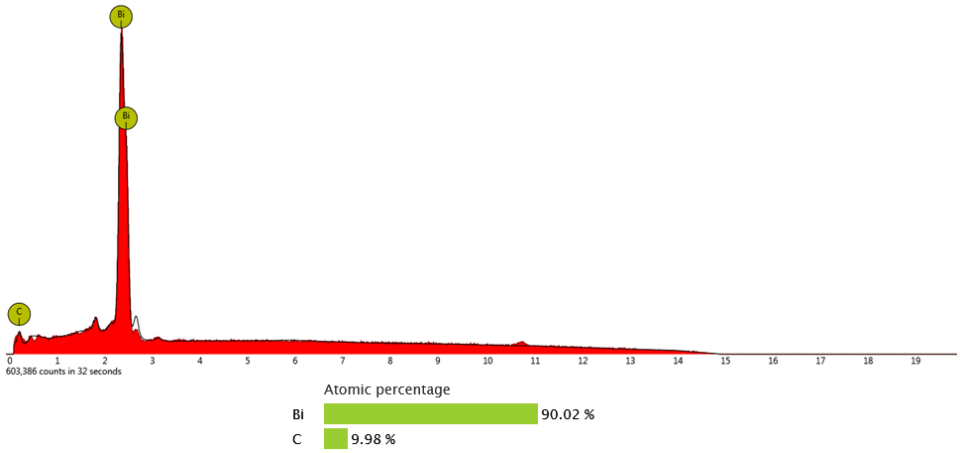

Figure 4.10 SEM-EDS analysis of Bi cathode used in EIS experiments of CsCl.

4.2 Studies with Strontium (Sr)

Sr-90 is another element found within the ER salt that contributes largely to the overall radioactivity of the salt. The selective removal of Sr from the salt would make shielding and handling easier during electrorefining, and also allow for a longer reuse of the ER salt. The electrochemical deposition of Sr into a Bi cathode in LiCl-KCl has been studied, but the fundamental electrochemical properties such as diffusion coefficient and exchange current characteristics on a liquid Bi cathode are lacking from the available literature [57]. Therefore, the $SrCl_2$-LiCl-KCl/liquid Bi system has been studied in this project via CV and EIS techniques to elucidate the electrochemical behavior of the Sr^{2+}/Sr redox couple on the liquid Bi cathode and provide experimental values for some of the electrochemical properties not yet reported in literature.

4.2.1 CV Measurements

The $SrCl_2$-LiCl-KCl system was studied with CV techniques on a cup-type liquid Bi cathode at varying temperatures of 723–823 K and varying SrCl concentrations of 0.5–4.0 wt% $SrCl_2$ in LiCl-KCl eutectic composition. Table 4.7 shows specific parameters of the CV studies of the $SrCl_2$-LiCl-KCl/liquid Bi system. After initial testing, a potential range of 0.22 to -1.55 V was

shown to produce repeatable CV curves. After all CV experiments, the Bi cathode was extracted and the surface area calculated to be 0.750 cm^2 according to Eq. (3.1).

Table 4.7 Experimental parameters for CV experiments of $SrCl_2$.

Temperature (K)	723, 748, 773, 798, 823
$SrCl_2$ Concentration (wt% in LiCl-KCl)	0.5, 1.0, 1.5, 2.0, 3.0, 4.0
Electrical Potential Range (V)	0.22 to -1.55
Scan rate (mV s^{-1})	25, 50, 75, 100, 150, 200
Bi Cathode Surface Area (cm^2)	0.750

Figure 4.11 shows cyclic voltammograms obtained for the $SrCl_2$-LiCl-KCl system on a liquid Bi cathode at 748 K and varying concentrations of $SrCl_2$ with a scan rate of 25 mV s^{-1}. After subtraction of the background current (see Figure 4.12), the presence of $SrCl_2$ is shown to cause a large variation in the reduction of Li at the negative end of the potential range. At 773 K, the Li reduction for the system which contains $SrCl_2$ occurs with approximately equivalent current-potential characteristics as the pure LiCl-KCl system. However, the presence of $SrCl_2$ seems to decrease the effect of temperature on the Li reduction. In the pure LiCl-KCl system, the current peaks at the end of the potential sweep (E = -1.55 V) vary by about 50 mA for each 25 K temperature difference. However, in the 2 wt% $SrCl_2$-LiCl-KCl system, there is no apparent variation of the reduction current-potential relationship with respect to temperature.

Although Lichtenstein and coworkers have report their successful deposition of Sr into a Bi cathode by cathodic discharge [57], the redox reaction of Sr^+/Sr and its intermetallic with Bi or Li were not observed in the current study. Based on the calculation from thermodynamic properties, the reduction potentials of Sr and Li are only -0.007 V apart for 5 mol% Sr in Bi (see Table 2.1).

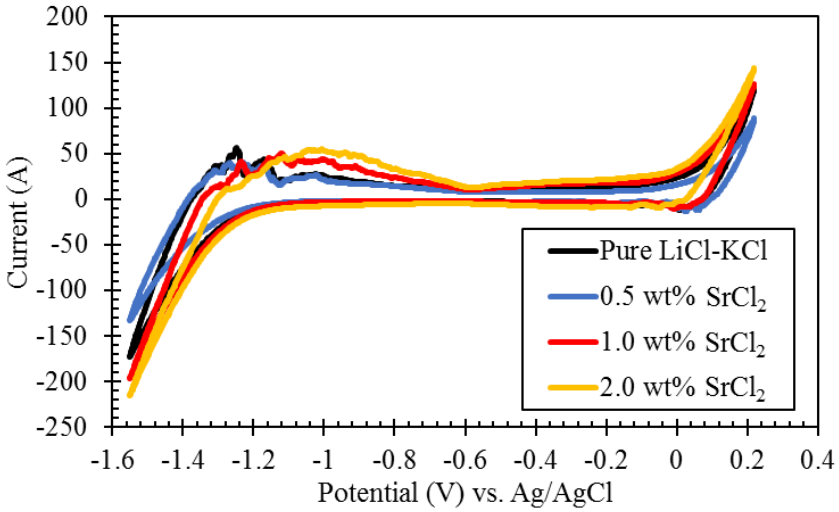

Figure 4.11 Cyclic voltammograms of $SrCl_2$-LiCl-KCl/ liquid Bi system at varying $SrCl_2$ concentrations and 748 K with scan rate of 25 mV s^{-1}.

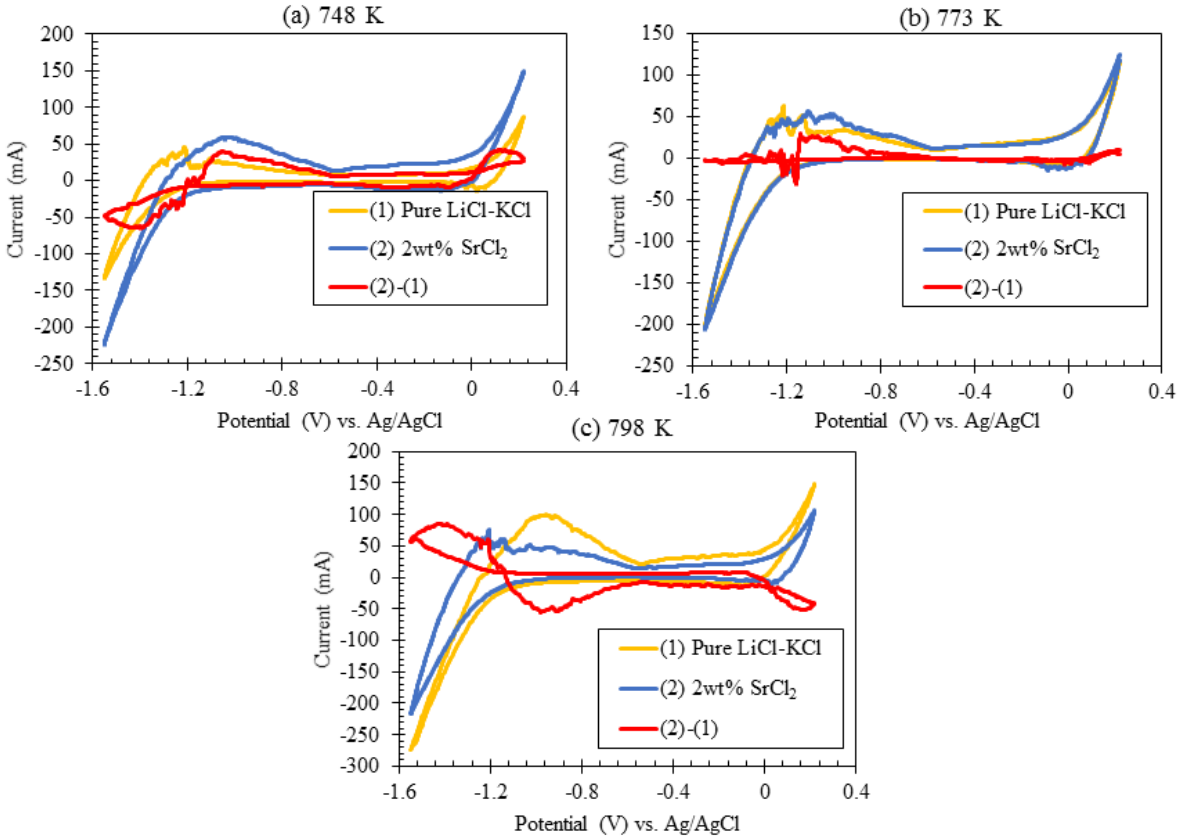

Figure 4.12 Cyclic voltammograms and background LiCl-KCl subtraction curve for 2 wt% $SrCl_2$-LiCl-KCl system at a scan rate of 25 mV s^{-1} and temperature of (a) 748 K, (b) 773 K, and (c) 798 K.

4.2.2 SEM-EDS Experimental Runs

After CV experiments, the Bi cathode was extracted and prepared for SEM-EDS analysis. Multiple image shots were taken with EDS analysis in order to confirm or otherwise discommend the presence of Sr-Bi intermetallics in the cathode. Figure 4.13 shows an image from the SEM analysis of the cathode cross section with target shots for EDS analysis labelled. Visual inspection of the cathode cross section yielded no visible phases of Sr-Bi intermetallics, which was confirmed by EDS analysis of the labelled target shots. Figure 4.14 shows the EDS results of target shot 1, indicating only the presence of Bi and the absence of Sr-Bi intermetallics. Although Lichtenstein and coworkers have discovered Sr-Bi intermetallics in a Bi cathode subjected to cathodic discharge in a $SrCl_2$-LiCl-KCl system, in our current study, we found no Sr-Bi intermetallics present by SEM-EDS analysis. Since the current study was performed with CV analysis, where any reduced Sr species are oxidized from the cathode on the cathodic sweep, Sr-Bi intermetallics should not be expected to be found in the Bi cathode unless they distribute favorably by thermodynamics. The results of the current study, finding no Sr-Bi intermetallics present in the Bi cathode, agree with a study by Kurata and coworkers, which found Sr to not distribute thermodynamically into a liquid Bi pool from LiCl-KCl [25].

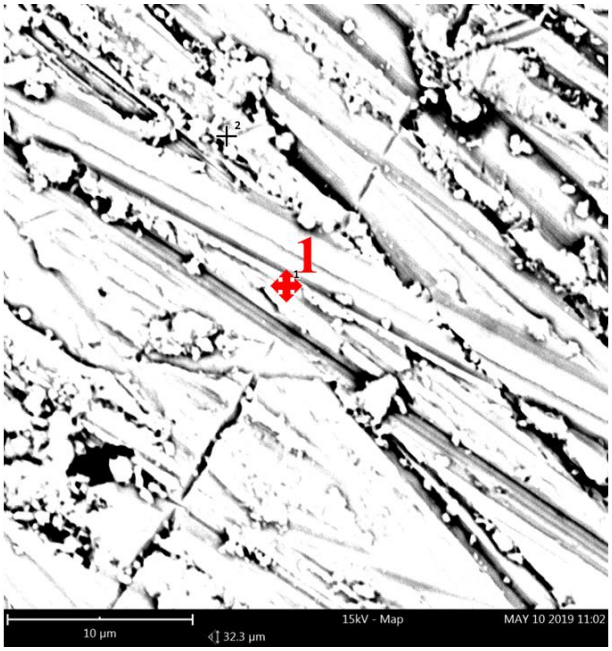

Figure 4.13 SEM picture of Bi cathode used in CV studies of $SrCl_2$.

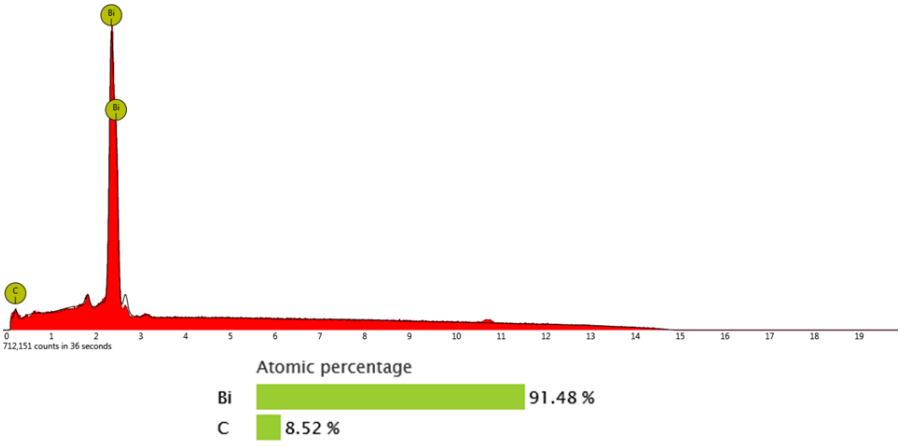

Figure 4.14 SEM-EDS analysis of Bi cathode used in CV studies of $SrCl_2$.

4.3 Studies with Barium (Ba)

The ER salt contains the alkaline-earth species Ba, which is created either as a fission product while the nuclear fuel is being burned up in the reactor or is in the UNF as the resulting decay product of Cs-137. In any case, the concentration of Ba in the ER salt will increase as more batch cycles of the ER are being performed and its presence will degrade the efficiency of the ER

in removing the actinides and REs. The removal of Ba from the ER salt will benefit the useful lifetime of the salt before it needs to be replaced. The removal of Ba alongside Sr from LiCl-KCl salt via a Bi cathode has been proven by Lichtenstein and co-workers [57]. However, the fundamental electrochemical properties of the Ba^{2+}/Ba redox couple on a liquid Bi cathode in LiCl-KCl eutectic salt has not been studied. The understanding of this electrochemical behavior and some of the relevant properties are necessary for studying the implementation of a liquid Bi cathode in the ER. Therefore, this work has focused on the electrochemical behavior of the $BaCl_2$-LiCl-KCl/liquid Bi system via CV and EIS techniques to give insight into the mass transport and exchange current behavior of Ba species in the salt and at the Bi cathode surface. From the CV experiments, the diffusion coefficient of $BaCl_2$ in the LiCl-KCl salt has been calculated from the current peaks of the voltammograms. The exchange current density has been calculated by both a CV technique and by and EIS technique. These values have been compared to give an assessment of i_0 measurement techniques and to describe the Ba^{2+}/Ba redox couple at the liquid Bi cathode.

4.3.1 CV Measurements

CV experiments were performed for the $BaCl_2$-LiCl-KCl/liquid Bi system for varying concentrations of $BaCl_2$ from 0.78 wt% to 4.0 wt% $BaCl_2$ in LiCl-KCl eutectic and at temperatures from 723 K to 823 K. After testing, the CV curves from the system were found to be repeatable with a potential sweep range of 0.3 to -1.5 V. After all experiments, the liquid Bi cathode was extracted, measured, and the surface area calculated to be 0.776 cm^2 according to Eq (3.1). Table 4.8 provides the summary of experimental parameters for $BaCl_2$.

Table 4.8 Experimental parameters for CV experiments of $BaCl_2$.

Temperature (K)	723, 748, 773, 798, 823
$BaCl_2$ Concentration (wt% in LiCl-KCl)	0.5, 1.0, 1.5, 2.0, 2.5, 3.0, 3.5, 4.0
Electrical Potential Range (V)	0.3 to -1.5
Scan rate (mV s^{-1})	50, 100, 150, 200
Bi Cathode Surface Area (cm^2)	0.776

Representative CV curves of the $BaCl_2$-LiCl-KCl/liquid Bi system for 1 wt% $BaCl_2$ at a scan rate of 150 mV s^{-1} and varying temperatures are shown in Figure 4.15. A redox reaction is observed at the negative potential end of the scan. This redox reaction shifts more negatively and positively in potential with increasing temperature for reduction and oxidation peaks, respectively. This indicates the somewhat reversible redox reaction of a Ba-Bi intermetallic species.

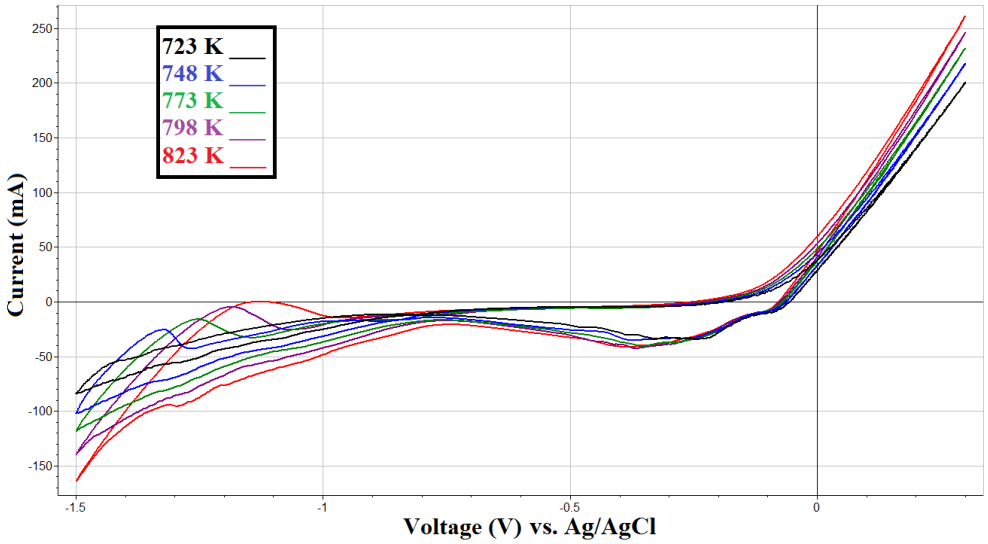

Figure 4.15 Cyclic voltammograms before subtraction of the background LiCl-KCl current for a 1 wt% $BaCl_2$-LiCl-KCl system with scan rate 150 mV s^{-1}.

Figure 4.16 shows the CV curves after subtraction of the background current. A redox reaction is seen with a reduction peak at approximately -1.40 V and an oxidation peak at roughly -1.27 V. Another noticeable aspect is the significant amount of variation in the current at neutral potentials. This has not been seen as much for LiCl-KCl/liquid Bi systems containing actinides or lanthanides [30], [47], [54], [55]. Here, for the $BaCl_2$ system, the only CV studies with repeatable CV curves came from the systems containing 1 wt% or 2 wt% $BaCl_2$. From the curves with prominent redox peaks in these systems, the anodic peaks of the redox reaction were measured. These current peaks, when plotted versus the square root of the scan rate, obey a linear relationship, as shown in Figure 4.17 for the 1 wt% $BaCl_2$ system, indicating a reaction controlled by diffusion.

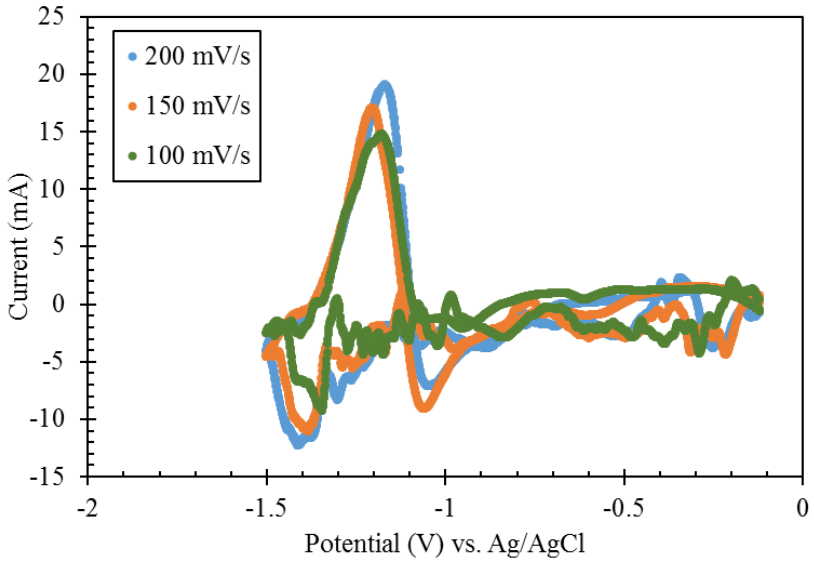

Figure 4.16 Subtracted CV curves for 1 wt% $BaCl_2$ system at 798 K.

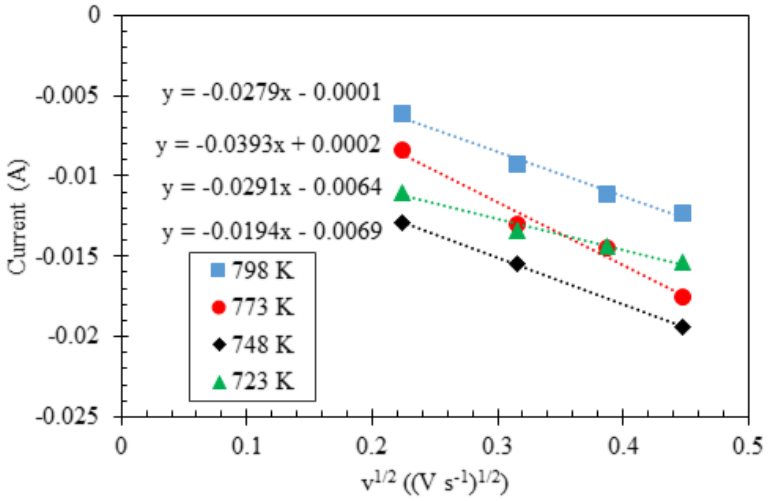

Figure 4.17 Anodic peak currents plotted versus the square root of the scan rate for the 1 wt% $BaCl_2$-LiCl-KCl/liquid Bi system.

From the slope of these plots, the diffusion coefficient of $BaCl_2$ was calculated by the Berzins-Delahay relationship for a soluble-insoluble reversible reaction (Eq. (2.6)), shown plotted versus inverse temperature in Figure 4.18. These diffusion coefficients were only calculated for systems which produced at least three reproducible peak currents for each scan rate. The calculated diffusion coefficients ranged from 0.0129×10^{-5} cm^2 s^{-1} to 0.0993×10^{-5} cm^2 s^{-1}, which is quite small when compared to other species in LiCl-KCl salt.

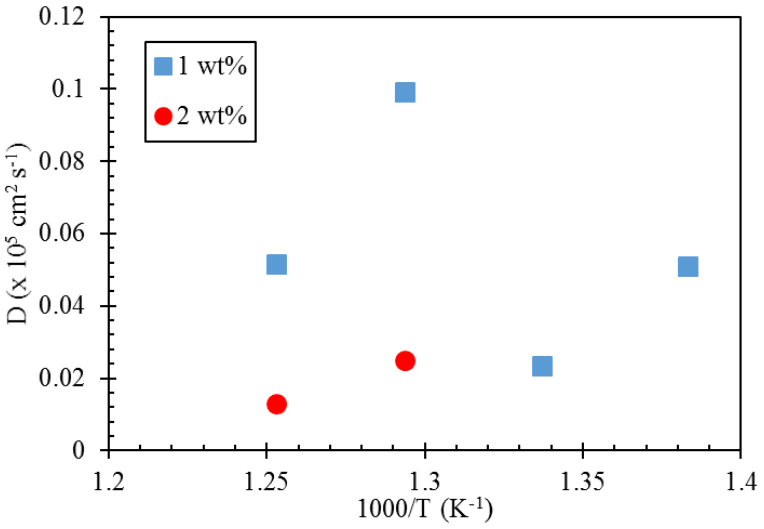

Figure 4.18 Plots of the diffusion coefficient of $BaCl_2$ in LiCl-KCl versus inverse temperature.

The CV curves were also used to give a calculation of the exchange current density of the Ba^{2+}/Ba redox couple at the liquid Bi surface. The slope of the CV curve at the small zero-current region on the cathodic sweep of the potential was measured, as shown in Figure 4.19. The simplified Butler-Volmer equation for very small overpotential regions (Eq. (2.9)) was then used to calculate values of the exchange current density from these slopes. Table 4.9 provides the i_0 values calculated for the 1 wt% $BaCl_2$-LiCl-KCl system at a scan rate of 50 mV s^{-1}.

Table 4.9 Calculated i_0 values for the 1 wt% $BaCl_2$-LiCl-KCl system from a CV technique.

T (K)	i_0 (A cm^{-2})
748	0.00264 ± 0.00015
773	0.00308 ± 0.00052
798	0.00307 ± 0.00018

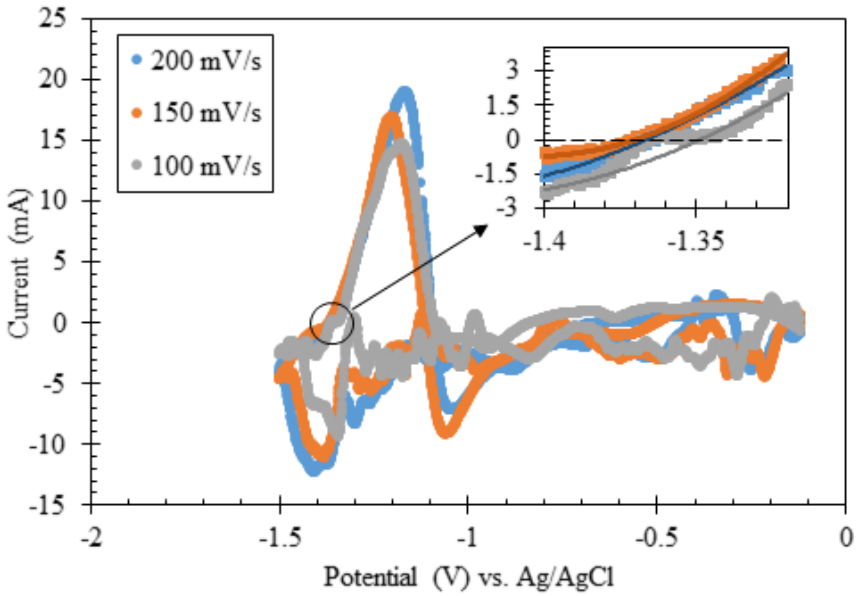

Figure 4.19 CV curves of 1 wt% $BaCl_2$-LiCl-KCl system at 798 K with inset showing the small zero-current overpotential region at the Bi cathode (S = 0.776 cm^2).

4.3.2 EIS Experimental Runs

To provide another measurement of the exchange current density of the Ba^{2+}/Ba redox couple at the Bi cathode, EIS techniques were performed on the $BaCl_2$-LiCl-KCl system at temperatures from 723–823 K and concentrations of 0.78, 1.5, and 3.0 wt% $BaCl_2$. A pool-type Bi cathode containing 10 mol% Ba was used for EIS experiments (refer to Section 3.2.2. for cathode preparation). The increase in the working area of the Bi cathode via pool-type cathode was chosen for a better EIS measurement. Additionally, the 10 mol% Ba in Bi cathode was prepared to create a more equilibrated Ba^{2+}/Ba concentration at the cathode surface layer.

Table 4.10 Experimental parameters for EIS experiments of $BaCl_2$.

Temperature (K)	723, 748, 773, 798, 823
$BaCl_2$ Concentration (wt% in LiCl-KCl)	0.78, 1.5, 3.0
Potential amplitude (mV)	10
Frequency Range	50 kHz – 50 mHz
Bi Cathode Surface Area (cm^2)	8.40 cm^2

Overpotentials of 2–10 mV were applied to the system during EIS measurements to initiate the Ba^{2+}/Ba reaction at the cathode surface. The Nyquist plots of the measured impedance spectra were fitted to an equivalent circuit using the Biologic Scientific Instruments Z-fit software. First, the software produced an autofit. Then, the values of the components in the equivalent circuit were manually adjusted to produce a fit with error below 0.10. Figure 4.20 shows the measured and fitted impedance spectra.

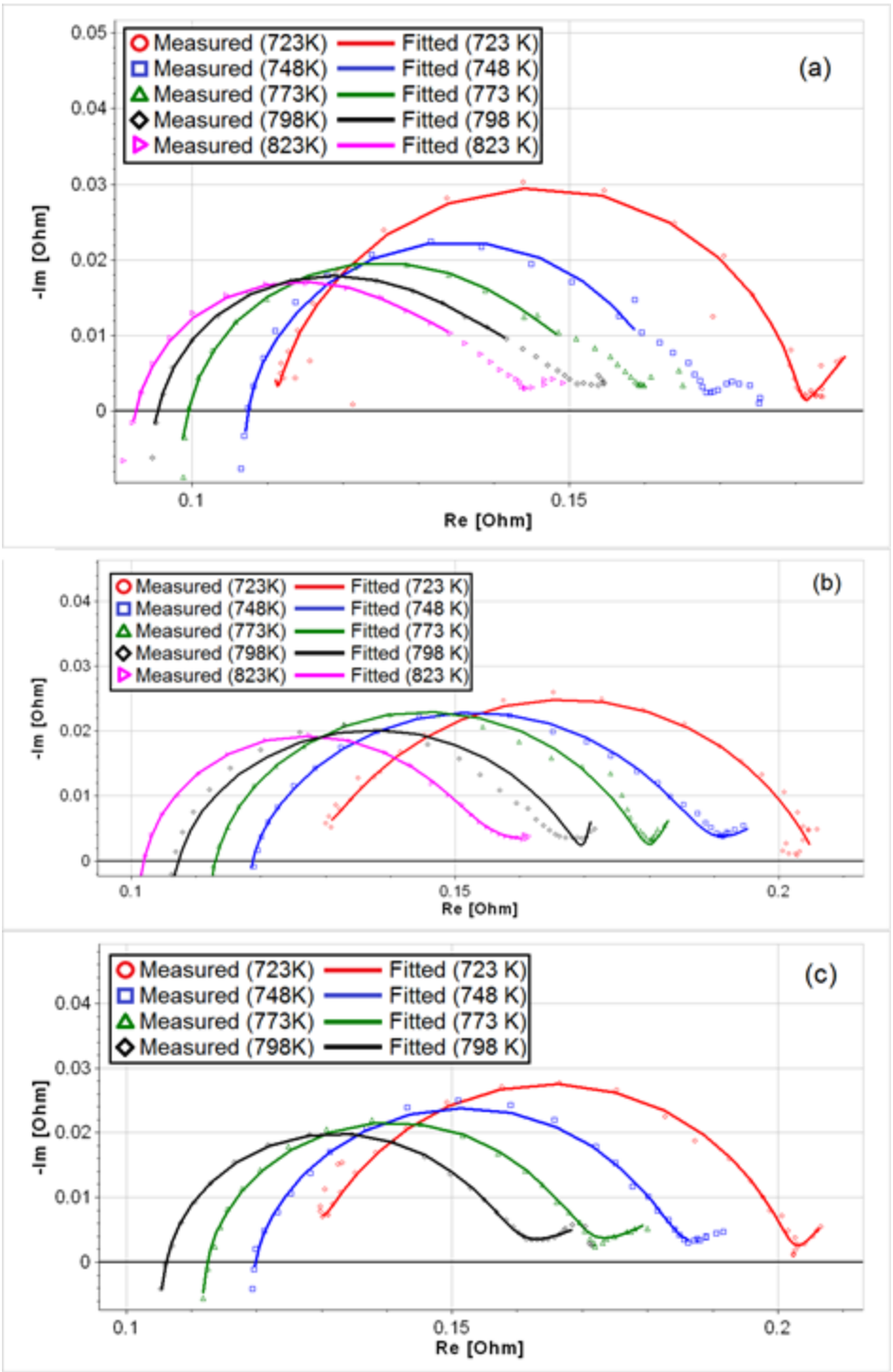

Figure 4.20 Measured and fitted impedance spectra for the LiCl-KCl/liquid Bi system with (a) 0.78 wt% $BaCl_2$, (b) 1.5 wt% $BaCl_2$, and (c) 3.0 wt% $BaCl_2$ at temperatures of 723–823 K.

The fitted impedance spectra provide a value of the charge transfer resistance (R_{ct}) times the cathode surface area (S), which allows the calculation of the exchange current density (i_0) by the relation of Eq. (2.16). Figure 4.21 shows the calculated i_0 values plotted versus the inverse temperature. Table 4.11 lists the experimentally attained R_{ct}*S and i_0 values. The results show that the exchange current density ranges from 0.055–0.0583 A cm^{-2} at 723 K to 0.118–0.121 A cm^{-2} at 823 K and does not vary much with increasing concentration of $BaCl_2$ in the salt. These i_0 values obtained by EIS are comparable to values obtained by Yoon and coworkers for the Ce^{3+}/Ce reaction on a liquid Cd cathode [65]. The i_0 values obtained by application of the Butler-Volmer relation to the CV curves are much smaller than those calculated from EIS techniques. This could be due to the weak redox reaction measured during the CV studies, which could itself be a result of the much smaller surface area of the working Bi cathode.

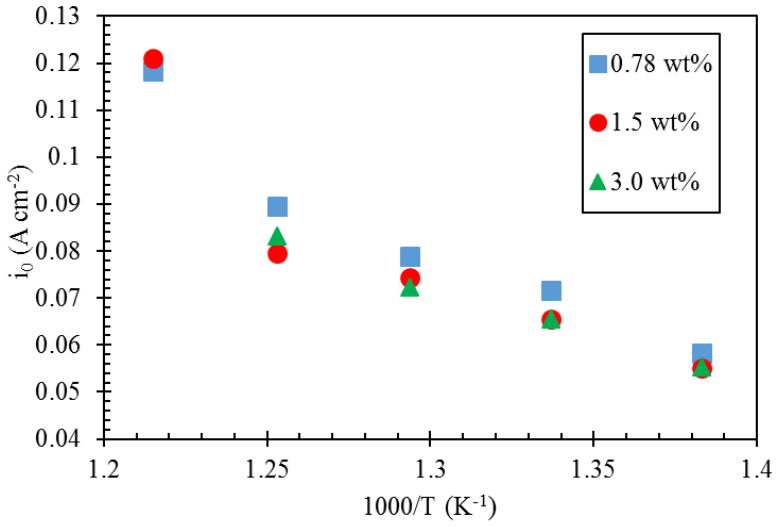

Figure 4.21 Plot of calculated i_0 values versus inverse temperature for varying $BaCl_2$ concentrations.

Table 4.11 Measured R_{ct}*S and calculated i_0 values for the Ba^{2+}/Ba reaction on the liquid Bi cathode by EIS technique.

	0.78 wt% $BaCl_2$		**1.5 wt% $BaCl_2$**		**3.0 wt% $BaCl_2$**	
T (K)	**R_{ct}*S (Ω cm^2)**	**i_0 (A cm^{-2})**	**R_{ct}*S (Ω cm^2)**	**i_0 (A cm^{-2})**	**R_{ct}*S (Ω cm^2)**	**i_0 (A cm^{-2})**
723	0.535	0.0583	0.569	0.0550	0.564	0.0553
748	0.453	0.0716	0.501	0.0655	0.492	0.0655
773	0.422	0.0790	0.463	0.0743	0.461	0.0723
798	0.395	0.0894	0.437	0.0796	0.413	0.0832
823	0.316	0.118	0.311	0.121	-	-

4.3.3 SEM-EDS Experimental Runs

After experiments, the Bi cathodes used in both the CV and EIS studies with Ba were characterized by SEM-EDS analysis. The process for preparation of the cup-type and pool-type cathodes used in CV and EIS experiments has been described in Section 3.3.

Figure 4.22 shows an image of the cup-type Bi cathode used in CV studies of $BaCl_2$. Inspection of the cathode cross section yielded no evidence of visible Ba-Bi intermetallics or other phases, which was confirmed by sampling with EDS analysis. Figure 4.23 shows EDS analysis of target spot 1 from Figure 4.22. All three target spots shown in Figure 4.22, as well as other target spots from the cross section of the cathode, yielded EDS results of 100% Bi composition.

Contrary to the cathode used in CV studies of $BaCl_2$, SEM-EDS study of the Ba-Bi cathode used in EIS studies showed presence of Ba-Bi intermetallics in the cathode cross section. Figure 4.24 shows an SEM image taken of the cathode cross section with the EDS target spot labelled and Figure 4.25 shows EDS analysis of the labelled target spot. EDS results showed a significant amount of oxygen present, likely from oxidation of the Bi surface, as well as the presence of Ba

in a 9 to 35 atomic ratio to Bi. This is close to the 31 mol% to 69 mol% ratio of Ba to Bi reported by Lichtenstein and coworkers for SEM-EDS analysis of a Bi cathode which has undergone constant current density cathodic discharge in a 5 mol% $BaCl_2$-LiCl-KCl system [57]. This comparison suggests presence of the same Ba-Bi intermetallic, likely $BaBi_3$ based on the molar ratio and the Ba-Bi phase diagram, shown in Figure 4.26 [63].

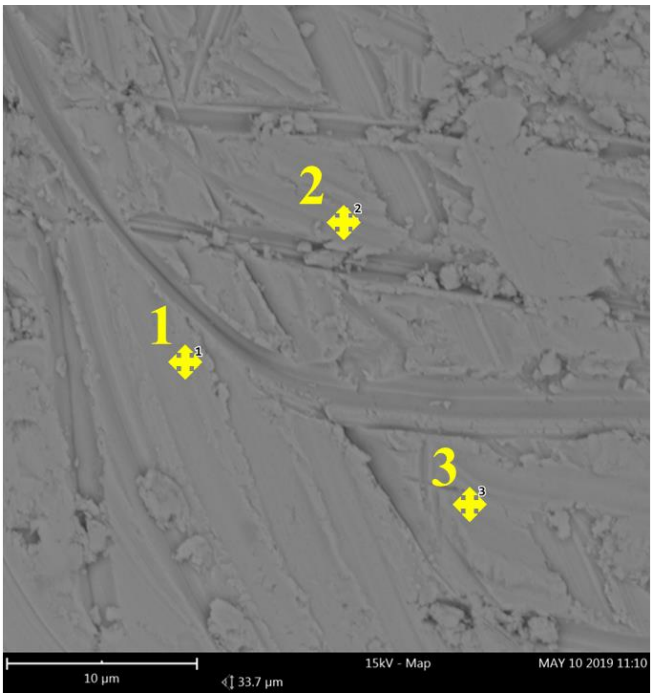

Figure 4.22 SEM picture of Bi cathode used in CV studies of $BaCl_2$.

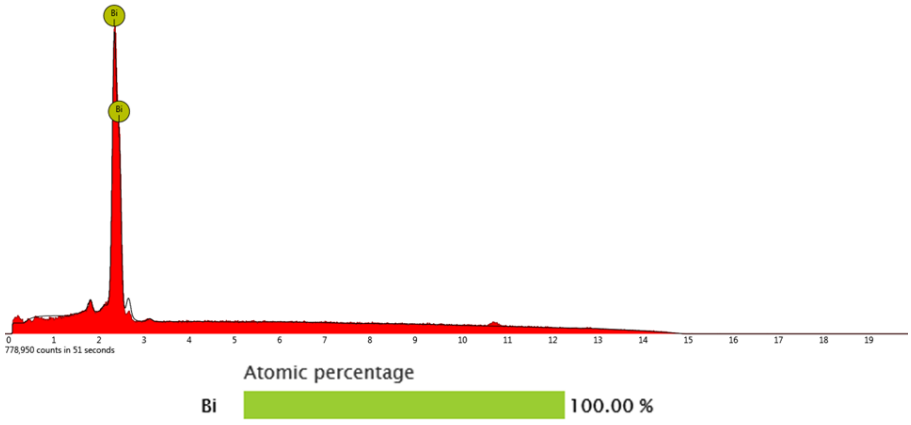

Figure 4.23 SEM-EDS analysis of Bi cathode used in CV studies of $BaCl_2$.

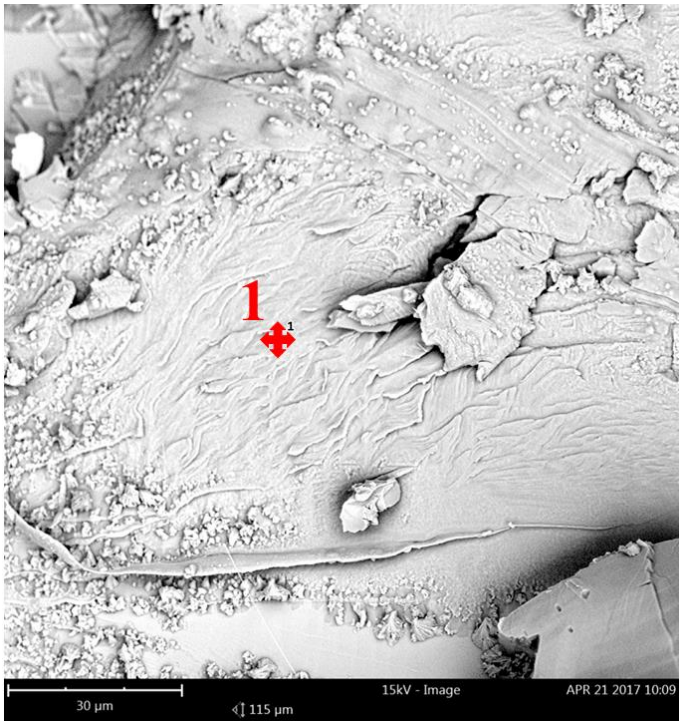

Figure 4.24 SEM picture of Ba-Bi cathode used in EIS studies of $BaCl_2$.

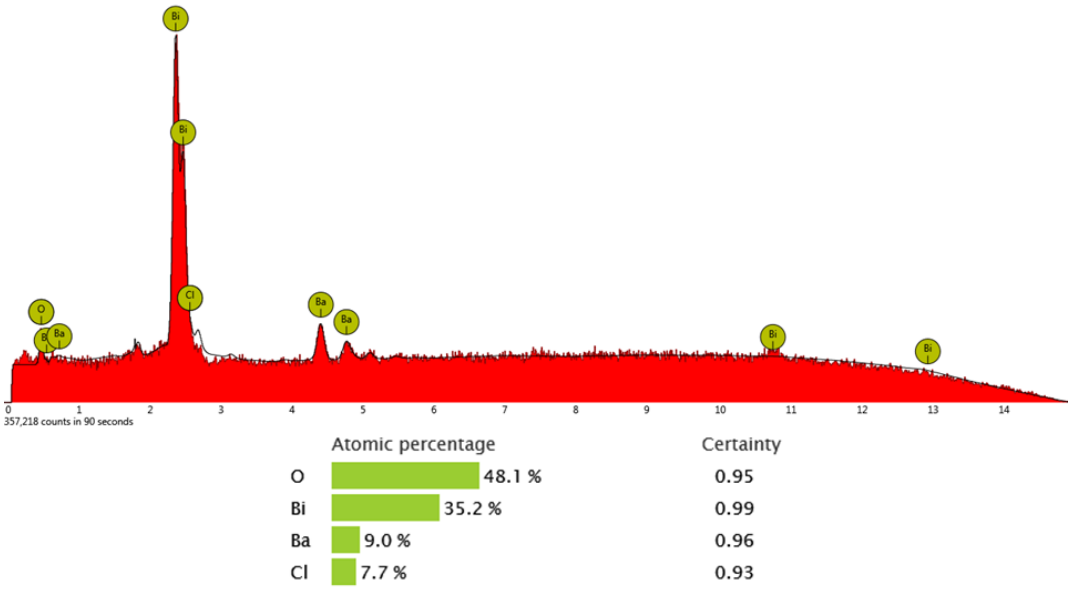

Figure 4.25 SEM-EDS analysis of Ba-Bi cathode used in EIS studies of $BaCl_2$.

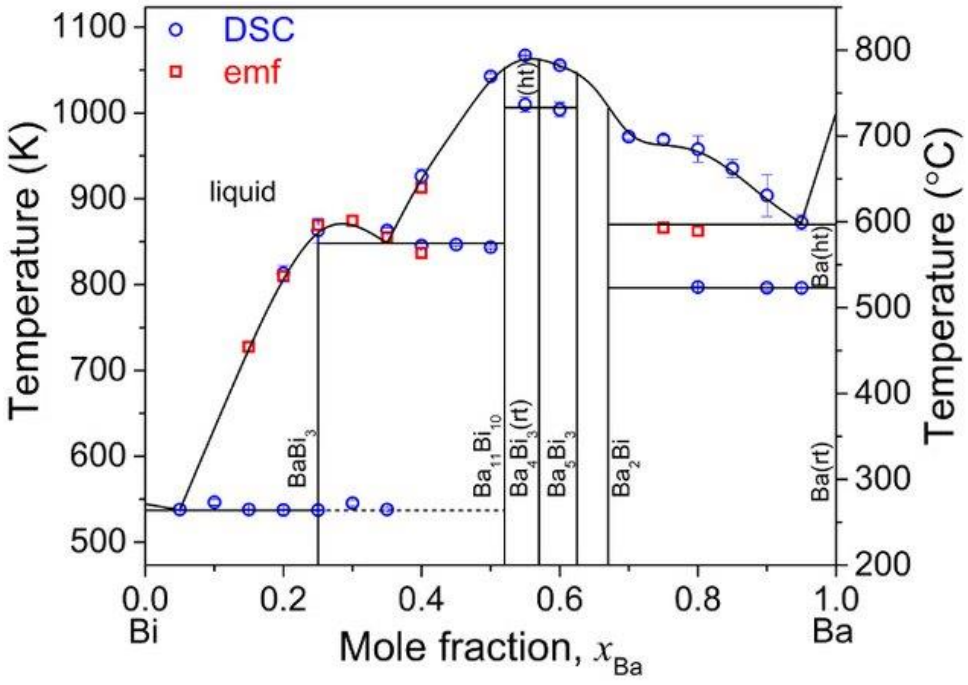

Figure 4.26 Ba-Bi phase diagram.

4.4 Studies with Cerium (Ce)

Many of the trivalent lanthanides in ER salt are captured by the LCC alongside U and TRUs. However, the inclusion of a liquid Bi cathode to the ER must take into account the electrochemical behaviors of lanthanide species on a Bi electrode. Many studies have been done to understand the electrochemical behavior of lanthanides on a liquid Bi surface [40], [49], [54]–[56], [61], but no studies have reported values for the diffusion coefficient of $CeCl_3$ in a LiCl-KCl/liquid Bi system. Therefore, the $CeCl_3$-LiCl-KCl/liquid Bi system was studied by CV techniques to give values for the diffusion coefficient. Furthermore, studying Ce allows for comparison of the experimental design of this project to a similar study reported by Castrillejo et al. [55]. The results of the CV study of the $CeCl_3$-LiCl-KCl system showed passing similarity to that of the previous study, suggesting an acceptable experimental design in this system and giving a soft validation of results of this project for the CV studies of Cs, Sr, and Ba.

4.4.1 CV Measurements

The $CeCl_3$-LiCl-KCl system was studied by CV on a Bi cathode to explore the mass transport behavior of the Ce^{3+}/Ce couple at the Bi cathode. The CV experiments were performed with the specific parameters summarized in Table 4.12.

Table 4.12 Experimental parameters for CV experiments of $CeCl_3$.

Temperature (K)	723, 748, 773, 798
$CeCl_3$ Concentration (wt% in LiCl-KCl)	0.5, 1.0, 2.0, 4.0
Electrical Potential Range (V)	0.22 to -1.55
Scan rate (mV s^{-1})	10, 15, 20, 30, 40, 50, 75, 100, 150, 200, 400, 600, 800, 1000
Bi Cathode Surface Area (cm^2)	0.736

The system was found to produce repeatable CV curves at scan rates below 100 mV/s, as also suggested by a previous study [55]. Figure 4.27 shows cyclic voltammograms obtained for the 4 wt% $CeCl_3$-LiCl-KCl system on a Bi cathode at 773 K after subtraction of the background LiCl-KCl voltammograms. From both the anodic and cathodic peaks of the potentials, it can be seen that they do not significantly shift at scan rates below 50 mV/s, indicating reversibility, and only to a small degree at scan rates greater than 50 mV/s, which suggests the overall quasi-reversibility of the system.

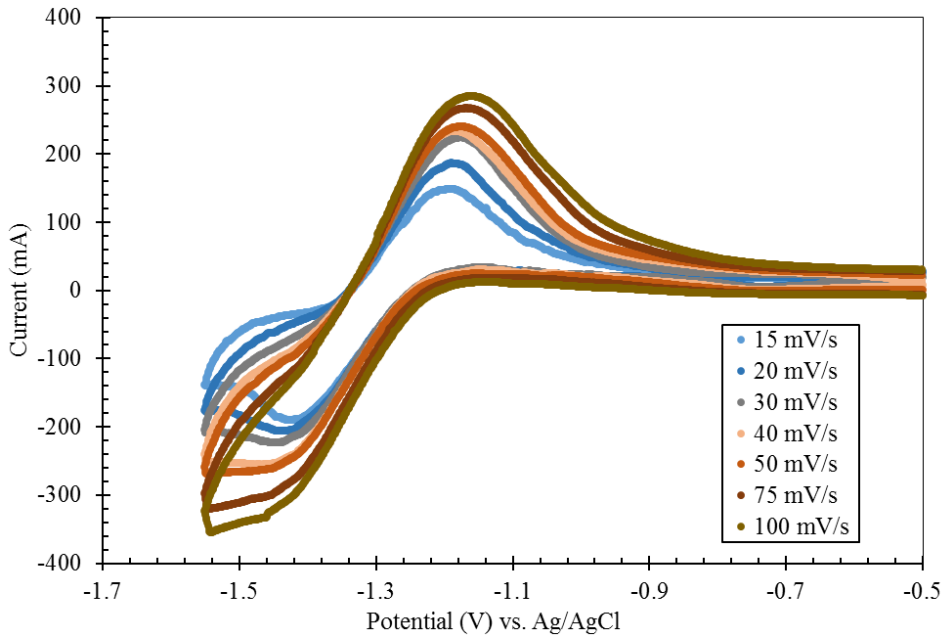

Figure 4.27 Subtraction CV curves for the 4 wt% $CeCl_3$-LiCl-KCl system at 773 K.

To confirm the quasi-reversibility of this system, the peak currents were plotted versus the square root of the scan rate for various $CeCl_3$ concentrations at 773K to show a linear dependence, as shown in Figure 4.28. This allows calculation of the diffusion coefficient of $CeCl_3$ in LiCl-KCl salt from the slope by the Berzins-Delahay relationship, given in Eq. (2.6), which can be applied to this diffusion controlled process of a soluble-insoluble reversible system. Figure 4.29 displays the calculated diffusion coefficients ranging from 1.05×10^{-5} cm^2 s^{-1} to 8.40×10^{-5} cm^2 s^{-1}; nevertheless, these large values for the diffusion coefficient, along with their high variance, suggest that there was some experimental system difference in this study compared to the one by Castrillejo and coworkers. Although the CV curves of this study exhibit strikingly familiar characteristics to those obtained by Castrillejo and coworkers, the slopes of the peak currents versus the square root of the scan rate appear to be much greater for this study [55].

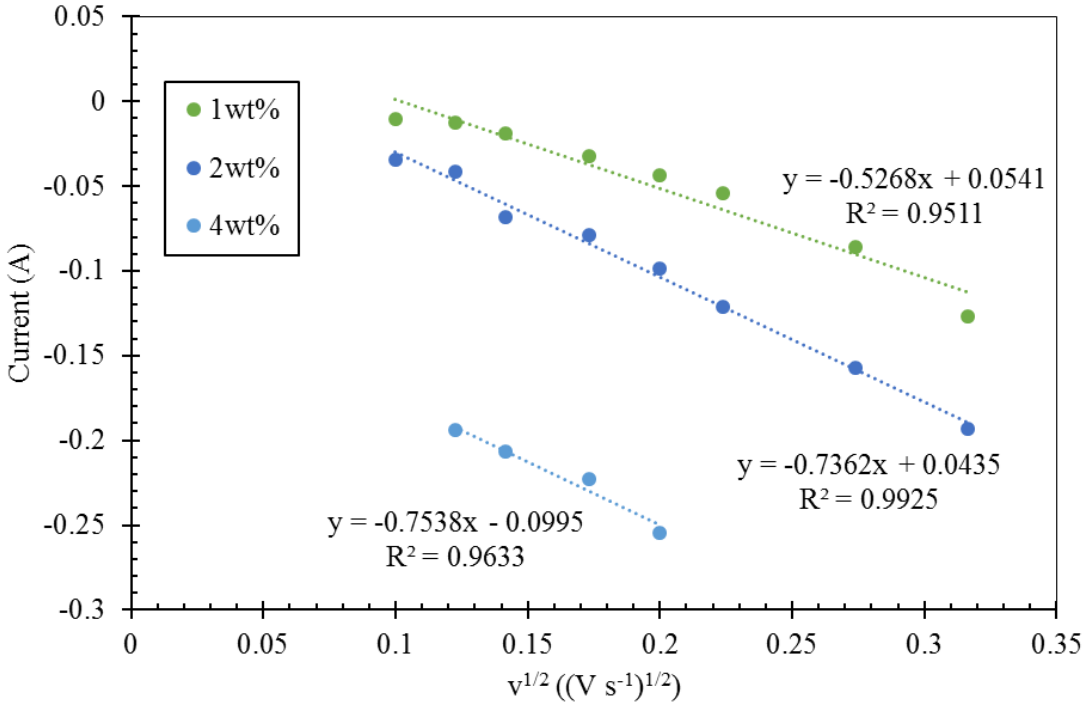

Figure 4.28 Plot of the peak anodic peak currents versus square root of the scan rate for $CeCl_3$-LiCl-KCl systems at 773 K.

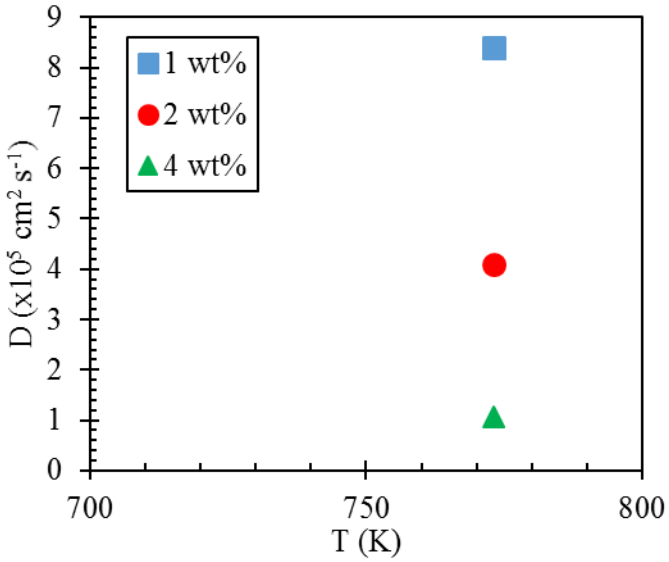

Figure 4.29 Calculated diffusion coefficient of $CeCl_3$ for varying concentrations.

4.4.1 SEM-EDS Experimental Runs

Here, multiple image shots were taken with EDS analysis to confirm or otherwise discommend the presence of Ce-Bi intermetallics in the cathode. Evidence of the presence of Ce

was found. Figure 4.30 displays an SEM picture of the Bi cathode cross section – with labels of the target areas where EDS was being applied. Visual inspection suggests that areas 2 and 3 might be Ce-Bi intermetallics. These Ce-Bi intermetallic compounds were confirmed by the spectra of the EDS analysis of these areas as well as the atomic quantification provided by the SEM-EDS software (see Figure 4.31, Figure 4.32, and Figure 4.33 for areas 1, 2, and 3, respectively). The spectra of target area 1 was used to confirm 100% Bi in the areas surrounding areas 2 and 3. The phase diagram of the Ce-Bi system, shown in Figure 4.34, shows five intermetallic compounds $CeBi_2$, CeBi, Ce_4Bi_3, Ce_5Bi_3, and Ce_2Bi [66]. Based on the rough quantitative analysis by the EDS, the present intermetallic compounds in areas 2 and 3 are likely $CeBi_2$, with the atomic ratio discrepancy likely due to experimental error and resolution of the spectrometer.

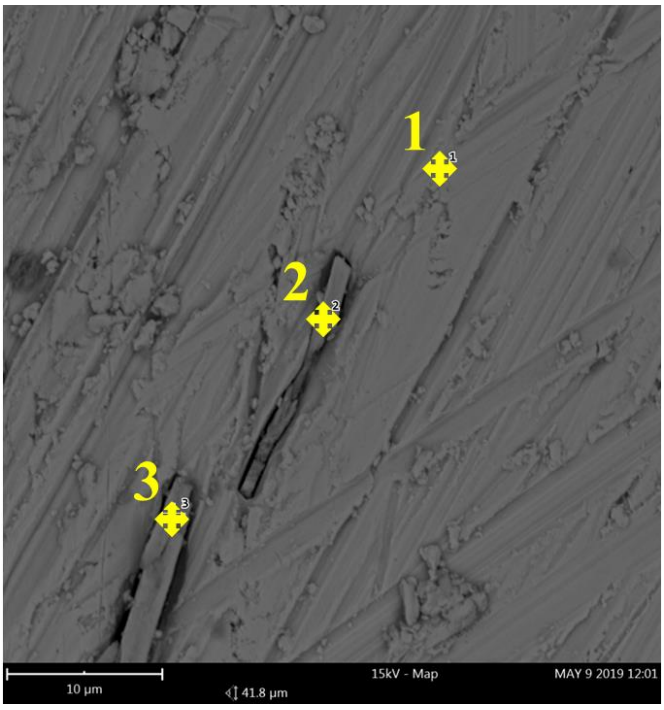

Figure 4.30 SEM picture of Bi cathode used in CV studies of $CeCl_3$.

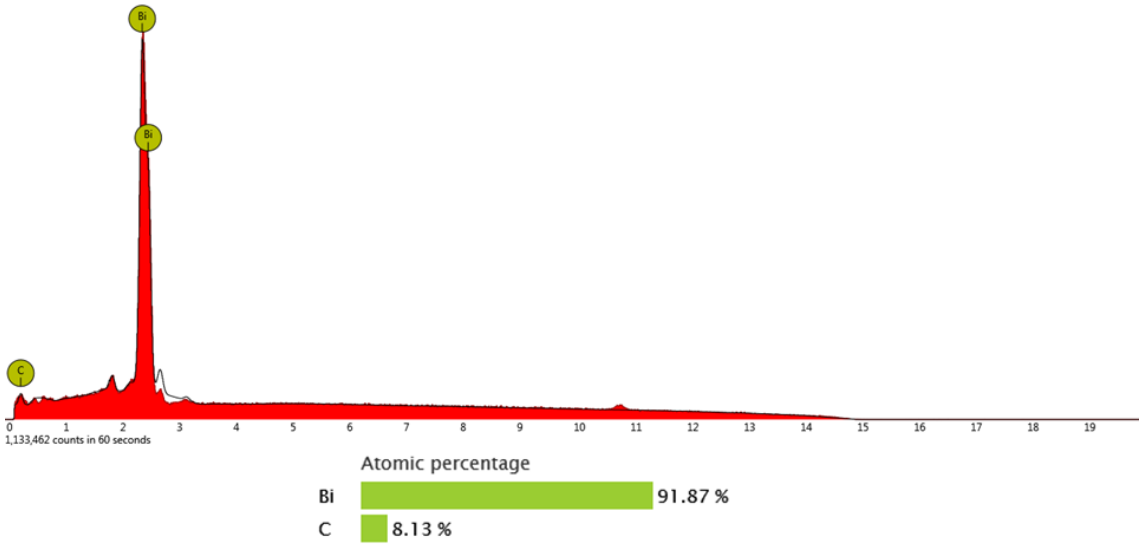

Figure 4.31 SEM-EDS analysis of target spot 1 of Bi cathode used in CV studies of $CeCl_3$.

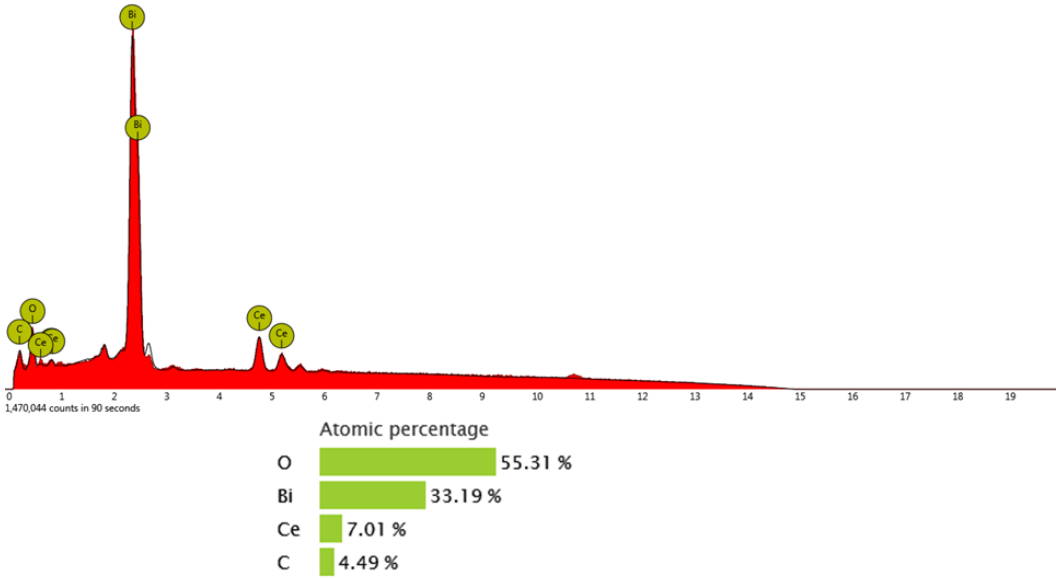

Figure 4.32 SEM-EDS analysis of target spot 2 of Bi cathode used in CV studies of $CeCl_3$.

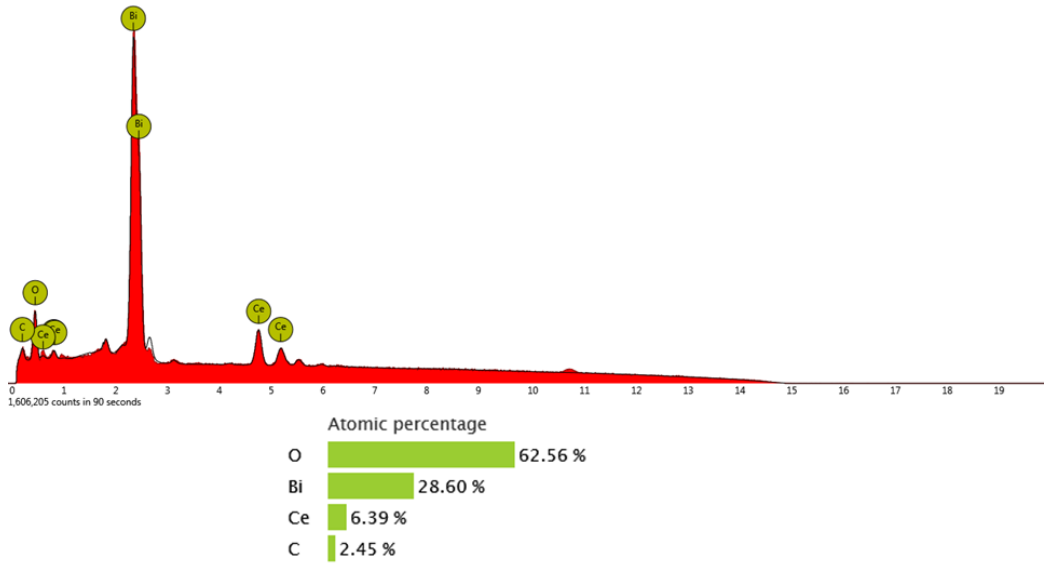

Figure 4.33 SEM-EDS analysis of target spot 3 of Bi cathode used in CV studies of $CeCl_3$.

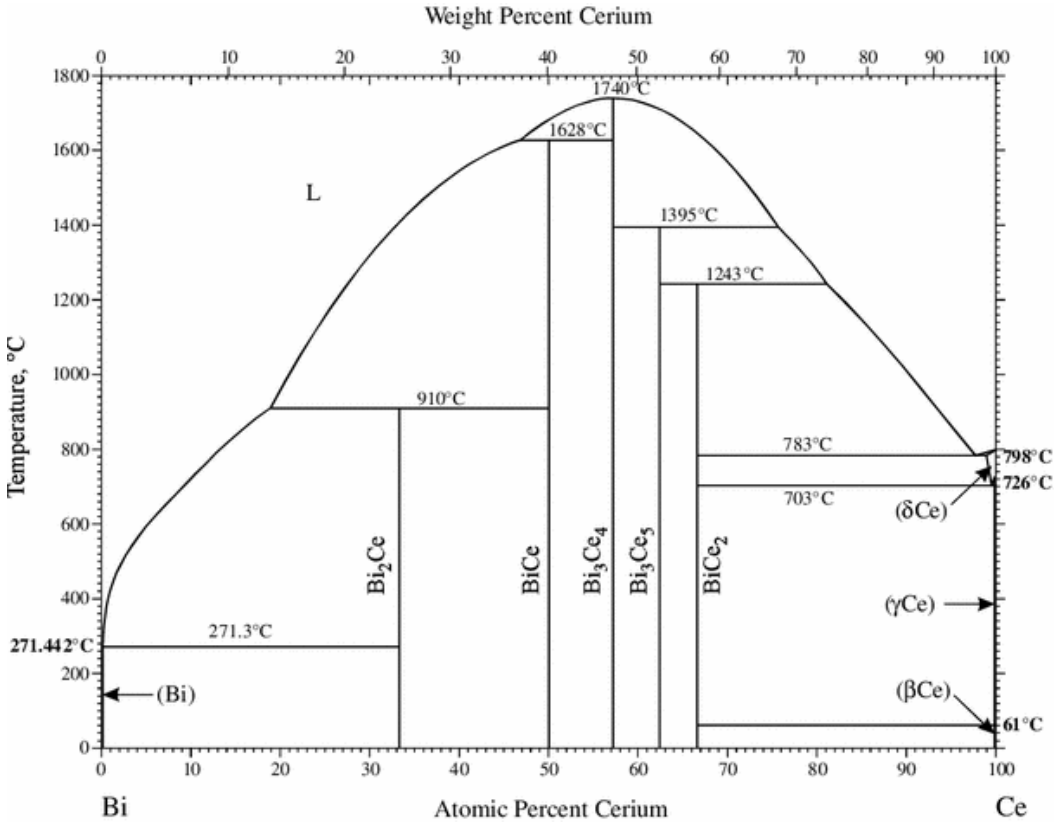

Figure 4.34 Ce-Bi phase diagram.

4.5 Assessment of Bi cathode for application in ER

The data and analyses presented in this study have shown electrochemical separation abilities of the liquid Bi cathode for some of the varied valency elemental species considered with certain conditions. In the case of CsCl, two redox peaks have been observed as more positive than that of Li, indicating that the controlled deposition of Cs from a CsCl-LiCl-KCl system into a liquid Bi cathode is possible. However, it should be noted that as diffusion of CsCl in LiCl-KCl is suggested by CV and EIS to be the rate-determining step, the sharp decrease in diffusivity of the CsCl at higher weight percentages means that the salt recycling process would become less efficient at higher concentrations of CsCl in the ER salt.

For the divalent species studied, Sr and Ba, redox reactions were less observable. In the $BaCl_2$ system, weak redox reactions due to $BaCl_2$ were seen to occur at potentials just slightly more positive than the reduction of Li. From the mass transport and exchange current kinetics values calculated in this study, the reduction of Ba into a Bi cathode should proceed limited by diffusion. In the case of the $SrCl_2$-LiCl-KCl system, no distinguishable redox reaction occurred which could be studied independently of the Li redox. However, from the electrochemical behavior observed, the presence of Sr influences the redox reactions occurring near the reduction potential of Li^+. Although SEM-EDS analysis showed no Sr present in the Bi cathodes post-examination, it could be possible that as other studies have shown, the separation of Sr into Bi from LiCl-KCl is not thermodynamically favorable. Lichtenstein and coworkers have separated Sr into a Bi cathode from LiCl-KCl [57]. Yet, this study has shown that sensitive redox control and electrochemical analysis of the system might not be feasible for Sr in the ER salt.

From the study with trivalent Ce, the experimental results agree with similar reported systems and there is in fact a Ce reduction occurring at the Bi cathode before reduction of Li. This

observation, along with some studies of other RE elements in a LiCl-KCl/liquid Bi system, suggests that the liquid Bi cathode could be employed for selective electrochemical extraction of RE elements from the LiCl-KCl salt [24], [25], [38], [67].

Taking into consideration the ER salt, which contains UCl_3 and $PuCl_3$, inclusion of a Bi cathode for any separation process must consider the separations of U and Pu from the salt and the degree to which they will occur. Np and U can be separated by reductive extraction into Bi from a mixed system [25]. However, if there is an applied potential, formation of Bi intermetallic compounds and the limited solubility of ER salt species in liquid Bi could allow for many different separation schemes. Here, temperature and redox control might be used in the ER to determine the equilibrium conditions and driving reactions within the ER salt and at the liquid Bi cathode surface.

4.6 Summary

This chapter has presented all of the experimental data collected and analysis performed for this study. This data includes cyclic voltammograms of CsCl, $SrCl_2$, $BaCl_2$, and $CeCl_3$ in LiCl-KCl with a liquid Bi cathode. Where redox reactions were repeatable, analysis of the peak currents led to calculation of values for the diffusion coefficient of the redox species in the bulk salt. For the $BaCl_2$ system, a region of the CV curves was used to approximate the value of the exchange current density of Ba^{2+}/Ba ions at the cathode surface. EIS measurements were also investigated for the systems containing CsCl and $BaCl_2$. Analysis of the Nyquist plots allowed for calculation of the exchange current density values of Cs^{+}/Cs and Ba^{2+}/Ba redox couples at the Bi cathode surface. Finally, all of the electrochemical data and observations from experiments were considered, along with reported thermodynamic and electrochemical behavior of the multivalent alkali, alkaline-earth and RE elements in the LiCl-KCl/liquid Bi system, to give an assessment of the liquid Bi cathode for electrochemical separations in the ER environment.

Chapter 5 Summary and Future Work

5.1 Background

Much research studies have been reported on pyroprocessing technology for recycling actinides and minimizing the final waste from UNF. Liquid Cd was selected as the cathode candidate for an electrochemical cell to recover actinides and RE elements, but there is still an appreciable amount of alkali/alkaline-earths and RE materials in the used salt from pyroprocessing batches. Among other ways to separate these species from the salt, other liquid metals could be potentially used alongside the liquid Cd as a cathode for selective recovery of the alkali/alkaline-earth and RE elements. There are few studies reported regarding the electrochemical and thermodynamic behavior of used nuclear fuel constituent species with liquid Bi. Therefore, the goal of this dissertation was to explore some of these systems containing alkali/alkaline-earth or RE species and calculate some mass transport and kinetics properties in order to gauge the possibility of separation of these species in LiCl-KCl eutectic salt.

5.2 Literature Survey

A survey of the available literature regarding liquid metal cathodes for pyroprocessing technology and experimental electrochemical methods was presented in Chapter 2. The information presented in brief:

- Reduction potentials determine if a species present in an electrochemical cell will be reduced or not for an applied electrical potential between two electrodes. On a steel or W electrode, the alkali/alkaline-earth species will have a reduction potential more negative than that of Li, which is bountifully present in the LiCl-KCl ER salt. However, due to the low activity of alkali-alkaline-earth species in liquid Bi, it is thermodynamically possible

to shift the reduction potential of alkali/alkaline-earth species by the Nernst relation to be more positive than that of Li.

- The mass transport of an electroactive species will commonly determine rates of reaction in a LiCl-KCl with liquid metal cathode system. Therefore, measuring the diffusion coefficient of a species is important for understanding the reaction rates and capabilities of an electrochemical separation. This can be done rapidly and accurately via CV experiments, providing information about the overall electrochemical behavior and reactions of the system.
- The kinetics occurring at the electrode surface are also crucial in determining the reactions occurring and their rates. At the liquid Bi cathode surface, the exchange current density is important to know in order to assess the maximum capabilities of the cathode for ion transfer at the interface. CV techniques can be used, but more robustly, EIS techniques can be applied for studying the kinetics at the cathode surface and measuring the exchange current density.
- Although many actinides and RE elements have been studied at liquid Cd and Bi cathodes, among others, there is very little reported research on the thermodynamics and electrochemical properties of alkali/alkaline-earth species in a LiCl-KCl/liquid Bi system.

5.3 Experimental Design

An experimental design and procedure has been established to study the LiCl-KCl/liquid Bi cathode system with monovalent, divalent, and trivalent species. Among many tools and equipment used, an inert argon atmosphere glovebox was used for all sample preparations and experiments. The key points of the experimental design were:

- Salts and crucibles were dried at high temperatures prior to experimentation. This is necessary in order to minimize oxygen present in the system.
- The Bi material was melted prior to use. This allowed the oxide layer to form on the top of the melt and pure Bi needles to be pulled from the bulk melt. These Bi needles were then used in either a pyrex cup type, contacted electrically by a Mo wire, or a pool-type cathode consisting of melted Bi on the crucible bottom, contacted electrically by a tungsten rod.
- Reference electrodes for electrochemistry experiments consisted of a Ag wire submerged in 5 mol% AgCl-LiCl-KCl within a pyrek tube. The pyrex tube closed end bottom was thinned to allow ionic conduction.
- Salt concentrations for the electrochemical studies were confirmed by ICP-MS analysis of samples taken at each experimental concentration. ICP-MS samples were carefully prepared and diluted to minimize error.
- The Bi cathodes were recovered after electrochemical experiments and characterized via SEM-EDS in order to visually look for intermetallic phases present in the Bi cathode and perform elemental composition analysis.

5.4 Results

5.4.1 Studies with Cs

- The fundamental behavior and properties of CsCl in the LiCl-KCl/liquid Bi system were explored via CV and EIS techniques with SEM-EDS analysis of the Bi cathodes. CV studies were performed at temperatures of 723–823 K and CsCl concentrations of 0.5–4.0 wt% CsCl in LiCl-KCl with a cup-type Bi cathode.
- Two redox peaks attributable to Cs were apparent in the background subtracted CV curves. Redox peak (I) had a reduction peak of approximately -1.1 V and oxidation peak of

approximately -0.15 V. Redox peak (II) had a reduction peak of approximately -1.24 V and oxidation peak of approximately -0.32 V.

- Based on the potential and current peaks from the CV curves with differing scan rates, the reaction was determined to be quasi-reversible. Values for the diffusion coefficient of Cs in each redox reaction were calculated. Table 5.1 displays the calculated diffusion coefficients from the peaks of redox reaction (I) and Table 5.2 displays the calculated diffusion coefficients from the peaks of redox reaction (II).

Table 5.1 Diffusion coefficients for Cs redox reaction (I) calculated from CV with scan rate of 100 mV s^{-1}.

	D ($\times 10^5$ cm^2 s^{-1})				
CsCl concentration	**0.5 wt%**	**1.0 wt%**	**1.5 wt%**	**2.0 wt%**	**3.0 wt%**
723 K	0.498	0.203	0.0359	-	-
748 K	0.857	0.385	0.0615	-	-
773 K	0.945	0.255	0.0679	0.0506	-
798 K	0.759	0.195	0.0832	0.0543	0.0181
823 K	0.867	0.410	0.103	0.0898	0.0176

Table 5.2 Diffusion coefficients for Cs redox reaction (II) calculated from CV with scan rate of 100 mV s^{-1}.

	D ($\times 10^5$ cm^2 s^{-1})				
CsCl concentration	**0.5 wt%**	**1.0 wt%**	**1.5 wt%**	**2.0 wt%**	**3.0 wt%**
723 K	1.551	0.546	0.203	0.101	0.027
748 K	0.702	0.326	0.326	0.049	-
773 K	-	0.389	-	0.052	-
798 K	-	0.301	-	-	-
823 K	1.189	0.371	-	-	-

- EIS studies were performed for a 0.5 wt% CsCl-LiCl-KCl system with a pool-type liquid Bi cathode at temperatures of 723–773 K.
- Impedance spectra were measured at frequencies of 50 kHz to 10 mHz with applied overpotentials of 2-4 mV. Nyquist plots were fitted to an equivalent circuit for the system. The measured charge transfer resistance and Bi cathode surface area were used to calculate i_0 of the Cs^+/Cs couple at the Bi cathode surface. Values of i_0 ranged from 0.0752 to 0.0911 A cm^{-2} for the system at 723 to 773 K.
- After CV and EIS experiments, the Bi cathodes used were analyzed by SEM-EDS for evidence of Cs in the form of intermetallic compounds.
- No Cs was found within the system, suggesting that the formation of Cs-Bi intermetallics from LiCl-KCl salt is not thermodynamically favorable at these experimental temperatures.

5.4.2 Studies with Sr

- The system of $SrCl_2$-LiCl-KCl was studied by CV and the Bi cathode used in CV experiments was analyzed by SEM-EDS. CV experiments were performed for the $SrCl_2$ system at temperatures of 723–823 K and concentrations of 0.5–4.0 wt% $SrCl_2$ in LiCl-KCl on a cup-type Bi cathode.
- No redox reaction of Sr was able to be discerned within the potential window between the reduction of Li^+ and anodic dissolution of Bi. However, the presence of $SrCl_2$ affected the reduction behavior of Li, decreasing the effect of temperature on current.
- After CV experiments, the Bi cathode was analyzed by SEM-EDS. No mixture of intermetallic phases was visually apparent and elemental composition analysis by EDS did not suggest any presence of Sr within the Bi cathode.

5.4.3 Studies with Ba

- The properties of $BaCl_2$ on a liquid Bi cathode in LiCl-KCl were studied via CV and EIS. CV experiments were carried out for the 0.5–4.0 wt% $BaCl_2$-LiCl-KCl system at temperatures of 723–823 K on a cup-type Bi cathode.
- Redox peak attributable to Ba seen with reduction peak at -1.40 V and oxidation peak at -1.27 V. Redox peak only seen for 1 and 2 wt% $BaCl_2$ systems. Large and unstable current at neutral potentials discouraged analysis of other concentration CV curves.
- Diffusion coefficients of the Ba species were calculated from the anodic peak currents of the 1 and 2 wt% $BaCl_2$ system. These ranged from 0.0129×10^{-5} cm^2 s^{-1} to 0.0993×10^{-5} cm^2 s^{-1} for temperatures of 723–798 K. Compared to other studies of elements within a LiCl-KCl/liquid Bi system, these values are rather small.
- The small zero-current overpotential region of the CV curves was used to calculate i_0 by the Butler-Volmer relation. Values of 0.00264–0.00308 A cm^{-2} were calculated for a scan rate of 50 mV s^{-1}. These values seem very small, and are likely due to the limitations of the applications of this measurement technique.
- EIS studies were also performed to study the charge transfer mechanisms of Ba^{2+}/Ba at the pool-type 10 mol% Ba in Bi cathode surface. The results as summarized:
- Impedance spectra were collected for systems of 0.78-3.0 wt% $BaCl_2$ at temperatures of 723–823 K with applied overpotentials of 2–10 mV and frequencies of 50 kHz–50 mHz. R_{ct}*S obtained from the fitting software of the Nyquist plots with the known surface area and the calculated i_0 values of Ba^{2+}/Ba at the Bi cathode are shown in Table 5.3. These i_0 values compare very similarly to studies of many other species on a liquid metal cathode

in LiCl-KCl pyroprocessing environment. Concentration variation in the experimental range did not appear to affect values of i_0.

Table 5.3 Measured R_{ct}*S and calculated i_0 values for the Ba^{2+}/Ba reaction on the liquid Bi cathode by EIS technique.

	0.78 wt% $BaCl_2$		**1.5 wt% $BaCl_2$**		**3.0 wt% $BaCl_2$**	
T (K)	**R_{ct}*S (Ω cm^2)**	**i_0 (A cm^{-2})**	**R_{ct}*S (Ω cm^2)**	**i_0 (A cm^{-2})**	**R_{ct}*S (Ω cm^2)**	**i_0 (A cm^{-2})**
723	0.535	0.0583	0.569	0.0550	0.564	0.0553
748	0.453	0.0716	0.501	0.0655	0.492	0.0655
773	0.422	0.0790	0.463	0.0743	0.461	0.0723
798	0.395	0.0894	0.437	0.0796	0.413	0.0832
823	0.316	0.118	0.311	0.121	-	-

- After CV and EIS studies, the Bi and Ba-Bi cathodes were investigated by SEM-EDS for compositional analysis.
- The Bi cathode used in CV experiments showed no visible signs of Ba intermetallics present and EDS analysis of target spots showed 100% Bi present.
- However, in SEM-EDS analysis of the 10 mol% Ba-Bi cathode used in EIS experiments, Ba was found in approximately 9:35 (Ba:Bi) molar ratio. This could be due to the formation of Ba-Bi intermetallics such as $BaBi_3$.

5.4.4 Studies with Ce

- CV studies were performed for the $CeCl_3$-LiCl-KCl system at temperatures of 723–798 K and $CeCl_3$ concentrations of 0.5–4.0 wt% on a cup-type liquid Bi cathode.

- Potential and current peaks of the CV suggested reversible behavior of the system for scan rates of 10–50 mV s^{-1}. Higher scan rates caused the system to slightly lose reversibility. Overall, the system can be considered quasi-reversible.
- The Berzins-Delahay relation was used to calculate diffusion coefficients from the slopes of the peak anodic current versus the square root of the scan rate. Calculated values for D of $BaCl_2$ in LiCl-KCl on a Bi cathode were 1.05×10^{-5} cm^2 s^{-1} to 8.40×10^{-5} cm^2 s^{-1}.
- After CV experiments, the Bi cathode was extracted and a cross section analyzed by SEM-EDS.
- Ce was found to be present in the Bi cathode cross section, in a roughly 7 to 33 Ce:Bi ratio. Based on a phase diagram of Ce-Bi, the intermetallic most present in the system is likely $CeBi_2$.
- Other than the mass transport and redox behavior studied, the CV experiments were useful for comparing the experimental apparatus and design of this dissertation to a previous study by Castrillejo and coworkers [55].
- Although the slopes of peak current versus square root of the scan rate were different between the two studies, the CV were otherwise very similar. This allowed for a conclusion that the experimental design of this dissertation is acceptable for CV studies.

5.4.5 Assessment of Bi cathode for application in ER

- The experimental work of this dissertation has shown the clear electrodeposition for some species into a liquid Bi cathode and more weak reactions for reactions
- Cs redox peaks observed. Diffusivity is strong at low concentrations in the salt but decreases significantly at higher concentrations of CsCl.

- Sr and Ba exhibited less clear redox reactions. Sr, in particular, at concentrations up to 4 wt% has a reduction potential very close to that of Li. Although controlled deposition into Bi from LiCl-KCl salts has been shown for both Sr and Ba, the avoidance of a large deposition of Li into the Bi will be difficult.
- The CV experiments performed here for Ce have shown favorable ability to separate Ce into Bi from LiCl-KCl salts.

Ultimately, the ER salt will be much harder to study and perform selective depositions of particular species with a liquid Bi cathode. The results of this dissertation help inform the design of a liquid Bi cathode in the ER regarding the expected behavior with alkali/alkaline-earth elements. Furthermore, some of the mass transport and kinetics values can be used in modelling the processes of redox and mass transport in the ER salt.

5.5 Future Work

From the results of this dissertation work, a few suggestions for future work to further the research base of the liquid Bi cathode for pyroprocessing technology applications are presented:

- Study electrochemical deposition of combined systems of two or more species of alkali/alkaline-earth, RE, and actinide species with a liquid Bi cathode. The chemistry, mass transport, and kinetics at the electrode surface will become much more complex for electrochemical studies of systems containing multiple species. As much as thermodynamic properties are used to predict the contents and behaviors of the species in the ER salt, electrochemical experiments are necessary to confirm things such as equilibrium and reduction potentials.

- Perform CP experiments to determine intermetallic compounds formed by Cs, Sr, and Ba with Bi and their energies of formation. Inclusion of thermodynamic data, confirmed by CP experiments, can give information about the alloy formation happening during electroreduction of the ionic species in the Bi and expected phases found within the cathode.

References

[1] World Nuclear Association, “World Nuclear Performance Report 2019,” 2019.

[2] N. E. Agency, “Nuclear Technology Development and Economics Économie et développement des technologies nucléaires 2018 Nuclear Energy Data Données sur l’énergie nucléaire,” 2018.

[3] J. K. Shultis and R. E. Faw, *Fundamentals of Nuclear Science and Engineering*. Boca Raton, FL: CRC Press, 2008.

[4] J. J. Laidler, J. E. Battles, W. E. Miller, J. P. Ackerman, and E. L. Carls, “Development of pyroprocessing technology,” *Prog. Nucl. Energy*, vol. 31, no. 1–2, pp. 131–140, 1997.

[5] V. K. Verma and K. Katovsky, *Spent Nuclear Fuel and Accelerator-Driven Subcritical Systems*. New York: Springer, 2018.

[6] L. Rodríguez-Penalonga and B. Yolanda Moratilla Soria, “A Review of the Nuclear Fuel Cycle Strategies and the Spent Nuclear Fuel Management Technologies,” *Energies*, vol. 10, no. 8, 2017.

[7] Michael F. Simpson, “Developments of Spent Nuclear Fuel Pyroprocessing Technology at Idaho National Laboratory,” no. April, 2012.

[8] T. Koyama, Y. Sakamura, M. Iizuka, T. Kato, T. Murakami, and J.-P. Glatz, “Development of Pyro-processing Fuel Cycle Technology for Closing Actinide Cycle,” *Procedia Chem.*, vol. 7, pp. 772–778, 2012.

[9] J. P. Glatz *et al.*, “Development of Pyrochemical Separation Processes for Recovery of Actinides from Spent Nuclear Fuel in Molten LiCl-KCl,” *Molten Salts Chem.*, pp. 541–560,

2013.

[10] D. Yoon, “Electrochemical Studies of Cerium and Uranium in LiCl-KCl Eutectic for Fundamentals of Pyroprocessing Technology,” Virginia Commonwealth University, 2016.

[11] Y. Sakamura, O. Shirai, T. Iwai, and Y. Suzuki, “Distribution behavior of plutonium and americium in LiCl-KCl eutectic/liquid cadmium systems,” *J. Alloys Compd.*, vol. 321, no. 1, pp. 76–83, 2001.

[12] M. Iizuka, T. Koyama, N. Kondo, R. Fujita, and H. Tanaka, “Actinides Recovery from Molten salt/Liquid Metal System by Electrochemical Methods,” *J. Nucl. Mater.*, vol. 247, pp. 183–190, 1997.

[13] S. Lee and J. Jang, “Distillation behavior of cadmium for U recovery from liquid cadmium cathode in pyroprocessing,” *J. Radioanal. Nucl. Chem.*, vol. 314, no. 1, pp. 491–498, 2017.

[14] E. Y. Choi and S. M. Jeong, “Electrochemical processing of spent nuclear fuels: An overview of oxide reduction in pyroprocessing technology,” *Prog. Nat. Sci. Mater. Int.*, vol. 25, no. 6, pp. 572–582, 2015.

[15] M. Shaltry, S. Phongikaroon, and M. F. Simpson, “Ion exchange kinetics of fission products between molten salt and zeolite-A,” *Microporous Mesoporous Mater.*, vol. 152, pp. 185–189, 2012.

[16] J. P. Ackerman, T. R. Johnson, and J. J. Laidler, “Waste Removal in Pyrochemical Fuel Processing for the Integral Fast Reactor,” in *The International Symposium on Actinides: Processing & Materials, 1994 TMS Annual Meeting, San Francisco, CA*, 1994.

[17] A. N. Williams, M. Pack, and S. Phongikaroon, “Separation of strontium and cesium from

ternary and quaternary lithium chloride-potassium chloride salts via melt crystallization," *Nucl. Eng. Technol.*, vol. 47, no. 7, pp. 867–874, 2015.

[18] Y. Z. Cho, T. K. Lee, J. H. Choi, H. C. Eun, H. S. Park, and G. Il Park, "Eutectic(LiCl-KCl) waste salt treatment by sequencial separation process," *Nucl. Eng. Technol.*, vol. 45, no. 5, pp. 675–682, 2013.

[19] Y. Cho, G. Park, H. Lee, and I. Kim, "Concentration of Cesium and Strontium Elements Involved in a LiCl Waste Salt by a Melt Crystallization Process," *Nucl. Technol.*, vol. 7, no. September, 2010.

[20] M. Shim, H. G. Choi, J. H. Choi, K. W. Yi, and J. H. Lee, "Separation of Cs and Sr from LiCl-KCl eutectic salt via a zone-refining process for pyroprocessing waste salt minimization," *J. Nucl. Mater.*, vol. 491, pp. 9–17, 2017.

[21] S. Phongikaroon, "Equilibrium Model for Ion Exchange Between Multivalent Cations and Zeolite-A in a Molten Salt," *VTT Publ.*, vol. 52, no. 504, pp. 3–194, 2003.

[22] H. Kim, N. Smith, K. Kumar, and T. Lichtenstein, "Electrochemical Separation of Barium into Liquid Bismuth by Controlling Deposition Potentials," *Electrochim. Acta*, vol. 220, pp. 237–244, 2016.

[23] J. Serp, P. Lefebvre, R. Malmbeck, J. Rebizant, P. Vallet, and J. P. Glatz, "Separation of plutonium from lanthanum by electrolysis in LiCl-KCl onto molten bismuth electrode," *J. Nucl. Mater.*, vol. 340, no. 2–3, pp. 266–270, 2005.

[24] K. Kinoshita *et al.*, "Separation of Uranium and Transuranic Elements from Rare Earth Elements by Means of Multistage Extraction in LiCl-KCl/Bi System," *J. Nucl. Sci. Technol.*,

vol. 36, no. 2, pp. 189–197, 1999.

[25] M. Kurata, Y. Sakamura, T. Hijikata, and K. Kinoshita, “Distribution behavior of uranium, neptunium, rare-earth elements (Y, La, Ce, Nd, Sm, Eu, Gd) and alkaline-earth metals (Sr,Ba) between molten LiCl-KCI eutectic salt and liquid cadmium or bismuth,” *J. Nucl. Mater.*, vol. 227, pp. 110–121, 1995.

[26] Y. Sakamura, O. Shirai, T. Iwai, and Y. Suzuki, “Thermodynamics of Neptunium in LiCl-KCl Eutectic/Liquid Bismuth Systems,” *J. Electrochem. Soc.*, vol. 147, no. 2, p. 642, 2000.

[27] N. Elgrishi, K. J. Rountree, B. D. McCarthy, E. S. Rountree, T. T. Eisenhart, and J. L. Dempsey, “A Practical Beginner’s Guide to Cyclic Voltammetry,” *J. Chem. Educ.*, vol. 95, no. 2, pp. 197–206, 2018.

[28] A. Bard and L. Faulkner, *Electrochemical Methods: Fundamentals and Applications*, 2nd ed. New York: Wiley, 2001.

[29] J. H. Sim, Y. S. Kim, S. W. Paek, S. H. Kim, and S. J. Lee, “Electrode reactions of Nd^{3+}/Nd couple in LiCl-KCl-$NdCl_3$ solutions at solid W and liquid Cd electrodes,” *Int. J. Electrochem. Sci.*, vol. 13, no. 3, pp. 2842–2859, 2018.

[30] O. Shirai, K. Uozumi, T. Iwai, and Y. Arai, “Electrode reaction of the U^{3+}/U couple at liquid Cd and Bi electrodes in LiCl – KCl eutectic melts,” *Anal. Sci.*, vol. 17 Supplem, pp. i959–i962, 2001.

[31] D. Yoon and S. Phongikaroon, “Measurement and Analysis of Exchange Current Density for U/U^{3+} Reaction in LiCl-KCl Eutectic Salt via Various Electrochemical Techniques,” *Electrochim. Acta*, vol. 227, pp. 170–179, 2017.

[32] H. D. Ertugrul and Z. O. Uygun, *State of the Art in Biosensors - General Aspects*. 2011.

[33] A. Lasia, *Electrochemical Impedance Spectroscopy and Its Applications*. New York: Springer, 2014.

[34] M. Matsumiya, M. Takano, R. Takagi, and R. Fujita, "Electrochemical Behavior of Ba^{2+} at Liquid Metal Cathodes in Molten Chlorides," *Zeitschrift fur Naturforsch.*, vol. 54a, pp. 1–8, 1999.

[35] L. Wang *et al.*, "Electrochemical Extraction of Cerium by Forming Ce-Zn Alloys in LiCl-KCl Eutectic on W and Liquid Zn Electrodes," *J. Electrochem. Soc.*, vol. 162, no. 9, pp. E179–E184, 2015.

[36] K. Liu, Y. L. Liu, Z. F. Chai, and W. Q. Shi, "Evaluation of the Electroextractions of Ce and Nd from LiCl-KCl Molten Salt Using Liquid Ga Electrode," *J. Electrochem. Soc.*, vol. 164, no. 4, pp. D169–D178, 2017.

[37] M. Kurata and Y. Sakamura, "Thermodynamic assessment of systems of actinide or rare earth with Cd," *J. Phase Equilibria*, vol. 22, no. 3, pp. 232–240, 2001.

[38] M. Kurata, Y. Sakamura, and T. Matsui, "Thermodynamic quantities of actinides and rare earth elements in liquid bismuth and cadmium," *J. Alloys Compd.*, vol. 234, no. 1, pp. 83–92, 1996.

[39] Y. Castrillejo, M. R. Bermejo, P. Díaz Arocas, A. M. Martínez, and E. Barrado, "Electrochemical behaviour of praseodymium (III) in molten chlorides," *J. Electroanal. Chem.*, vol. 575, no. 1, pp. 61–74, 2005.

[40] Y. Castrillejo, R. Bermejo, A. M. Martínez, E. Barrado, and P. Díaz Arocas, "Application

of electrochemical techniques in pyrochemical processes - Electrochemical behaviour of rare earths at W, Cd, Bi and Al electrodes," *J. Nucl. Mater.*, vol. 360, no. 1 SPEC. ISS., pp. 32–42, 2007.

[41] Y. Castrillejo, P. Hernández, R. Fernández, and E. Barrado, "Electrochemical behaviour of terbium in the eutectic LICl-KCl in Cd liquid electrodes.- Evaluation of the thermochemical properties of the $TbCd_x$ intermetallic compounds," *Electrochim. Acta*, vol. 147, pp. 743–751, 2014.

[42] H. Shibata, H. Hayashi, M. Akabori, Y. Arai, and M. Kurata, "Evaluation of Gibbs free energies of formation of Ce-Cd intermetallic compounds using electrochemical techniques," *J. Phys. Chem. Solids*, vol. 75, no. 8, pp. 972–976, 2014.

[43] V. Smolenski, A. Novoselova, P. Mushnikov, and A. Osipenko, "Study of the electrochemical behavior of U(III) ions on liquid Cd electrode and preparation of the U–Cd intermetallic compound in fused 3LiCl–2KCl eutectic," *J. Radioanal. Nucl. Chem.*, vol. 311, no. 1, pp. 127–133, 2017.

[44] D. Yoon, S. Phongikaroon, and J. Zhang, "Electrochemical and Thermodynamic Properties of $CeCl_3$ on Liquid Cadmium Cathode (LCC) in LiCl-KCl Eutectic Salt," *J. Electrochem. Soc.*, vol. 163, no. 3, pp. E97–E103, 2016.

[45] S. H. Kim, S. Paek, T. J. Kim, D. Y. Park, and D. H. Ahn, "Electrode reactions of Ce^{3+}/Ce couple in LiCl-KCl solutions containing $CeCl_3$ at solid W and liquid Cd electrodes," *Electrochim. Acta*, vol. 85, pp. 332–335, 2012.

[46] O. Shirai, M. Iizuka, T. Iwai, Y. Suzuki, and Y. Arai, "Electrode reaction of plutonium at liquid cadmium in LiCl-KCl eutectic melts," *J. Electroanal. Chem.*, vol. 490, no. 1, pp. 31–

36, 2000.

[47] O. Shirai, K. Uozumi, T. Iwai, and Y. Arai, “Electrode reaction of the Np^{3+}/Np couple at liquid Cd and Bi electrodes in LiCl – KCl eutectic melts,” *J. Appl. Electrochem.*, pp. 323–330, 2004.

[48] O. Shirai, H. Yamana, and Y. Arai, “Electrochemical behavior of actinides and actinide nitrides in LiCl-KCl eutectic melts,” *J. Alloys Compd.*, vol. 408–412, pp. 1267–1273, 2006.

[49] Y. Castrillejo, M. R. Bermejo, P. D. Arocas, A. M. Martínez, and E. Barrado, “The electrochemical behaviour of the Pr(III)/Pr redox system at Bi and Cd liquid electrodes in molten eutectic LiCl-KCl,” *J. Electroanal. Chem.*, vol. 579, no. 2, pp. 343–358, 2005.

[50] B. R. Westphal, J. C. Price, D. Vaden, and R. W. Benedict, “Engineering-scale distillation of cadmium for actinide recovery,” *J. Alloys Compd.*, 2007.

[51] T. Toda, T. Maruyama, K. Moritani, H. Moriyama, and H. Hayashi, “Thermodynamic properties of lanthanides and actinides for reductive extraction of minor actinides,” *J. Nucl. Sci. Technol.*, vol. 46, no. 1, pp. 18–25, 2009.

[52] K. Liu *et al.*, “Electrochemical reactions of the Th^{4+}/Th couple on the tungsten, aluminum and bismuth electrodes in chloride molten salt,” *Electrochim. Acta*, vol. 130, 2014.

[53] O. Shirai, M. Iizuka, T. Iwai, and Y. Arai, “Electrode reaction of Pu^{3+}/Pu couple in LiCl-KCl eutectic melts: comparison of the electrode reaction at the surface of liquid Bi with that at a solid Mo electrode.,” *Anal. Sci.*, vol. 17, no. 1, pp. 51–57, 2001.

[54] M. Li *et al.*, “Electrochemical behavior of La(III) on liquid Bi electrode in LiCl–KCl melts. Determination of thermodynamic properties of La–Bi and Li–Bi intermetallic compounds,”

RSC Adv., vol. 5, no. 100, pp. 82471–82480, 2015.

[55] E. Castrillejo, Y.; Bermejo, M.R.; Rosa, F. de la; Barrado, "Electrode reaction of cerium into liquid bismuth in the eutectic LiCl-KCl," *Denki Kagaku Oyobi Kogyo Butsuri Kagaku*, vol. 37, no. 03, pp. 636–643, 2005.

[56] W. Han *et al.*, "Electrochemical formation and thermodynamic properties of Tb–Bi intermetallic compounds in eutectic LiCl–KCl," *RSC Adv.*, vol. 7, no. 50, pp. 31682–31690, 2017.

[57] T. Lichtenstein, T. P. Nigl, N. D. Smith, and H. Kim, "Electrochemical deposition of alkaline-earth elements (Sr and Ba) from LiCl-KCl-$SrCl_2$-$BaCl_2$ solution using a liquid bismuth electrode," *Electrochim. Acta*, vol. 281, pp. 810–815, 2018.

[58] M. Matsumiya, R. Takagi, and R. Fujita, "Recovery of Eu^{2+} and Sr^{2+} using liquid metallic cathodes in molten NaCl-KCl and KCl system," *J. Nucl. Sci. Technol.*, vol. 34, no. 3, pp. 310–317, 1997.

[59] M. Matsumiya, M. Takano, R. Takagi, and R. Fujita, "Recovery of Ba^{2+} using liquid metallic cathodes in molten chlorides," *J. Nucl. Sci. Technol.*, vol. 35, no. 11, pp. 836–839, 1998.

[60] M. Matsumiya, H. Matsuura, R. Takagi, and R. Fujita, "Continuous recovery of concentrated solute from the melt by countercurrent electromigration," *J. Alloys Compd.*, vol. 306, no. 1–2, pp. 87–95, 2000.

[61] M. Matsumiya and R. Takagi, "Electrochemical impedance spectroscopic study on Eu^{2+} and Sr^{2+} using liquid metal cathodes in molten chlorides," *Zeitschrift fur Naturforsch. - Sect. A*

J. Phys. Sci., vol. 55, no. 8, pp. 673–681, 2000.

[62] A. V. Volkovich, "Diffusion Coefficients of Alkaline-Earth Metal Ions in Molten Equimolar Mixtures of Potassium and Sodium Chlorides," *Melts*, vol. 7, no. 106, 1993.

[63] T. Lichtenstein, N. D. Smith, J. Gesualdi, K. Kumar, and H. Kim, "Thermodynamic properties of Barium-Bismuth alloys determined by emf measurements," *Electrochim. Acta*, vol. 228, pp. 628–635, 2017.

[64] J. M. P. Q. Delgado and M. Vazquez da Silva, "Analytical Solutions of Mass Transfer around a Prolate or an Oblate Spheroid Immersed in a Packed Bed," in *Multiphase System and its Applications*, 2011.

[65] D. Yoon and S. Phongikaroon, "Electrochemical Properties and Analyses of $CeCl_3$ in LiCl-KCl Eutectic Salt," *J. Electrochem. Soc.*, vol. 162, no. 10, pp. E237–E243, 2015.

[66] H. Okamoto, "Supplemental literature review of binary phase diagrams: Bi-Ce, Bi-Er, C-Ce, C-La, C-Pr, Cd-I, Cr-Cu, Cu-Er, Er-Sb, F-Sm, F-Yb, and Fe-Gd," *J. Phase Equilibria Diffus.*, vol. 34, no. 4, pp. 350–362, 2013.

[67] H. Yamana, J. Sheng, N. Souda, and H. Moriyama, "Thermodynamic properties of lanthanide metals in liquid bismuth," *J. Nucl. Mater.*, vol. 294, pp. 232–240, 2001.

Appendix A. Thermophysical Properties of $BaCl_2$-LiCl-KCl

To confirm the dissolution of $BaCl_2$ in the LiCl-KCl eutectic, the thermophysical properties of $BaCl_2$ in varying concentrations of LiCl-KCl were studied via differential scanning calorimetry (DSC). This produced a basic binary phase diagram for the $BaCl_2$:LiCl-KCl system.

Samples of $BaCl_2$-LiCl-KCl were prepared in an argon atmosphere glovebox. Salts were weighed and mixed to give a 10 g sample, which was then placed into an alumina crucible and dried in a Kerrlab Auto Electro Melt furnace for 5 hours at 573 K to remove any remaining moisture content. The salts were then melted at 773 K for 24 hours before being extracted by dipping a clean pyrex tube into the molten salt and removing it, leaving a rod-shaped salt sample inside the tube. A TA Instruments TGA-DSC model Q600 was used to study the thermal transitions via DSC, measuring the amount of heat required to increase the temperature of the sample versus a reference. Alumina pans were used both to hold the salt sample and to act as the empty reference pan. Salt sample size and heating rate have significant effects on the shape of the DSC scan. A high heating rate enhances the instrumental sensitivity but decreases the resolution; that is, it results in thermograph peaks that are taller, but also broader. The mass of the DSC sample also has an effect on the heat flow measurement. Using small sample masses will achieve high resolution but poor sensitivity. In contrast, larger samples increase sensitivity but can also cause thermal lag due to heat transfer effects within the sample. After testing several experiments with different sample sizes and heating rates, the parameters were chosen for this study, being a sample size of 10 mg and a heating rate of 5 K min^{-1} up to 973K. Two peaks were observed for each composition, correlating to the solidus line and the liquidus line phase changes. Detailed temperature values for observed peaks are listed in Table A.1.

Table A.0.1 Data for DSC experiments.

$BaCl_2$ (wt%)	**Weight (mg)**	**Peak 1 Temp. (K)**	**Peak 2 temp. (K)**
1	8.2562	625.98	754.50
10	9.0789	619.36	722.59
20	9.0203	616.12	653.75
30	8.1955	616.56	702.81
40	13.916	610.61	749.16
50	9.8121	620.01	780.03
60	7.8963	623.27	902.96

The temperature values for the first and second peak were then plotted vs. weight fraction of $BaCl_2$ to construct a partial binary phase diagram of the $BaCl_2$ and LiCl-KCl system, as shown in Figure A.0.1. The first peak temperatures represent values on the solidus line, below which the composition is completely crystalline. The second peak temperatures represent values on the liquidus line, above which the solution is completely liquid. The eutectic composition of the salt is seen to exist somewhere between 10 and 30 wt%. The importance of this study to the overall study is a confirmation that $BaCl_2$ is fully liquid in the system at the temperatures of the electrochemical study. This DSC study has shown that at the low weight percentages used in the electrochemistry studies (1 to 4 wt%), the $BaCl_2$ might not be fully liquid at temperatures below 754.50 K.

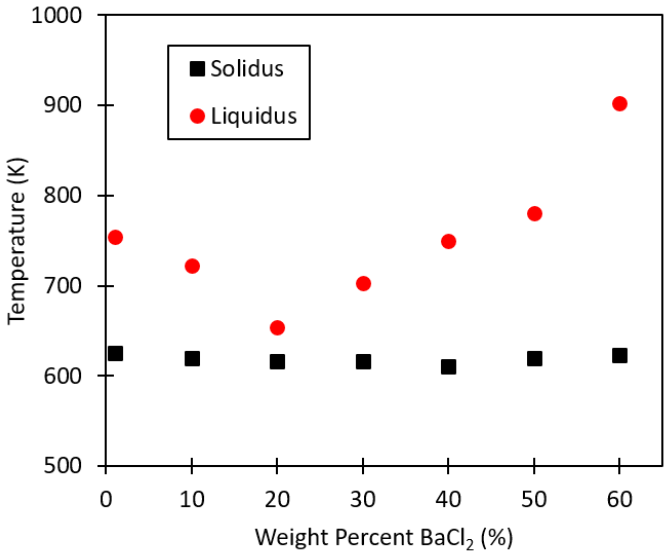

Figure A.0.1 Binary phase diagram of the $BaCl_2$:LiCl-KCl eutectic salt system.

Appendix B. Catalyzed Electrochemical Plutonium Oxide Dissolution

This appendix presents work conducted at Oak Ridge National Laboratory (ORNL) and is based on the manuscript, which has been created and is in the approval process for submission to a journal (ONRL Publication Tracking System). The full list of authors includes Michael E. Woods, Paul D. Benny, Aaron J. Unger, Supathorn Phongikaroon, and Kristian G. Myhre. The role of Michael E. Woods was to design and perform the experiments, process and analyze all data collected, and prepare the manuscript for submission.

Abstract

The production of ^{238}Pu heat source material at Oak Ridge National Laboratory for use by the National Aeronautic and Space Administration results in a solid Pu oxide that is shipped to Los Alamos National Laboratory for fabrication into General Purpose Heat Sources. Prior to shipment, it is crucial that the product Pu oxide be analyzed for plutonium isotopics and impurities. The quantitative dissolution of solid Pu oxide is quite difficult with the current method involving lengthy several-day exposures to solutions containing some hydrofluoric acid and high molarity of nitric acid. This limits the rapidness at which solid Pu oxide can be analyzed at various stages during production. The adaptation of a different dissolution strategy, Mediated Electrochemical Oxidation (MEO), has been explored as a rapid approach for quantitatively dissolving solid Pu oxide. The process involves the electrochemical production of a strongly oxidizing species in an electrolyte solution which then reacts with and dissolves the solid Pu oxide. MEO for Pu oxide, which is often referred to as Catalyzed Electrochemical Plutonium Oxide Dissolution (CEPOD), has been applied at production scale levels to dissolve solid Pu oxide with great success for several decades. The application to quantitatively dissolve solid Pu oxide for chemical analysis has not been explored though. In this study, a small scale apparatus was used to explore the use of MEO

for rapid quantitative dissolution of solid Pu oxide with the application of preparing samples for analysis (e.g. gamma spectroscopy, alpha spectroscopy, mass spectrometry). The effects of temperature, electrode material, and electrocatalyst on the dissolution kinetics were explored. Under conditions examined in this study, complete dissolution of tens of milligrams of solid Pu oxide can be achieved in less than an hour at ambient temperature.

Introduction

Radioisotope Thermoelectric Generators (RTGs) are an enabling technology for deep space exploration that function by converting the decay heat from a radioactive material into electricity through the Seebeck effect – a direct conversion of temperature difference to electricity at the junction of two different material wires. The National Aeronautic and Space Administration (NASA) has used RTGs in numerous missions, including to power the Voyager I and II spacecraft. Originally launched in 1977, the twin Voyager spacecraft have received multiple new missions. In the last several years, both spacecraft exited the heliosphere thereby becoming the first and second manmade objects to enter interstellar space. One of the key components enabling their significantly longer than expected lifetimes is the RTGs that have provided reliable power for more than 40 years. The radioisotope of choice for use in RTGs for NASA is ^{238}Pu (E_{α} = 5.593 MeV, $t_{1/2}$ = 87.7 years), though other radioisotopes such as ^{90}Sr ($E_{\beta-}$ = 0.546 MeV, $t_{1/2}$ = 28.8 years), ^{210}Po (E_{α} = 5.408 MeV, $t_{1/2}$ = 138 days), ^{241}Am (E_{α} = 5.486 MeV, $t_{1/2}$ = 432.2 years), etc. can be used in RTGs. The United States' ^{238}Pu bulk production capability was originally housed at the Savannah River Site but ceased in 1988. Additional ^{238}Pu was then purchased from Russia until their production ceased and decreasing stockpiles prevented continued purchases. In 2012, the United States Department of Energy (DOE) and NASA announced that a domestic capability to produce bulk quantities of ^{238}Pu would be established within the DOE complex. Today, Oak Ridge National

Laboratory (ORNL) is leading this effort in collaboration with Idaho National Laboratory (INL) and Los Alamos National Laboratory (LANL). This collaboration has successfully produced pilot scale quantities of ^{238}Pu exceeding the isotopic and impurity specifications and is continuing to ramp production efforts up to reach a production capacity goal of 1.5 kg per year by 2025[1].

The production process starts with ^{237}Np feedstock material being shipped from INL to the Radiochemical Engineering Development Center (REDC) at ORNL, where Np feedstock material is dissolved, chemically processed to remove impurities and decay products, and converted into an Np oxide powder. The Np oxide powder is then mixed with Al powder and pressed into cermet pellets, which are inserted into aluminum target bodies for irradiation in the High Flux Isotope Reactor at ORNL or Advanced Test Reactor at INL. Once the targets have been irradiated, they are returned to REDC for radiochemical processing to recover the produced ^{238}Pu. The remaining ^{237}Np is also recovered such that it can be reused as target material. The radiochemical processing of the irradiated targets involves numerous steps including solvent-extraction, ion exchange, and resin firing before the final ^{238}Pu oxide product is produced and ready for shipment to LANL. The entire production process is complex and a significant amount of work is required to reach the 1.5 kg per year production capacity goal by 2025. This production rate target is achievable but requires optimization of operations within the chemical processing flowsheet.

Throughout the production process it is necessary to perform quantitative isotopic and elemental analysis of Pu oxide samples. The dissolution of PuO_2 in any acid media is difficult, but a combination of nitric acid with fluoride and heat is typically used in many processes[2,3]. However, the presence of fluoride is undesirable because of its corrosive nature on stainless steel, and its added expenses in processing and waste remediation. Additionally, the total dissolution time to achieve complete dissolution can exceed several days. To avoid the use of fluoride and increase

the dissolution rate, a process utilizing mediated electrochemical oxidation (MEO) known as CEPOD, standing for Catalyzed Electrolytic Plutonium Oxide Dissolution, has been developed at Pacific Northwest National Laboratory (PNNL) by which electrochemically generated metal ions oxidize the PuO_2 to PuO_2^+ and then again to PuO_2^{2+} thereby increasing the solubility[2,4]. A representation of this process is shown in Figure B.0.1. The most attractive metal cations for this process are Ag^{2+} ($E° = 1.98$ V), Co^{3+} ($E° = 1.84$ V), and Ce^{4+} ($E° = 1.74$ V) due to their reduction potentials all being higher than the standard oxidation potential for PuO_2 to PuO_2^+ ($E^o = 1.58$ V).

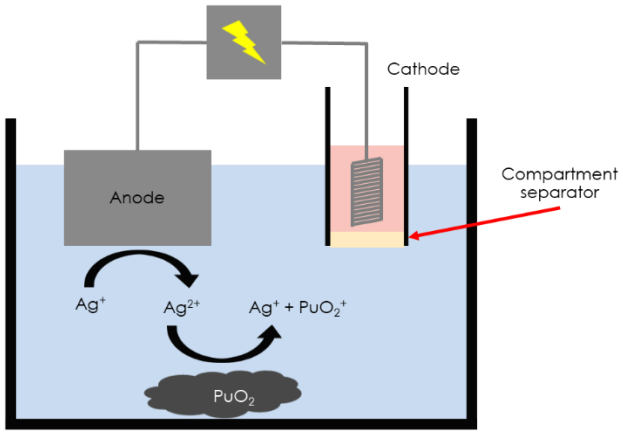

Figure B.0.1 Simplified diagram of the dissolution process.

This process for the dissolution of PuO_2 and mixed oxide (MOX) materials has been studied only for applications in large processing scales[4–7]. In France, it has been implemented at a production scale for nuclear waste treatment using Ag^{2+} ions[8]. MEO has also been studied with various electrocatalysts for the destruction of organic compounds, such as phenol[9,10].

To date, the mediated electrochemical oxidation process has been studied for use only within large scale processing schemes. This paper presents a process for rapidly dissolving samples

of PuO_2 from a processing scheme for analytical measurements. This changes the emphasis of the dissolution method from minimal resource cost (electricity, waste, etc.), which is a key consideration for production scale dissolutions, to a preference for rapid and quantitative dissolution for analytical measurements. If complete dissolution can be achieved within an hour, then a same-day quantitative composition analysis measurement is possible in a processing scheme.

Materials and equipment

Experiments were conducted in a negative pressure glovebox at ambient temperature. The electrochemical cell was set up as shown in Figure B.0.2. A bulk electrolysis cell kit (MF-1056) was purchased from Bioanalytical Systems, Inc. (BASi). The bulk anolyte solution was contained in the large compartment and consisted of 4 M HNO_3 with the addition of either 0.1 M $AgNO_3$ or 0.1 M $Co(NO_3)_2$. The smaller chamber was utilized as a cathode chamber and consisted of a spiral Pt wire within 8 M HNO_3, separated from the bulk anolyte by a Nafion membrane that was held in place by an open-bottom threaded cap. The reticulated vitreous carbon (RVC) electrode and a platinum gauze electrode (BASi NM-D001), both with an open bottom, were each tested as an anode. PuO_2 powder was obtained from the ORNL ^{238}Pu production program and contained 88% ^{238}Pu isotopically. A magnetic stirrer was employed to increase the dissolution rate. A thermocouple was adhered to the side of the glass beaker and insulated with tape for different temperature studies. Heating was achieved via the hot plate stirrer upon which the whole experimental vessel rested.

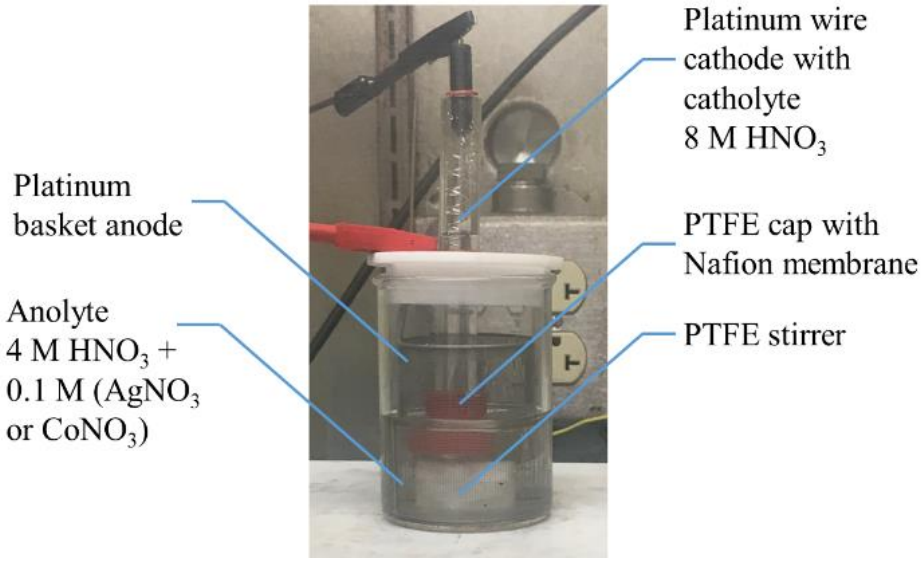

Figure B.0.2 Experimental vessel labelled with components, shown with Pt basket and Ag reagent.

Dissolution experiments

Prior to each experiment, the apparatus and other components were triple rinsed with 0.1 M HNO_3 to minimize any possible cross contaminations. Between 12 and 17 mg of PuO_2 powder were weighed and added to the vessel containing 40 mL of 4 M HNO_3 with either 0.1 M $AgNO_3$ or 0.1 M $Co(NO_3)_2$. The electrodes were then lowered into the solution and connected to the power supply. Stirring was then started in parallel with heating, if necessary. The power supply was then turned on with a constant voltage of 5 V. The maximum current of the power supply (378 mA) was infrequently reached for all dissolution experiments. The voltage did not drop significantly (typically ~0.1 to 0.3 V) during those events. The current typically stayed within a range of 300-340 mA. Small 100 µL samples were withdrawn every ten minutes by turning the stirring off, waiting to allow undissolved solids to settle, and then pipetting from just underneath the top surface of the anolyte. The samples were then diluted and prepared for radioanalytical measurements.

Radioanalytical measurements.

Alpha spectroscopy was used to quantify the amount of plutonium dissolved into the anolyte solutions. The activity of the Pu-238 within the sample was calculated from the total counted 5.5 MeV alpha emissions. This was then used with the dilution factor to give a measure of the specific activity within the anolyte. The total expected activity was calculated from the specific activity of Pu-238 and sample mass. The calculated activity and expected activity were then used to create a measurement of the percentage of dissolution achieved.

Results and Discussion

The first dissolution experiment tested the effectiveness of Ag^{2+} ions with a Pt anode and varying temperature from ambient to 80 °C. The percent of dissolution with respect to time is shown in Figure B.0.3. The rate of dissolution decreased sharply with increased temperature above 42 °C. At temperatures less than or equal to 42 °C, dissolution of PuO_2 appears to be near completion within one hour with a slightly decreased rate of dissolution for increased temperatures in the first 40 minutes. Reasons for the decreased dissolution rate at increased temperatures for the Ag^{2+} system are the oxidation of H_2O, which has a high activation energy, and the increased production of nitrous acid in the anolyte, reactions which have been suggested by similar studies[4,7,10]. In particular, Ryan et al. documented in their patent that the reduction of Ag^{2+} ions at a temperature of 104 °C was visually apparent by the solution color shift of brown to clear. From our study, it appears that a temperature around 30 °C allows near complete dissolution after approximately 60 min.

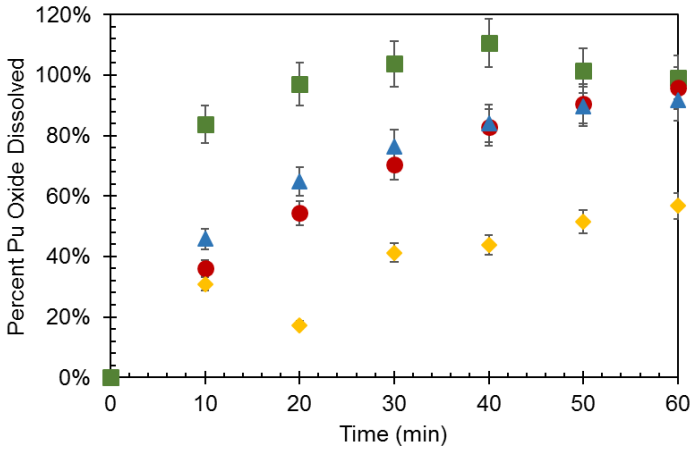

Figure B.0.3 Percentage of plutonium dissolved as a function of time using MEO with Ag^{2+} oxidant and a Pt anode. Temperatures are 25 °C (■), 32 °C (▲), 42 °C (●), and 80 °C (♦).

A similar temperature study using a Pt anode and Co^{3+} ions was then conducted. The dissolution results shown in Figure B.0.4 demonstrate the temperature did not seem to affect the rate of dissolution. Interestingly, at all four experimental temperatures, approximately 10 to 20% of PuO_2 dissolved within the first ten minutes and the amount of dissolved PuO_2 did not change appreciably afterward. Therefore, compared to Ag^{2+}, the use of Co^{3+} ions for this MEO system was not as effective.

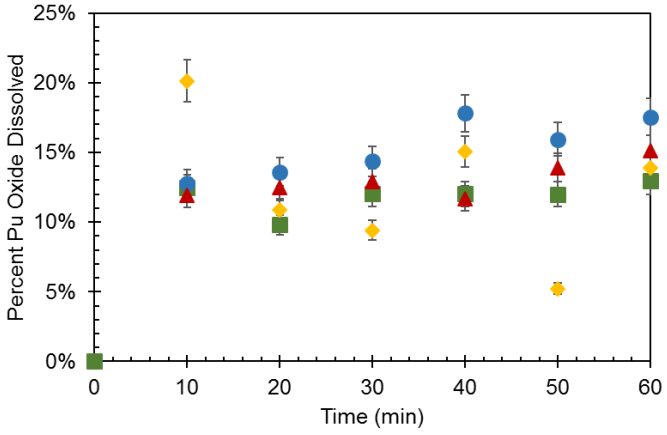

Figure B.0.4 Percentage of plutonium dissolved as a function of time using MEO with Co^{3+} oxidant and a Pt anode. Temperatures are 25 °C (■), 32 °C (●), 42 °C (▲), and 80 °C (♦).

Finally, the RVC anode was tested with conditions of 0.1 M $AgNO_3$ in 4 M HNO_3 for the anolyte and at a temperature of 25 °C, mimicking one of the earlier experiments done with a Pt anode. These comparative studies are shown in Figure B.0.5 and it can be seen that the RVC anode contributes to a much slower rate of dissolution, appearing to plateau at around 20% dissolution. The difference of rates of Ag^{2+} generation at the anode was visually apparent between the studies with the Pt and RVC anodes. In the experimental runs with a Pt anode, the solution went from clear to near black in a manner of seconds, indicating Ag^{2+} generation at the anode. In the RVC anode experimental runs, this solution color shift progressed over the order of minutes indicating a slower rate of Ag^{2+} generation. The RVC anode was tested because it would be much cheaper than platinum as an anode material and should have sufficient inertness in the harsh oxidizing environment. However, the results show that the performance of the RVC anode was far below that of Pt. In addition, the RVC was prone to breakage during the experiment, owing to occasional contact with the stirring bar.

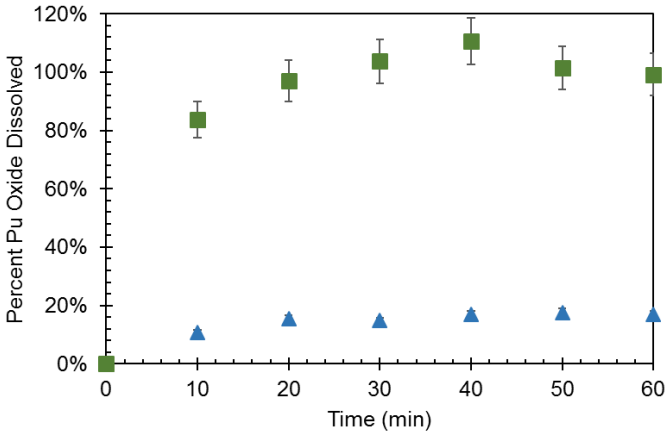

Figure B.0.5 Comparison of MEO dissolutions using Ag^{+} at two different electrode materials, platinum (■) and RVC (▲), at 25 °C.

Another important parameter which affects the dissolution rate is the particle size of the PuO_2. Smaller particles and greater surface area would increase the rate of dissolution, so the

particle size of the PuO_2 feedstock to be analyzed must be taken into account when applying this method of dissolution. A possible method to increase the dissolution rate is the addition of other metal ion catalysts to increase the oxidation rate by the primary electrocatalyst. This has been studied with various metal ion catalysts for Ce^{4+} based MEO[11,12]. Systems of MEO electrocatalysts with additional metal ion oxidation catalysts would be worthwhile to study for this PuO_2 dissolution system, such as Ag^{+} with a small addition of Ce^{3+}. However, it is attractive to use only Ag ions, as their recovery from the solution via electrodeposition is easier to achieve[13,14].

Conclusions

An approach to quantitatively dissolve small amounts of solid Pu oxide for isotopic and impurity analysis was successfully developed. This involved adapting the MEO approach known as CEPOD from the well-developed production scale to the unexplored analytical scale. The effects of two electrocatalysts (Ag^{2+} and Co^{3+}), two electrode materials (Pt and RVC), and temperature from ambient to 80 °C on the completeness and rapidness of dissolution were explored. It was found that complete dissolution of analytical scale samples, tens of milligrams, can be achieved using Ag as the electrocatalyst with a platinum anode under ambient conditions. Continued work on this dissolution approach is underway with the focus on establishing a routine procedure and direct comparison to the nitric acid/hydrofluoric acid approach. It is envisioned that this new approach for analytical scale dissolutions of solid Pu oxide may be widely applicable to other media, such as environmental samples with applications in nuclear forensics analysis, or adapted slightly to analyze similar production feedstock, such as Np oxide.

Acknowledgements

The authors thank Miting Du and Tom Hylton for providing results from the nitric/hydrofluoric acid dissolutions and general discussions on dissolving plutonium oxide. The

authors thank the Nuclear Analytical Chemistry and Isotopics Laboratory Group for performing the radioanalytical measurements. This study was performed partially using funding received from the DOE Office of Nuclear Energy's Nuclear Energy University Programs (NEUP) in collaboration with The Pennsylvania State University (NEUP-15-8126). This manuscript has been authored by UT-Battelle, LLC under Contract No. DE-AC05-00OR22725 with the U.S. Department of Energy. The United States Government retains and the publisher, by accepting the article for publication, acknowledges that the United States Government retains a non-exclusive, paid-up, irrevocable, world-wide license to publish or reproduce the published form of this manuscript, or allow others to do so, for United States Government purposes. The Department of Energy will provide public access to these results of federally sponsored research in accordance with the DOE Public Access Plan (http://energy.gov/downloads/doe-public-access-plan).

References

(1) Oakley, S. S. Space Exploration: Improved Planning and Communication Needed for Plutonium-238 and Radioisotope Power Systems Production. **2017**.

(2) Bray, L. A.; Ryan, J. L.; Wheelwright, E. J. Development of the CEPOD Process for Dissolving Plutonium Oxide and Leaching Plutonium from Scrap and Wastes. **1985**.

(3) Machuron-Mandard, X.; Madic, C. Basic Studies on the Kinetics and Mechanism of the Rapid Dissolution Reaction of Plutonium Dioxide under Reducing Conditions in Acidic Media.Pdf. *J. Alloys Compd.* **1994**, *213/214*, 100–105.

(4) Ryan, J.; Bray, L.; Boldt, A. United States Patent (19) 11 Patent Number : Date of Patent : **1990**, No. 19, 3–6. DOI: 10.1007/s00253-005-1916-3.

(5) Zundelevich, Y. The Mediated Electrochemical Dissolution of Plutonium Oxide: Kinetics and Mechanism. *J. Alloys Compd.* **1992**, *182* (1), 115–130. DOI: 10.1016/0925-8388(92)90580-3.

(6) Bourges, J.; Maixc, C. DISSOLUTION DU BIOXYDE DE PLANS PAR L ’ ARGENT (II) ELECTBOGENERE * EN ~ IL ~ U N ~ RIQUE Resume La ~ Solution Oxydante Du Bioxyde de Plutonium Par l ’ ~ Ent (II) Electrogenere a 6te Etudiee B Echelle Analytique Dans Le but de DQgager Les Parametres C. **1986**, *122*, 303–311.

(7) Brown, J.; Campbell, C.; Carrigan, C.; Carrott, M.; Greenough, K.; Maher, C.; McLuckie, B.; Mason, C.; Gregson, C.; Griffiths, T.; et al. Americium and Plutonium Purification by Extraction (the AMPPEX Process): Development of a New Method to Separate 241Am from Aged Plutonium Dioxide for Use in Space Power Systems. *Prog. Nucl. Energy* **2018**, *106* (March 2017), 396–416. DOI: 10.1016/j.pnucene.2018.02.008.

(8) Izquierdo, J.-J.; Lavenu, A.; Kniebihli, B. The Centralized Alpha Waste Treatment Facility (UCD) at La Hague. In *RECOD, 5th International Nuclear Conference on Recycling, Conditioning and Disposal*; RECOD, 5th International Nuclear Conference on Recycling, Conditioning and Disposal: Nice, France; p 11. Vol. 1.

(9) Farmer, J. C. Destruction of Chlorinated Organics by Cobalt(III)-Mediated Electrochemical Oxidation. *J. Electrochem. Soc.* **2006**, *139* (11), 3025. DOI: 10.1149/1.2069027.

(10) Matheswaran, M.; Chung, S. J.; Moon, I. S. Cobalt(III)-Mediated Oxidative Destruction of Phenol Using Divided Electrochemical Cell. *Korean J. Chem. Eng.* **2008**, *25* (5), 1031–1035. DOI: 10.1007/s11814-008-0168-1.

(11) Das, A. K. Kinetic and Mechanistic Aspects of Metal Ion Catalysis in Cerium(IV) Oxidation. *Coord. Chem. Rev.* **2001**, *213* (1), 307–325. DOI: 10.1016/S0010-8545(00)00376-3.

(12) Matheswaran, M.; Balaji, S.; Chung, S. J.; Moon, I. S. Silver Ion Catalyzed Cerium(IV) Mediated Electrochemical Oxidation of Phenol in Nitric Acid Medium. *Electrochim. Acta* **2007**, *53* (4), 1897–1901. DOI: 10.1016/j.electacta.2007.08.042.

(13) Chandrasekara Pillai, K.; Chung, S. J.; Moon, I. S. Studies on Electrochemical Recovery of Silver from Simulated Waste Water from Ag(II)/Ag(I) Based Mediated Electrochemical Oxidation Process. *Chemosphere* **2008**, *73* (9), 1505–1511. DOI: 10.1016/j.chemosphere.2008.07.047.

(14) Raju, T.; Chung, S. J.; Moon, I. S. Electrochemical Recovery of Silver from Waste Aqueous Ag(I)/Ag(II) Redox Mediator Solution Used in Mediated Electro Oxidation Process. *Korean J. Chem. Eng.* **2009**, *26* (4), 1053–1057. DOI: 10.1007/s11814-009-0175-x.